SEASONAL CLIMATE PREDICTIONS WITH A COUPLED ATMOSPHERE-OCEAN GENERAL CIRCULATION MODEL

CJ de W Rautenbach

WRC Report No. 904/1/03

Water Research Commission

SEASONAL CLIMATE PREDICTIONS WITH A COUPLED ATMOSPHERE-OCEAN GENERAL CIRCULATION MODEL

(CLIPWATER)

by

C J de W RAUTENBACH

Department of Geography, Geoinformatics and Meteorology
Faculty of Natural and Agricultural Sciences
University of Pretoria
Pretoria

Final Report to the Water Research Commission

2002

WRC Report No 904/1/03
ISBN NO 1-77005-049-3

Disclaimer

This report emanates from a project financed by the Water Research Commission (WRC) and is approved for publication. Approval does not signify that the contents necessarily reflect the views and policies of the WRC or the members of the project steering committee, nor does mention of trade names or commercial products constitute endorsement or recommendation for use.

Printed by Silowa Printers: 012 804 7565

SEASONAL CLIMATE PREDICTIONS WITH A COUPLED ATMOSPHERE-OCEAN GENERAL CIRCULATION MODEL

(CLIPWATER)

by

C.J.deW. RAUTENBACH

Department of Geography, Geoinformatics and Meteorology
Faculty of Natural and Agricultural Sciences
University of Pretoria, Pretoria

EXECUTIVE SUMMARY

---

1. INTRODUCTION

Many industrial sectors, especially the agriculture and food production sectors, exhibit a strong seasonal character. In addition, climate variability is factored into the performance of such industries. The availability of relatively accurate seasonal forecasts would therefore be invaluable for production prediction and operational planning. Seasonal climate variability is modulated by atmospheric circulation features, which are considered non-linear of nature.

Progress in the field of seasonal forecasting over the last couple of decades has revealed that the processes involved in seasonal forecasting are complex. Not only do seasonal changes in global Sea Surface Temperatures (SSTs) and land surface characteristics interfere with the conventional El Niño Southern Oscillation (ENSO) signal, but natural variability in the atmosphere (also known as random internal variability or chaos) also appears to be a major contributing factor that prevents forecasters from producing the so called "perfect deterministic seasonal forecast". Since anomalous changes in the ocean circulation evolve over longer periods than in the atmosphere, the response of atmospheric circulation (and therefore rainfall) to the global SST variability is still regarded as a key factor in the process of longer term forecasting. Both statistically and numerically-based (also dynamic) models have shown significant skill in the forecasting of rainfall at many locations on the globe. One benefit of numerically-based models is that natural variability forms part of the general or overall climate variation simulated by these models.

In this study the CSIRO9 Atmospheric Circulation Model (AGCM) with a R21 resolution is used in an effort to produce improved seasonal rainfall forecasts for South Africa. The COCA Coupled Atmosphere Ocean General Circulation Model (CGCM) simulates forecasted SST patterns that serve as boundary forcing for the AGCM. Both the AGCM and CGCM models were developed by the CSIRO Atmospheric Research in Australia. SST forecasts are supplied by Australian collaborators, while AGCM rainfall simulations are performed on a local super computer.

2. OBJECTIVES OF THE CLIPWATER PROJECT

The two main objectives of the CLIPWATER project can be summarised as follows:

a. *To collaborate with the CSIRO Atmospheric Research in Australia in order to develop a CGCM (referred to as the COCA CGCM) by coupling a dynamic OGCM to the CSIRO9 Mark II global AGCM with a T63 resolution (referred to as the CSIRO9(T63) AGCM). The CSIRO Atmospheric Research has developed both models.*

b. *To prescribe the CGSM simulated SST forecasts generated and issued by the CSIRO Atmospheric Research as boundary forcing in a coarser resolution model locally available (CSIRO9 Mark II global AGCM with a R21 resolution or CSIRO9(R21) AGCM) in order to investigate the skill and ability of this model to generate seasonal rainfall forecasts for Southern Africa.*

The research objectives were successfully achieved:

Good collaboration was established between the research team and the CSIRO Atmospheric Research in Australia. The CGCM was developed during the research project and the research team as well as students involved benefit significantly in terms of knowledge transfer from an international research organisation. The research team obtained code for the CSIRO9 Mark II AGCM (T63 resolution) and a number of simulations were completed on a local supercomputer.

Monthly SST forecasts generated by the CGCM were acquired from the CSIRO and these forecasts were compared to local SST forecasts. A thourough investigation indicated that CGCM forecasts are superior to persistence and locally generated statistical forecasts. CGCM SST forecasts were prescribed as boundary forcing to the CSIRO Mark II AGCM (R21 resolution). A forecasting technique was developed and probabilistic rainfall forecasts were successfully generated on a local super computer for the 2001/2002 summer season.

3. SUMMARY OF RESEARCH

In this study observed rainfall over South Africa was analysed from spatial and temporal perspectives and was compared with the associated AGCM simulated rainfall, where rainfall climatologies were derived in accordance with the CSIRO9(R21) and T(63) spectral resolutions. These climatologies formed the basis from which deviations in forecast rainfall were assessed.

A first numerical rainfall forecast was obtained by using the CSIRO9(R21) AGCM for the 1998/1999 summer season and verified against observations. Instead of CGCM SST forecasts, statistical Canonical Correlation Analysis (CCA) SST forecasts were employed as surface boundary forcing in this first experiment.

The research team collaborated closely with Australian scientists during the development phase of the COCA CGCM. Aspects of anomaly coupling, nudging and the initialisation procedure for forecast simulations were addressed and complex processes involved in ocean-atmosphere coupling as well as forecasting procedures were considered. In this project the COCA CGCM was primarily used for global SST forecasts.

Finally, COCA CGCM SST forecasts were evaluated against persisted SST forecasts and compared with forecasts generated by a statistical model. The CGCM forecasts outscored

persistence and statistical forecasts, which motivated why CGCM SST forecasts were used. Spatial anomaly correlation patterns between observations and CGCM SST forecasts were illustrated and ocean regions with significant skill were highlighted.

The CSIRO9(R21) AGCM was forced with CGCM SST forecast fields to in an effort to generate probabilistic seasonal forecasts for the 2001/2002 summer season. An 18-year hindcast simulation was used to determine the skill of the AGCM, and different rainfall categories were defined. Hit rate scores were calculated. CGCM SST forecasts for the October, November, December (OND) 2001 and January, February, March (JFM) 2002 seasons were prescribed as boundary forcing for the AGCM and rainfall simulations were performed. Probabilistic forecasts were prepared for the three rainfall categories.

The OND 2001 (early-summer) and JFM 2002 (late-summer) forecasts favoured wetter conditions during the early-summer season followed by somewhat drier conditions during the late-summer season. ***These forecasts agreed with observations during the 2001/2002 summer season.***

The report on capacity building and technology (knowledge) transfer gives an overview on the knowledge that was generated and how it will be applied in future.

4. OUTLOOK FOR THE FUTURE

The CLIPWATER project established a firm basis for further research in the field of numerical-based rainfall forecasting. A most challenging prospect is to produce improved seasonal forecasts on the regional scale. The CLIPWATER research team will continue with their efforts to investigate means of improving seasonal forecasts, and will most probably focus on the development of regional scale rainfall forecasting.

REPORT ON CAPACITY BUILDING

The CLIPWATER project extended over a period of three years. The primary objective of the project was to establish a numerically-based seasonal rainfall forecasting facility. For this purpose a numerical model (CSIRO9 (R21) AGCM) has been installed on a local super computer, and numerous simulations were performed to achieve what is outlined in the final report. Although probabilistic rainfall forecasts are locally generated, coupled model SST forecasts that serve as boundary forcing for the local atmospheric model, are still required from Australia.

1. INTERNATIONAL COLLABORATION

The CLIPWATER project encouraged international collaboration, in particular between the CSIRO Atmospheric Research in Australia and the Meteorology Group at the University of Pretoria. During the execution of the project three international scientists, all experts in the fields of either numerical modelling or seasonal forecasting, visited South Africa and contributed to transfer of knowledge to local scientists and students. The visiting scientists were:

1.1 1998: Barrie Hunt (Program Leader, CSIRO Atmospheric Research, Australia)
1.2 1999: Dr Steve Wilson (Ocean modeller, CSIRO, Atmospheric Research, Australia.
1.3 2000: Dr Ian Smith (Seasonal forecasting, CSIRO Atmospheric Research, Australia)

During visits these scientists participated in local workshops and conferences.

The project leader visited the CSIRO Atmospheric Research on an annual basis to assist with the development of the coupled atmosphere-ocean model.

2. QUALIFICATIONS

2.1 As part of their studies, many undergraduate students worked on aspects of seasonal forecasting and model verification in internal research projects.

2.2 The project leader obtained his PhD in 1999. His research focused on model development and verification (CSIRO9 (R21) AGCM). His PhD studies established a basis from which the model could be applied in the CLIPWATER project.

2.3 Ms A.G. Bartman from the South African Weather Service enrolled for her MSc studies at the University of Pretoria. The purpose of her research was to employ an empirical recalibration technique in order to improve rainfall forecasts over South Africa. The CSIRO9 (R21) AGCM was used for this purpose. Me Bartman submitted her dissertation entitled *PATTERN ANALYSIS AND RECALIBRATION OF A PERFECTLY FORCED ATMOSPHERIC GENERAL CIRCULATION MODEL* in 2002.

2.4 Ms A. Thackrah from the Institute for Soil Climate and Water enrolled for her MSc studies at the University of Pretoria. She will use seasonal rainfall forecasts from the CLIPWATER project to develop an early warning system for Brown Locust Outbreaks over the western parts of South Africa. Ms Thackrah will submit her dissertation before the end of 2003.

2.5 The modelling facility and international collaboration established by the CLIPWATER project contributed to the initiation of research in the field of Regional Modelling. Many students from previously disadvantaged communities are currently entering the University of Pretoria and sharing in the knowledge gained over the past few years.

3. CONFERENCE PRESENTATIONS

Nationally

1. Rautenbach C.J.deW (1998) Teleconnections between global sea-surface temperatures and the inter-annual variability of observed and model simulated rainfall over Southern Africa. *Skool vir Mynbou & Mineraalwetenskap, Navorsingseminaar, Universiteit van Pretoria, Pretoria, Suid-Afrika* (poster presentation)

2. Rautenbach, C.J.deW. (2000) Seasonal surface temparature and rainfall projections with a coupled atmosphere-ocean General Circulation Model (GCM). *2000 Annual Conference of the South African Society of Atmospheric Science, 16-17 October 2000, Sanlam Auditorium, University of Pretoria*

3. Rautenbach, C.J.deW. (2001) A cost effective procedure to construct coupled ocean-atmosphere model seasonal rainfall forecasts for South Africa. *2001 Annual Conference of the South African Society of Atmospheric Science, 6,7,September 2001, University of Cape Town.*

Internationally

1. Rautenbach, C.J.deW. (1998) The CSIRO-9 AGCM and climate variability over Southern Africa. *Presentation during the annual AMOS conference in Wellington, New Zealand.* (oral presentation) (***Session chairman during this conference***)

2. Engelbrecht, F.A. and Rautenbach, C.J.deW. (1999) The contribution of extra tropical sea-surface temperature anomalies to the 1996/97 rainfall simulations over the South African summer rainfall region. *UNESCO International conference on integrated drought management, CSIR, Pretoria, South Africa.* (oral presentation).

3. Rautenbach, C.J.deW. (1999) Numerical rainfall forecasts for the South African 1998/99 summer season using the CSIRO-9 (R21) AGCM. *UNESCO International conference on integrated drought management, CSIR, Pretoria, South Africa.* (oral presentation).

4. PUBLICATIONS IN PEER-REVIEWED JOURNALS

4.1 Jury, M.R., Mulenga, H. and Rautenbach, C.J.deW. (2000) Tropical Atlantic variability and Indo-Pacific ENSO: Statistical analysis and numerical simulation. *The Global Atmosphere and Ocean System*, **7(2)**, 107-124.

4.2 Rautenbach, C.J.deW. and Smith, I.N. (2001) Teleconnections between global sea-surface temperatures and the interannual variability of observed and model simulated rainfall over Southern Africa. *Journal of Hydrology*, **254**, 1-15.

The availability of the CSIRO9 (R21) AGCM also encouraged the project leader to publish the following paper:

4.3 Rautenbach, C.J.deW. A hypothetical approach to determining the effect of palaeorotational rates on late Precambrian Earth's palaeoclimate. *Accepted for publication in the African Journal of Geology in 2002.*.

5. CONTRIBUTION TO THE SADC COMMUNITY

The project leader attended all the Southern African Regional Climate Outlook Forum (SARCOF) meetings presented from 1998 to 2000. CSIRO9(R21) rainfall forecasts were presented.

6. OTHER PROJECTS

Research achievements in the CLIPWATER project enabled the project leader to become involved and to make a significant contribution to a project funded by the South African Department of Arts, Culture, Science and Technology entitled *SEASONAL WEATHER FORECASTING FOR AGRICULTURAL, WATER AND FISHERIES IMPACT PLANNING THROUGH INNOVATED COMPUTING* (2000 to 2002). The project is managed by the University of Cape Town.

REPORT ON TECHNOLOGY TRANSFER

1. Probabilistic seasonal rainfall forecasts will be made available on the World-Wide-Web (WWW) through the Seasonal Forecasting facility at the South African Weather Service (SAWS). To facilitate this process, a WWW link will be created between the SAWS and University of Pretoria. Here the Water Research Commission will be acknowledged for their involvement and contribution that made such a facility possible.

2. The University of Pretoria will build on the knowledge gained in the CLIPWATER project. Emanating from the CLIPWATER project, a *LABORATORY FOR POST-GRADUATE RESEARCH IN ATMOSPHERIC MODELLING (LRAM)* has already been established in the Department of Geography, Geoinformatics and Meteorology, Faculty of Natural and Agricultural Sciences, University of Pretoria. This facility will encourage local students and scientists to become involved in the field of atmospheric modelling and numerical seasonal forecasting.

SEASONAL CLIMATE PREDICTIONS WITH A COUPLED ATMOSPHERE-OCEAN GENERAL CIRCULATION MODEL

(CLIPWATER)

by

C.J.deW. RAUTENBACH

Department of Geography, Geoinformatics and Meteorology
Faculty of Natural and Agricultural Sciences
University of Pretoria
Pretoria

Final Report to the Water Research Commission

2002

PROJECT: K5 / 904

ACKNOWLEDGEMENTS

The author and project leader wishes to express his appreciation to the following persons and organisations for their assistance and contribution to the final report.

1. The Water Research Commission for funding the research and, in particular, *Dr George Green* for his interest and guidance during the project.

2. The steering committee for their advice during the project. The following persons have been involved: *Dr. G.C.Green, Mr H. Maaren, Prof M. Jury, Prof B.E.M.L. Kelbe, Mr E. Poolman, Ms E. Klopper, Dr C. Reason, Prof R.E. Schulze, Mr C. Turner, Mr S. van Biljon, Mr A.T. van Coller and Prof J van Heerden.*

3. *Mr Barrie Hunt* (Program leader, Climate Modelling) from the CSIRO Atmospheric Research, Australia. I wish to thank him for supporting this research and providing the necessary office space and computer facilities during my many visits to the CSIRO.

4. *Dr Ian Smith* and *Dr Steve Wilson* from the CSIRO Atmospheric Research for their enthusiasm while developing the coupled atmosphere-ocean model. Thanks a lot for their time and contribution during their visits to South Africa.

5. *Dr Hal Gordon* from the CSIRO Atmospheric Research, Australia, for his assistance with the model code.

6. All the staff in the Department of Geography, Geoinformatics and Meteorology at the University of Pretoria who provide the time, space and support to perform this research which take us one step further in the complex, but encouraging, field of seasonal forecasting.

7. The South African Weather Service for the availability and maintenance of the CRAY(EL). The research would have been impossible without this valuable hardware platform.

8. The Drought Monitoring Centre (DMC) in Harare, and in particular *Brad Garanganga*, who regularly invited me to present results from this research at the annual Southern African Regional Climate Outlook Forum (SARCOF) meetings.

9. *Francois Engelbrecht* (staff member at the University of Pretoria) for his willingness to perform some of my duties while I spent time on research and activities in seasonal rainfall forecasting.

10. *Mr Louis Botha* who made the observed Namibian rainfall data available for model verification.

11. *Mr Richard Sewell, Dr Warren Tennant, Dr Willem Landman, Dr Emsie Klopper* and *Ms Anna Bartman* for their contributions and advice.

TABLE OF CONTENTS

LIST OF FIGURES

Kelvin. Because of negative spatial loadings the PC scores are inverted so that negative values indicate wet conditions.

FIGURE 2.9
The first *AGCM simulated* summer (October-March) rainfall principal component pattern (PC1) with the associated amplitude time series (1961-1990) for southern Africa. The pattern accounts for 39% of the total variance. The bar-chart depicts the Niño4 Sea Surface Temperature (SST) variation in Kelvin. Because of negative spatial loadings the PC scores are inverted so that negative values indicate wet conditions.

FIGURE 2.10
The first *observed* mid-summer (December, January) rainfall principal component pattern (PC1) with the associated amplitude time series (1961-1990) for southern Africa. The pattern accounts for 54 % of the total variance. The bar-chart depicts the Niño4 Sea Surface Temperature (SST) variation in Kelvin. Because of negative spatial loadings the PC scores are inverted so that negative values indicate wet conditions

FIGURE 2.11
The first *AGCM simulated* mid-summer (December, January) rainfall principal component pattern (PC1) with the associated amplitude time series (1961-1990) for southern Africa. The pattern accounts for 29 % of the total variance. The bar-chart depicts the Niño4 Sea Surface Temperature (SST) variation in Kelvin. Because of negative spatial loadings the PC scores are inverted so that negative values indicate wet conditions.

FIGURE 2.12.
The first *observed* winter (May-August) rainfall principal component pattern (PC1) with the associated amplitude time series (1961-1990) for southern Africa. The pattern accounts for 36 % of the total variance. Because of negative spatial loadings the PC scores are inverted so that negative values indicate wet conditions.

FIGURE 2.13
The first *AGCM simulated* winter (May-August) rainfall principal component pattern (PC1) with the associated amplitude time series (1961-1990) for southern Africa. The pattern accounts for 55 % of the total variance. Because of negative spatial loadings the PC scores are inverted so that negative values indicate wet conditions.

FIGURE 2.14.
Correlation coefficients (r x 10) between the *observed* summer (October-March) rainfall PC1 time series (Figure 2.8) over southern Africa and global observed sea-surface temperatures (SSTs). Solid and dashed lines denote positive and negative values respectively. Spatially coherent correlations with values higher than the 99% significance level (0.47) are shaded. The symbols A, B, C and D denote the geographical location the Niño1.2 (0°-5°S)(90°-80°W), Niño3 (5°N-5°S)(150°-90°W), Niño3.4 (5°N-5°S)(170°-120°W) and Niño4 (5°N-5°S)(160E °-150°W) regions respectively.

FIGURE 2.15
Correlation coefficients (r x 10) between the *AGCM simulated* summer (October-March) rainfall PC1 time series (Figure 2.9) over southern Africa and global observed sea-surface temperatures (SSTs). Solid and dashed lines denote positive and negative values respectively. Spatially coherent correlations with values higher than the 99% significance level (0.47) are shaded.

FIGURE 3.1
Spatial regions used in the forecast analyses, namely (a) seven separate model grid boxes (G1 to G7), (b) a composite of four model grid boxes to form a central continental region (A1) and (c) a composite of seven model grid boxes to form one region (SA) that covers most parts of South Africa.

FIGURE 3.2
Area averages of observed rainfall calculated from land rainfall records alone (gray areas). In model grid boxes where the ocean forms part of the grid box area, it was assumed that the average rainfall over the land fraction represents the total grid average rainfall.

FIGURE 3.3
Spatial distribution of the SST anomaly grid used as AGCM boundary input during rainfall forecast simulations.

FIGURE 3.4
Canonical Correlation Analysis (CCA) Sea Surface Temperature (SST) anomaly forecast issued during May 1998 for the July, August, September (JAS) 1998 season.

FIGURE 3.5
Canonical Correlation Analysis (CCA) Sea Surface Temperature (SST) anomaly forecast issued during May 1998 for the October, November, December (OND) 1998 season

FIGURE 3.6
Three separate twelve-month AGCM rainfall forecast simulations, each initiated from a different month (namely January, April and June 1998), and each representing a five-member ensemble mean, have been compiled. Monthly Sea Surface Temperature (SST) anomalies were prescribed as ocean boundary forcing. Shaded / unshaded months denote observed/predicted SSTs. Forecast SSTs were issued as three-month averages. Weights of 1/3, 2/3 and 3/3 were applied to rainfall forecasts with 3, 2 and 1 month lead times, respectively in the forecast seasons (October, November, December (OND) 1998 and January, February, March (JFM) 1999).

FIGURE 3.7
Percentage of months (from the 12-year hindcast) where the model simulated and observed rainfall fell in the same category (hits). Categories are in terms of terciles indicating above-normal (AN), near-normal (NN) and below-normal (BN) rainfall.

FIGURE 3. 8(a)
Accumulated monthly observed rainfall (thick black line), forecast rainfall (shaded line) and the five ensemble members (thin black lines), measured in mm/season, for the OND 1998 and JFM 1999 seasons over region G1. Vertical thick black and shaded bars depict the near-normal (NN) category for the observed and AGCM simulated (forecast) rainfall, respectively.

FIGURE 3. 8(b)
As figure 3.8(a) but for region G6

FIGURE 3. 8(c)
As figure 3.8(a) but for region G7

FIGURE 3. 8(d)
As figure 3.8(a) but for region A1

FIGURE 3. 8(e)
As figure 3.8(a) but for region SA

FIGURE 3.9
Categorical probabilistic rainfall forecasts (left) for the (a) OND 1998 and (b) JFM 1999 seasons over regions G1, G6, G7 and A1. Observed rainfall catogaries are shown on the right. Probabilities have been derived from a 12-year hindcast simulation. The interpertation of the forecast probabilities is depicted by figure 3.10.

FIGURE 3.10
Interpretation of the diagram printed in the forecast regions (maps on the left in figure 3.9(a) and (b))

FIGURE 4.1
Diagram of COCA CAGCM Coupling (CSIRO9(T63) AGCM and ACOM2 OGCM)

FIGURE 5.1
Anomaly correlations between CGCM forecast SSTs and persistence over the NINO34 region. The correlations have been calculated from 48 hindcast simulations where the model was initialised at the beginning of January, February, March (1987 to 1999 = 13 years) and October (1990 to 1998 = 9 years). The 99% significance level is 0.33.

FIGURE 5.2
Anomaly correlations between COCA CGCM (solid black lines) SST forecasts and observations, and CCA/POPs (dotted black lines) SST forecasts and observations in the NINO34 region over a 13-year period (1987 to 1999) for different month lag times (+3, +6, +9, +12). Correlations are for the seasons (a) OND, (b) JFM, (c) AMJ and (d) JAS. The 95% and 99% significance levels are 0.54 and 0.69 respectively.

FIGURE 5.3
Global spatial anomaly correlations between CGCM forecast SSTs with a time lag of 6 months and observations. The correlations have been calculated from 48 hindcast simulations where the model was initialised at the beginning of January, April, July (1987 to 1999 = 13 years) and October (1990 to 1998 = 9 years). The 95% and 99% significance levels are 0.29 and 0.33 respectively.

FIGURE 5.4 Regional spatial anomaly correlations between CGCM forecast SSTs with a time lag of 6 months and observations. The correlations have been calculated from 13 hindcast simulations (1987 to 1999 = 13 years) where the model was initiated at the beginning of (a) July to forecast for January and (b) January to forecast for July. The 95% and 99% significance levels are 0.54 and 0.69 respectively.

FIGURE 5.5(a)
NINO34 SST forecast simulations by the COCA CGCM for the 2001/2002 summer season. Neutral ENSO conditions are expected.

FIGURE 5.5(b)
CGCM forecast Sea Surface Temperature (SST) anomalies for December 2001 measured in °C. The forecast simulation has been initialised from the beginning of August 2001. The dotted line represent the zero isotherm and the shaded areas has temperatures of 0.2 degrees and higher.

FIGURE 5.6(a)
Categorical probabilistic rainfall forecasts for the (a) OND 2001 and (b) JFM 2002 seasons over regions G1 to G7 as calculated for category classification A (6:6:6). Probabilities have been derived from a 18-year hindcast simulation. The interpretation of the forecast probabilities is depicted by figure 3.10.

FIGURE 5.6(b)
As figure 5.6(a) but for region A1.

FIGURE 5.6(c)
As figure 5.6(a) but for region SA.

FIGURE 5.7(a)
Categorical probabilistic rainfall forecasts for the (a) OND 2001 and (b) JFM 2002 seasons over regions G1 to G7 as calculated for category classification B (5:8:5). Probabilities have been derived from a 18-year hindcast simulation. The interpretation of the forecast probabilities is depicted by figure 3.10.

FIGURE 5.7(b)
As figure 5.7(a) but for region A1.

FIGURE 5.7(c)
As figure 5.7(a) but for region SA.

FIGURE 5.8(a)
Categorical probabilistic rainfall forecasts for the (a) OND 2001 and (b) JFM 2002 seasons over regions G1 to G7 as calculated for category classification C (4:10:4). Probabilities have been derived from a 18-year hindcast simulation. The interpretation of the forecast probabilities is depicted by figure 3.10.

FIGURE 5.8(b)
As figure 5.8(a) but for region A1.

FIGURE 5.8(c)
As figure 5.8(a) but for region SA.

LIST OF TABLES

TABLE 7(b)
Percentages of three-month average (seasonal) hit rate scores for the more extreme AN and BN categories in regions G1 to G7, A1 and SA. Hit rate scores are calculated for three category classifications (6:6:6, 5:8:5 and 4:10:4) as defined in table 5. Periods with scores bigger than 33% are shaded.

LIST OF ABBREVIATIONS

AGCM:	Atmospheric General Circulation Model
CAR:	CSIRO Atmospheric Research
CGCM:	Coupled Atmosphere Ocean General Circulation Model
COCA:	Coupled Oasis CAR-AGCM ACOM2 model
CPC:	Climate Prediction Centre
CSIRO:	Commonwealth Scientific and Industrial Research Organisation
DMC:	Drought Monitoring Centre
ENSO:	El Nino Southern Oscillation
EOF:	Empirical Orthogonal Function
FSU:	Florida State University (*wind stress data*)
GISST:	Global Sea Ice and Sea Surface Temperature (*data set*)
HR:	Hellerman and Rosenstein (*wind stress data*)
LEPS:	Linear Error in Probability Space
OASIS:	Ocean Atmosphere Sea Ice Soil (*coupler*)
OGCM:	Ocean General Circulation Model
PC:	Principal Component
POPs:	Principal Oscillation Patterns
RGSCS:	Research Group for Statistical ClimateStudies at the SAWS
SAWS:	South African Weather Service
SOI:	Southern Oscillation Index
SST:	Sea Surface Temperature
UP:	University of Pretoria
WRC:	Water Research Commission

Deviation indicators

AN:	Above-Normal
NN:	Near-Normal
BN:	Below-Normal

Seasons

JFM:	January, February, March	FMA:	February, March, April
MAM:	March, April, May	AMJ:	April, May, June
MJJ:	May, June, July	JJA:	June, July, August
JAS:	July, August, September	ASO:	August, September, October
SON:	September, October, November	OND:	October, November, December
NDJ:	November, December, January	DJF:	December, January, February

CHAPTER 1

INTRODUCTION

1.1 BACKGROUND

Many industrial sectors, especially the agriculture and food production sectors, exhibit a strong seasonal character. In addition, climate variability is factored into the performance of such industries. The availability of relatively accurate seasonal forecasts would therefore be invaluable for production prediction and operational planning.

During the 1980s forecasts of summer rainfall over South Africa was closely associated with the phase of the El Niño Southern Oscillation (ENSO) with above/below-normal rainfall driven by cold/warm ENSO phases. The association was mostly based upon a statistically significant linear correlation between the Southern Oscillation Index (SOI) in the equatorial Pacific Ocean and summer rainfall over the central continental parts of South Africa. In recent years statistical models have provided valuable information concerning the complex behaviour of atmospheric flow, and even succeeded to a certain degree of accuracy, in forecasting year-to-year changes in climate.

Progress in the field of seasonal forecasting over the last couple of decades has revealed that the processes involved in seasonal forecasting are much more complex. Not only do seasonal changes in global Sea Surface Temperatures (SSTs) and land surface characteristics interfere with the conventional ENSO signal, but natural variability in the atmosphere (also known as random internal variability or chaos) also appears to be a major contributing factor that prevents forecasters from producing the so called "perfect deterministic seasonal forecast". Since anomalous changes in the ocean circulation evolve over longer periods than in the atmosphere, the response of atmospheric circulation (and therefore rainfall) to the global SST variability is still regarded as a key factor in the process of longer term forecasting.

Both statistically and numerically-based (also dynamic) models have shown significant skill in the forecasting of rainfall at many locations on the globe (Kumar et. al., 1996). One benefit of numerically-based models is that natural variability forms part of the general or overall climate variation simulated by these models. Improvements in super computer technology contributed significantly to better global climate field simulations by numerically-based Atmospheric General Circulation Models (AGCMs).

In this study (also known as the CLIPWATER project) an AGCM that runs on a local super computer is used in an effort to produce improved seasonal rainfall forecasts for South Africa. Coupled Atmosphere Ocean General Circulation Model (CGCM) simulations from Australia supply forecast SSTs that serve as boundary forcing for the AGCM. CGCM generated SST forcing is employed to modulate future rainfall deviations in the AGCM.

1.2 TELECONNECTIONS BETWEEN OCEANS AND LOCAL RAINFALL

Rainfall is one of the most important atmospheric variables as far as agriculture and water resource management is concerned, but is difficult to predict at the seasonal time scale. Global SST anomalies have often been analysed in an effort to better understand the factors that may be

responsible for anomalously drier or wetter rainfall seasons for various regions. It has been demonstrated, for instance, that ENSO events, which evolve in the equatorial Pacific Ocean region, are a significant contributor to the inter-annual rainfall variability throughout much of the global tropics and beyond (Ropelewski and Halpert, 1987).

1.2.1 Equatorial Pacific Ocean

Statistically significant correlation patterns between SST anomalies over the equatorial Pacific Ocean and rainfall over South Africa have been described by many researchers (van Heerden *et al.*, 1988; Lindesay and Vogel, 1990 and Allan *et al.*, 1996). Warm ENSO phases, also known as El Niño events, usually coincide with below-normal summer rainfall over the central and western continental regions of South Africa. In general, these drier conditions have a detrimental impact on the availability of water resources, agricultural activities and food production. It has also been demonstrated that cold ENSO phases (La Niña events) are often associated with wet summer seasons over the same region.

1.2.2 Indian Ocean

Walker (1990), Jury and Pathack (1993) and Reason and Mulenga (1999) also indicated that wet summer rainfall conditions over the continental parts of South Africa are usually associated with relatively warmer SSTs in the south-west Indian Ocean south of 25° south, and lower SSTs north of this region to the east of Madagascar. Landman (1995, 1997) also found that SST anomalies over the tropical western Indian Ocean are negatively correlated with summer rainfall over the South African plateau, with the most significant correlations occurring during February. Landman and Mason (1999) later demonstrated that the latter association had been more profound prior to the late-1970s, and that warm/cold events in the tropical western Indian Ocean are, at present, more frequently associated with above-normal/below-normal rainfall conditions over South Africa.

Statistically significant links between South African rainfall and SST anomalies over both the Pacific and Indian Oceans might imply a semi-consistent remote response of the atmospheric circulation to ocean thermal boundary forcing.

1.2.3 Adjacent regional oceans

The effects of more localised forcing have also been explored. Lutjeharms and Ruijter (1996), for example, found that atmospheric convection induced by the warm Agulhas Ocean current might contribute to local precipitation along the south and southeastern coastline of South Africa. Walker (1990) and Crimp *et al.* (1998) postulated that surface heat and moisture fluxes, which appear in the Agulhas retroflection region during the summer months, may have an influence on the continental atmospheric pressure (tropical-temperate trough formation), and therefore can contribute to summer rainfall patterns over southern Africa (Harrison, 1984). It has also been suggested that SST fluctuations in the South Atlantic Ocean may contribute to cyclogenesis, which usually enhances favourable winter rainfall conditions confined to the southwestern parts of South Africa (Brundrit and Shannon, 1989; Majodina and Jury,1996). Comprehensive statistical studies by Walker (1990); Mason *et al.* (1994); Mason (1995), Jury (1996); Reason (1998) and Reason and Mulenga (1999) have conclusively indicated that links between regional SST anomalies and South African rainfall are complex and difficult to formulate.

1.2.4 SST as boundary forcing

The ability of an AGCM to represent monthly average climatic conditions on a global scale (McGregor *et al.*, 1993; Rautenbach, 1999) suggests that it may also be suitable for estimating the combined effects of both remote and localised SST forcing. For example, the effect of Indian Ocean SSTs on the large-scale atmospheric circulation and associated rainfall patterns have been investigated by Jury *et al.* (1996) and Tennant (1996) who performed AGCM simulations with prescribed above-normal SST anomalies for the central Indian Ocean. Reason (1998) and Reason and Mulenga (1999) used the same principle to investigate the impact of SST changes in the southeast Atlantic and southwest Indian Oceans on atmospheric circulation and rainfall patterns over southern Africa.

Furthermore, AGCMs offer the opportunity of forecasting seasonal climate anomalies (e.g. rainfall) if the relevant SST anomalies can be reliably forecast in advance. Most rainfall forecasting schemes make use of prescribed SSTs as boundary forcing for an AGCM, which then produces monthly or seasonal simulated mean atmospheric circulation anomalies. Unlike extra-tropical SSTs, tropical SSTs related to ENSO variability are predictable with lead times of several months (Zebiak and Cane, 1987; Landman, 1999). Since the atmospheric response to SST variability in the tropics is more direct than in the extra-tropics (Webster, 1981; Lau and Nath, 1994), AGCM simulated forecasts usually exhibit better skill over regions directly affected by tropical ocean teleconnections (Hunt *et al.*, 1994; Palmer and Anderson, 1994; Kumar *et al.*, 1996; Mason *et al.*, 1996; Hunt, 1997; Rowell, 1998; Yang *et al.*, 1998).

1.3 CLIMATE SIMULATIONS WITH NUMERICAL MODELS

1.3.1 *Boundary forcing and initial conditions*

Atmospheric mechanisms that contribute to teleconnections between globally-observed SST fields and South African rainfall can be investigated by forcing AGCMs with observed SST fields at the lower surface boundary (thermal boundary forcing). This approach is also followed when hindcast simulations are prepared in order to estimate the reliability of a model in producing seasonal forecasts. Even if one assumes that perfectly observed SST fields are used to force the same AGCM at its boundaries, noticeable deviations may occur in different simulations that start with a slight difference in initial conditions (Dix and Hunt, 1995). As demonstrated by Lorenz (1964), this is a result of the presence of natural variability in the non-linear dynamic system of the atmosphere. The implication is that even if a perfect SST field is forecast and fed into an AGCM, diverse atmospheric circulation anomalies (rainfall included) are most likely to appear in model simulations that start off with a slight difference in initial conditions.

According to Kumar et al. (1996) anomalies that result from climate variability in AGCM simulations may be expressed in terms of the following two components:

a) ***Boundary-forced component***

b) ***Random internal variability component***

The *boundary-forced component* of the resulting anomaly of an atmospheric variable is due to modulation of the atmospheric circulation by local or remote boundary forcing through SSTs and land cover characteristics, while the *random internal variability component* forms part of the internal nature of atmospheric flow as indicated by the non-linear atmospheric equations. It is therefore recommended that a number of model simulations be performed with the same

response of the model is to be examined. One such simulation is known as an ensemble member. An estimation of the climate variability of an AGCM can be obtained by calculating the average (ensemble mean) of all the individual model simulations (ensemble members). To a certain extent, ensemble averaging might smooth random internal variability, meaning that ensemble averaged AGCM anomalies give a good estimation of boundary-forced results.

1.3.2 Probabilistic nature of seasonal forecasting

A simple procedure to distinguish between the boundary-forced (for example fluxes from SST anomalies) and random internal variability components in observed climate anomalies does not exist, which implies that AGCM ensemble simulations for a particular observed event are difficult to interpret. There will always be a degree of uncertainty caused by actual random internal variability. In addition SST forecasts, which are still far from perfect, are needed as boundary forcing. The following statement is therefore extremely important:

THE PROBLEM OF SEASONAL FORECASTING IS INHERENTLY PROBABILISTIC BY NATURE

1.4 SEASONAL FORECASTING WITH NUMERICAL MODELS

Numerical models might be suitable for producing relatively reliable forecasts from certain long-lived boundary forcing conditions (Kamur et al., 1996). Remarkable progress has been made in forecasting SST anomalies in the equatorial Pacific Ocean up to one year in advance. Rainfall in regions, which experience a local or remote response to these SSTs, might therefore be successfully forecast to a certain degree of skill.

Two procedures are currently followed in seasonal climate forecasting:

a) TWO-TIERED FORECASTING PROCEDURE

An AGCM is employed exclusively to produce future climate simulations with prescribed or imposed SST input at the lower surface boundary. These observed or forecast SSTs might be produced by either CGCM or empirical techniques.

b) ONE-TIERED FORECASTING PROCEDURE

An AGCM is coupled to interact with a numerically based Ocean General Circulation Model (OGCM) to form a CGCM. The CGCM is then released from a given point in time, allowing it to evolve and produce estimates (scenarios) of future climate.

Both AGCM and OGCM models solve the equations of motion. Physical parameterisation is applied, where sub-grid scale processes are parameterised empirically.

When used alone the AGCM may be forced with either persistence (here one assumes that the SST field at the point of release will persist during the period of prediction), future SST projections from empirical models or future SST projections generated independently by a CGCM. Climate or rainfall forecasts therefore depend purely upon the AGCMs response to the prescribed SST input. This method of forecasting is a two-tiered forecasting procedure in which SSTs are forecast during the first phase and a climate variable during the second phase as indicated in figure 1.1 (Hunt, 1997; 1994).

More advanced and faster super computers have made it possible to introduce the one-tiered forecasting approach of using a CGCM to generate future climate projections. The forecasting procedure involves a strong nudging, during pre-forecast simulations, of CGCM simulated parameters towards the observed climate and the use of anomaly coupling. This prevents the model from "drifting" away from realistic values as the integration proceeds. During forecast simulations, the CGCM is released from a given point in time allowing it to evolve freely and produce future scenarios of estimated climate (one-tiered forecasting procedure).

As a consequence of the boundary-forced and random internal variability components in deviations from the normal in the climate system (discussed in section 1.2.1), it is required that numerical forecasts consist of an ensemble of simulations, which obviously leads to probabilistic climate forecasts.

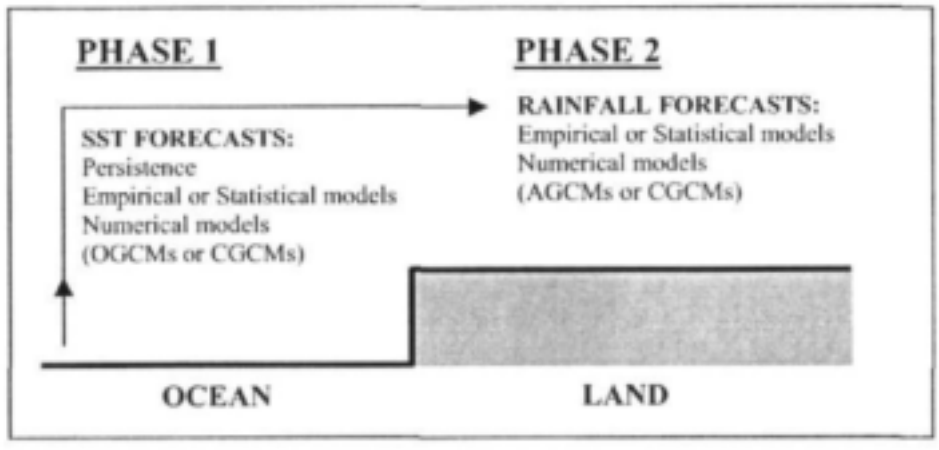

FIGURE 1.1: A typical example of the various models (or methods) used during the two phases of a two-tiered forecasting procedure. As a result of the response of the atmosphere to ocean forcing, Sea Surface Temperature (SST) forecasts are normally used to estimate future rainfall projections over land (or ocean).

A first attempt using the Australian CSIRO9 Mark II global AGCM with a R21 resolution (refer to as the CSIRO9(R21) AGCM) to produce two-tiered rainfall forecasts for lead times of up to twelve months was made by Hunt *et al.* (1994). Forecast SST anomalies were imposed over the equatorial Pacific Ocean as ocean thermal forcing (Zebiak and Cane, 1987). In a follow-up study Hunt (1997) investigated the prospects and problems concerning these rainfall forecasts.

In this study a CGCM, known as the Coupled Oasis CAR-AGCM ACOM2 model (COCA CGCM described in CHAPTER 4), developed in Australia was used to forecast global SST fields. These SSTs will then be prescribed as surface boundary forcing for an AGCM available in South Africa, which will finally produce the probabilistic seasonal rainfall forecasts. However, during the development phase of the CGCM, the AGCM was forced with statistically (Canonical Correlation Analysis: CCA) predicted SST fields obtained from the South African Weather Service (SAWS). A two-tiered forecasting procedure was employed.

An outstanding overview of current approaches followed in seasonal to inter-annual climate predictions can be found in Goddard et al. (2001).

1.5 OBJECTIVES OF THE CLIPWATER PROJECT

The two main objectives of the CLIPWATER project can be summarised as follows:

a. *To collaborate with the CSIRO Atmospheric Research in Australia in order to develop a CGCM (referred to as the COCA CGCM) by coupling a dynamic OGCM to the CSIRO9 Mark II global AGCM with a T63 resolution (referred to as the CSIRO9(T63) AGCM). The CSIRO Atmospheric Research has developed both models.*

b. *To prescribe the CGSM simulated SST forecasts generated and issued by the CSIRO Atmospheric Research as boundary forcing in a coarser resolution model locally available (CSIRO9 Mark II global AGCM with a R21 resolution or CSIRO9(R21) AGCM) in order to investigate the skill and ability of this model to generate seasonal rainfall forecasts for Southern Africa.*

South Africa (in this project the University of Pretoria or UP) does not have adequate computer resources to run the complete COCA CGCM on a routine basis. Local and international researchers agreed to perform CGCM simulations in Australia, and to use the CGCM forecast SST anomalies to force the coarser resolution version of the CSIRO9(R21) to produce future rainfall projections for South Africa. The CSIRO9(R21) AGCM does run on a local supercomputer at the SAWS, which enabled the research team to perform local analyses. A more detailed description of the various atmospheric models used in the CLIPWATER project is outlined in CHAPTER 2.

1.6 ORGANISATION OF THE REPORT

CHAPTER 1 has given an overview of relevant teleconnections between rainfall over South Africa and the global oceans. The concept of numerical seasonal forecasting has also been discussed and it was emphasised that numerical seasonal forecasting is probabilistic in nature. The first chapter also contains the objectives of the research.

Observed rainfall over South Africa is analysed from spatial and temporal perspectives in CHAPTER 2 and is compared with the associated AGCM simulated rainfall. Rainfall climatologies are provided in terms of the CSIRO9(R21) and T(63) spectral resolutions. These climatologies provide a basis for evaluating deviations in forecast rainfall.

A first numerical rainfall forecast by using the CSIRO9(R21) AGCM for the 1998/1999 summer season is presented and verified against observations in CHAPTER 3. At this point in the CLIPWATER project the COCA CGCM was still in a developing stage, and statistical (CCA) SST forecasts are therefore employed as surface boundary forcing.

The research team collaborated closely with Australian scientists during the developing phase of the COCA CGCM. A detailed description of the configuration of the COCA CGCM is outlined in CHAPTER 4. Aspects of anomaly coupling, nudging and the initialisation procedure for forecast simulations are some of the points that are addressed. The complex process of ocean-atmosphere coupling and forecasting is illustrated. The CGCM is primarily used for global SST forecasts.

In CHAPTER 5 COCA CGCM SST forecasts are verified against persistence and forecasts generated by a statistical model. These forecasts serve as base line against which the performance

of CGCM forecasts is measured. Spatial anomaly correlation patterns between observations and CGCM forecasts are illustrated and discussed. The CSIRO9(R21) AGCM is forced with CGCM SST forecast fields to in an effort to generate a seasonal forecast for the 2001/2002 summer season. An 18-year hindcast simulation is used to determine the skill of the AGCM, and different rainfall categories are defined. Hit rate scores are calculated. SST forecasts for the October, November, December (OND) 2001 and January, February, March (JFM) 2002 seasons are prescribed as boundary forcing for the AGCM and rainfall simulations are performed. Probabilistic forecasts are prepared for the three category classifications and rainfall forecast results are discussed.

It is concluded in CHAPTER 6 that the research indicates that it is feasible to prepare and issue seasonal rainfall forecast with the CSIRO9(R21) AGCM over South Africa. As an alternative, AGCM recalibration techniques should be considered for rainfall estimations. Concluding remarks and recommendations are made in this final chapter.

CHAPTER 2

OBSERVED AND MODEL SIMULATED RAINFALL

2.1 INTRODUCTION

Rainfall is one of the most complex atmospheric variables to simulate. Rainfall climate simulated by AGCMs typically has biases in relation to observed rainfall. In both the CSIRO9(R21) and (T63) AGCMs (described in sections 2.2.1 and 2.2.2), rainfall is overestimated over most of the eastern parts of South Africa. It is therefore more appropriate to compare anomalous rainfall fields produced by an AGCM with the associated observed rainfall anomaly fields and therefore to express AGCM forecasts in terms of anomalies rather than to make direct comparisons between observed and model-simulated rainfall projections.

Because rainfall anomalies rather than actual rainfall totals are forecast, end users of seasonal forecasts, whether probabilistic or deterministic, always need a reference base from which to interpret the results. The average rainfall measured over a given period of time is an obvious part of such a reference base. Knowing this, and given a seasonal rainfall forecast, a user can estimate whether dry or wet conditions are likely to occur in the coming season. For this reason, rainfall maps of observed averages are displayed in this chapter.

2.2 ATMOSPHERIC GENERAL CIRCULATION MODELS (AGCMs)

The CSIRO9 Mark II AGCM with both a R21 and T63 spectral resolution has been used. The R21 resolution has been used in local forecast integrations forced by prescribed SSTs while the T61 resolution model serves as the atmospheric component of the CGCM (the configuration of the COCA CGCM is described in detail in CHAPTER 3). Forecast SST fields are made available in T63 resolution and are interpolated to R21 resolution for use as surface boundary fields in local rainfall forecast simulations.

2.2.1 CSIRO9 Mark II AGCM (R21 spectral resolution)

The horizontal grid of the CSIRO9(R21) AGCM comprises 64 zonal and 56 meridional (gaussian) grid points, which yields a resolution of approximately 5.6^{O} by 3.3^{O}. In zonal-meridional dimension that gives a grid box of approximately 622 km x 360 km at the equator and 180 km x 317 km at a latitude of 30^{O} south. In the AGCM dynamics the spectral atmospheric equations in flux formulation (Gordon, 1981; Rautenbach, 1999) are integrated over nine sigma model levels (Phillips,1957) in the vertical. A comprehensive range of physical processes like radiation and rainfall are also included (Rotstayn, 1996, 1997). The model has full diurnal and annual cycles, gravity wave drag, a mass flux scheme for convection, semi-Lagrangian water vapour transport and a relative humidity-based cloud parameterisation. Surface interactions are parameterised using a soil-canopy model (Kowalczyk et al. 1994). A more detailed description of the model is provided in McGregor *et al.* (1993).

2.2.2 CSIRO9 Mark II AGCM (T63 spectral resolution)

The horizontal grid of the CSIRO9(T63) AGCM comprises 192 zonal and 96 meridional (gaussian) grid points, which yields a resolution of approximately 1.9^{O} by 1.9^{O}. In zonal-meridional dimension that gives a grid box of approximately 208 km x 208 km at the equator and 180 km x 208 km at a latitude of 30^{O} south. With the exception of horizontal grid resolution, the dynamical and physical configuration is similar to that of the CSIRO9(R21) AGCM described in SECTION 2.2.1.

2.3 OBSERVED AND MODEL SIMULATED RAINFALL

The final probabilistic rainfall forecasts made in this report by means of a two-tiered forecasting procedure (the COCA CGCM is employed to produce SST forecasts while a local AGCM produces probabilistic rainfall forecasts - CHAPTER 5) as produced by the CSIRO9(R21) AGCM are time averaged over the months OND and JFM. These two seasons have been selected since the Southern African Regional Climate Outlook Forum (SARCOF) regards OND and JFM as standard pre-summer and post-summer seasons. Observed rainfall averages and medians calculated over a period of 18-years are therefore displayed and compared with AGCM results for these two seasons only.

Likewise rainfall variability characteristics of the CSIRO9(T63) AGCM (atmospheric component of the COCA CGCM) are also compared with the associated observed fields and global SSTs. This part of the study, however, focuses on the October to March, December to January and the May to August seasons. Comparisons made refer to the development phase of the COCA CGCM, and give an overview of how the atmospheric component of the CGCM perform with regard to rainfall simulations. Since the primary purpose of the CGCM was to produce SST forecasts for use as boundary fields for the CSIRO9(R21) AGCM, it is important to note that rainfall simulations from the CGCM were not considered for seasonal forecasts.

2.3.1 CSIRO9(R21) AGCM simulated vs observed rainfall

2.3.1.1 Average or mean rainfall

CSIRO9(R21) AGCM simulated rainfall averages over seven grid boxes from the R21 horizontal spectral resolution that cover South Africa, are compared with the equivalent observed climate fields acquired from the SAWS. Rainfall averages for the pre-summer (namely OND) and post-summer (namely JFM) seasons are illustrated in figures 2.1 and 2.2. Rainfall averages are expressed in mm per season. Model simulated rainfall averages represent ten-year ensemble averages obtained from a seasonal cycle control simulation. Observed rainfall averages had been calculated from model grid box area averages of point stations.

In agreement with results of Joubert (1997), the model significantly overestimates rainfall totals over the eastern interior for both the OND and JFM and seasons (figures 2.1 and 2.2). The observed increase of summer rainfall totals from west to east over the country is well captured by the CSIRO9(R21) AGCM simulations for both seasons. In reality most parts of South Africa receive more rain during the post-summer (JFM) than during the pre-summer (OND) season - a feature also well reproduced by the model simulations.

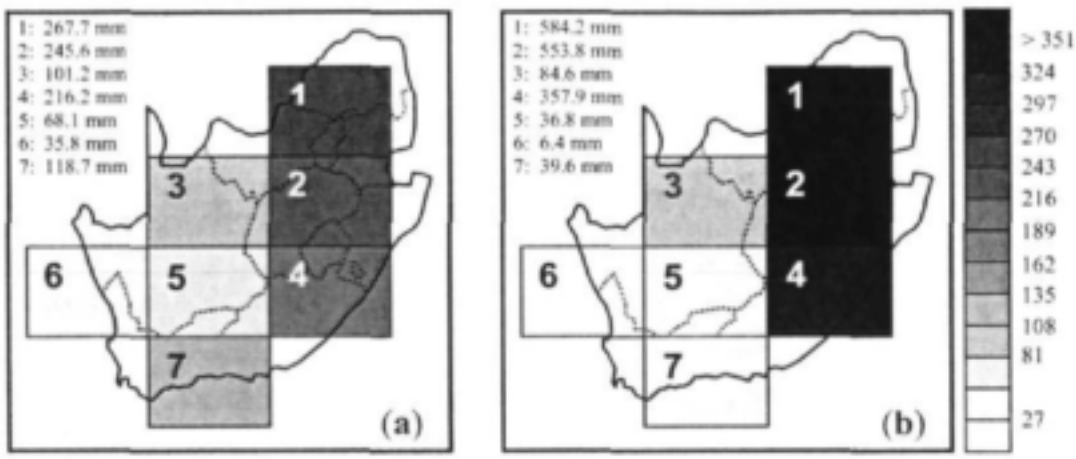

FIGURE 2.1 Averages of (a) observed October, November, December (OND) rainfall and (b) CSIRO9(R21) AGCM simulated OND rainfall in mm/season. Model simulated fields represent ten-year ensemble means obtained from a seasonal cycle control simulation.

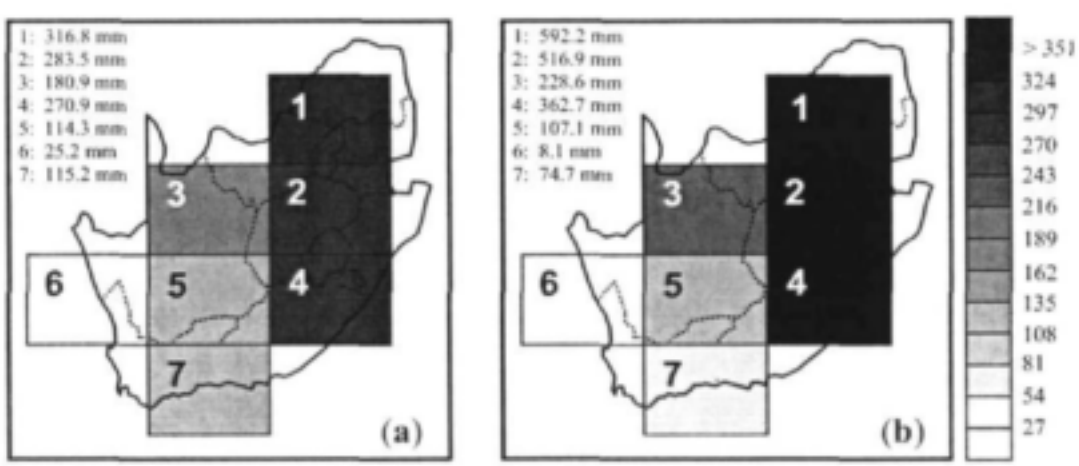

FIGURE 2.2 Averages of (a) observed January, February, March (JFM) rainfall and (b) CSIRO9(R21) AGCM simulated JFM rainfall in mm/season. Model simulated fields represent ten-year ensemble means obtained from a seasonal cycle control simulation.

2.3.1.2 Rainfall median

It is sometimes more appropriate to use the median rainfall instead of average or mean rainfall values. For example, differences between the average and median may be significant in a dry region where a few unusually high rainfall figures might result in a skew frequency distribution. In such an event the mean will be higher (as a result of the odd high rainfall episodes) than the median which will give a much more realistic value of the prevailing rainfall.

The rainfall median for the pre-summer (OND) and post-summer (JFM) seasons is illustrated in figures 2.3 and 2.4. Observed and AGCM simulated (rainfall from prescribed observed SST simulations) medians have been calculated from an 18-year rainfall record (1982 to 1999).

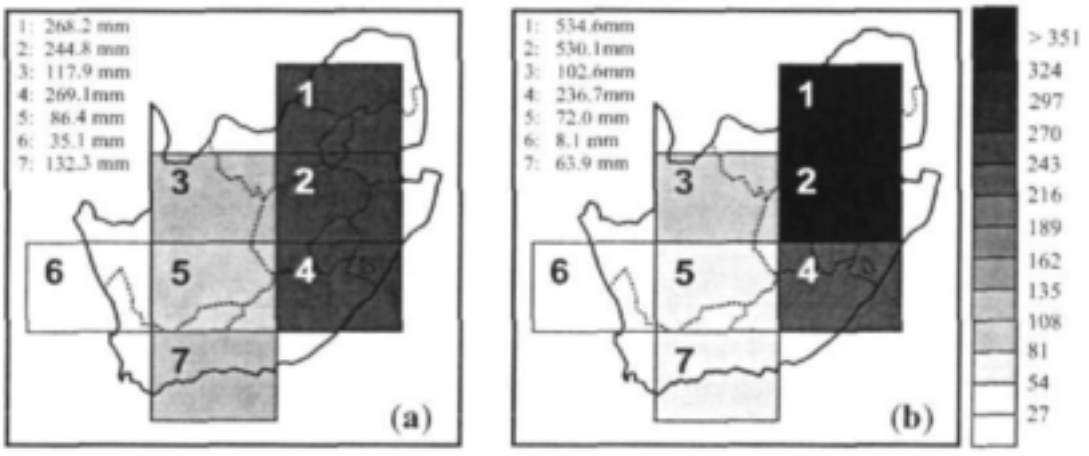

FIGURE 2.3 Median of (a) observed October, November, December (OND) rainfall and (b) CSIRO9(R21) AGCM simulated OND rainfall in mm/season. Observed and AGCM simulated (from prescribed SST simulations) rainfall medians have been calculated from an 18-year rainfall record (1982 to 1999).

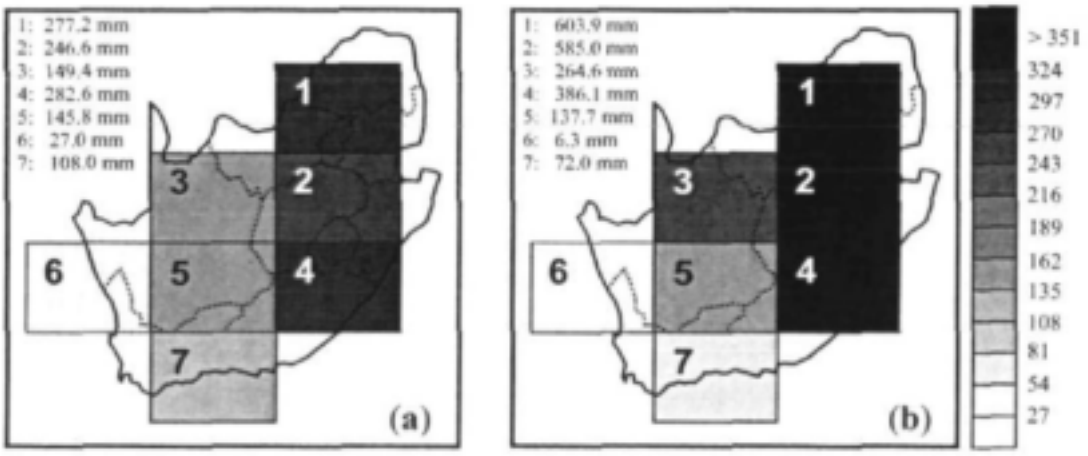

FIGURE 2.4 Median of (a) observed January, February, March (JFM) rainfall and (b) CSIRO9(R21) AGCM simulated JFM rainfall in mm/season. Observed and AGCM simulated (from prescribed SST simulations) rainfall medians have been calculated from an 18-year rainfall record (1982 to 1999).

2.3.2 CSIRO9(T63) AGCM simulated vs observed rainfall

During the development phase of the CGCM a comprehensive analysis was done on the dominant rainfall variability pattern of the CSIRO9(T63) AGCM. This AGCM serves as the atmospheric

component of the coupled model developed by the CSIRO Atmospheric Research in the CLIPWATER project.

The objective of this part of the study is to investigate the CSIRO9(T63) AGCM's response to some of the major global SST forcing that contributes to observed rainfall patterns over South Africa and Namibia. This will give an indication whether the model is suitable for use in seasonal forecasting research. Globally observed SSTs of a 30-year period (1961 to 1990) have been prescribed as boundary forcing for the AGCM. Since global SST forcing responsible for southern African rainfall variability is regarded as complex, only dominant rainfall patterns are considered.

2.3.2.1 SST data and hindcast simulations

The Hadley Centre of the United Kingdom Meteorological Office compiled, and is revising, global data for SSTs and sea-ice for the purpose of analysing climatic variations (Parker *et al.*, 1995; Folland and Rowell, 1995). An early version of this data (referred to as GISST1.1) comprises monthly mean SST values from 1871 to 1991. This data, interpolated to daily values, were prescribed as the lower boundary condition in a series of climate simulations as described by Smith *et al.* (1998) and Smith (1999).

Five separate 120-year long CSIRO9(T63) AGCM simulations were completed using the same SST forcing, each starting with different initial conditions. However, only results from a shorter period (1961 to 1990) are considered here as this period coincides with the period when the observed rainfall data used for verification are regarded as complete and reliable. For a given year and month, the AGCM simulated rainfall from each of the 5 simulations will differ because of the internal random variability introduced by the different initial conditions. When calculating the long-term average means, we average the results over 30 years and across the 5 simulations (sample size of 150). When dealing with a given year and month, we average the results across the 5 simulations (sample size of 5). These monthly values were then aggregated into summer (October to March) average values (sample size of 30), mid-summer (December to January) (sample size of 10) and winter (May to August) (sample size of 20). The effect of averaging across the ensemble is to reduce the noise due to chaos in the data and to better exhibit any underlying signals.

SST anomalies in the Niño1.2, Niño3, Niño3.4 and Niño4 regions (indicated by A, B, C and D in figure 2.14 which will be discussed in further detail later), were obtained from the June 1998 calculated monthly atmospheric and SST index values of the Climate Prediction Centre (CPC), Washington, USA. Niño4 SST anomalies are depicted by bar charts in figures 2.8 to 2.11. The report will focus on these figures in greater detail later. The ENSO classification proposed by Zhang (1997) is used in this study to distinguish between El Niño and La Niña events.

2.3.2.2 Observed rainfall data

Figure 2.5 shows that South Africa and Namibia are geographically located in the subtropical high-pressure zonal belt where the atmospheric circulation is governed by dry descending air. Arid regions such as the Namib Desert, Atakama desert as well as the Australian deserts all lie in the subtropics. During summer, however, contrasts in the horizontal temperature distribution result in relatively low surface pressure over continents compared to the oceans. These pressure features (subtropical troughs), in conjunction with mid-latitude westerly waves (cyclonic frontal systems) and tropical circulation perturbations (tropical lows and easterly waves), form the major driving forces behind moisture advection and finally summer rainfall over southern Africa (Hattle, 1968; Harrison, 1984; Tyson, 1986; Preston-Whyte and Tyson, 1993).

Observed rainfall data from 93 homogeneous rainfall districts over South Africa for the period 1961 to 1990 were acquired from the SAWS. In previous studies, the rainfall value allocated to each rainfall district in South Africa represented the area average of the measured rain gauge values over the given district (Harrison, 1984; van Heerden *et al.*, 1988). In this study, however, a rainfall value for a specific district has been calculated from rain gauge values weighted according to data point concentration distribution (Tennant ,1995: *personal communication*).

FIGURE 2.5 A map depicting the location of South Africa and Namibia. The grid points of the CSIRO9(T63) Atmospheric General Circulation Model (AGCM) are located at the centre of each shaded grid box. The rainfall value at each grid point represents the spatial average of the rainfall of the overlying grid box.

Weighted means were used to calculate a final rainfall value for each South African rainfall district. It was subsequently assumed that the rainfall value allocated to each one of the 93 rainfall districts is geographically located at the centre of the district. In addition to the South African rainfall district values, 96 complete rainfall records from point stations (rain gauges) were available for the period 1961 to 1990 from the Namibian Weather Service (Botha, 1997). These point stations are well distributed over the entire country. Finally, rainfall values at these positions (central points of rainfall districts over South Africa and rain gauge points over Namibia) were area averaged to obtain the rainfall for each model grid box over South Africa and

Namibia or southern Africa (depicted as shaded boxes in Figure 2.5). Grid boxes containing less than two rainfall observation points have been ignored.

Figure 2.6(a) shows average observed summer (October to March) rainfall (measured in millimetres per day) on the model grid. The pattern is characterised by a gradual increase in rainfall towards the eastern parts of the country.

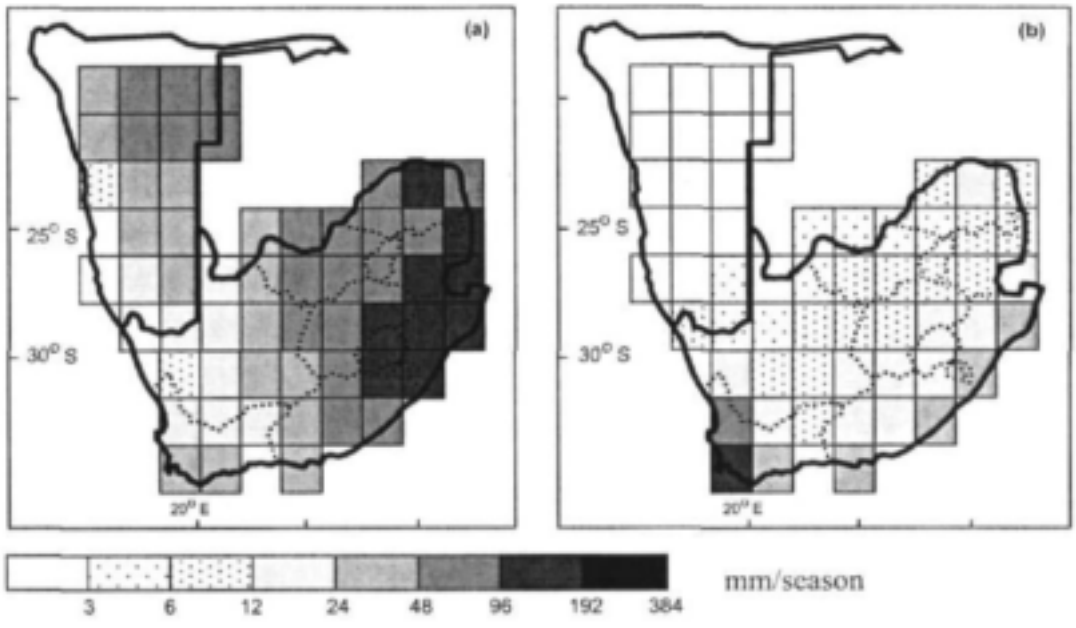

FIGURE 2.6 The observed rainfall climate for the (a) austral *summer* season (October to March) and (b) austral *winter* season (May to August) in millimetres per day over southern Africa.

During the same season, the northern part of Namibia receives more rain than the rest of the country, with the first significant rains appearing in January (Botha, 1997). Figure 2.6(b) shows average winter (May to August) rainfall that, unlike the summer rainfall, is confined to the south and southwestern coastline and the adjacent interior, and is almost entirely modulated by the eastward propagation of mid-latitude cyclonic frontal systems. Namibia receives little or no rain during this season. Both the summer and winter seasons exhibit high inter-annual variability.

2.3.2.3 Model simulated rainfall climate

Figures 2.7(a) and (b) show the long-term average (1961 to 1990) AGCM simulated rainfall for the summer (October to March) and winter (May to August) rainfall seasons respectively.

The AGCM adequately captures the general spatial distribution of higher and lower seasonal rainfall patterns for both the summer and winter seasons, but overestimates the mean summer rainfall for the entire South African region east of 20°E, as well as over the northeastern parts of Namibia. This agrees well with results previously obtained by Joubert (1997) in validation studies that involved the coarser resolution version (R21) of the AGCM as well as results from this report

(figures 2.1 to 2.4). The rainfall comparison for the western region, which receives little rain during the summer season, shows smaller differences with the AGCM simulated rainfall - even slightly lower than observed. The AGCM also overestimates winter rainfall for most grid points over southern Africa (figure 2.7(b)). The highest observed rainfall (figure 2.7(b)) for the winter season, however, occurs over the southwestern parts of the southern Africa region (West Cape province). It is important to note from figure 2.7(b) that the AGCM underestimates the mean seasonal rainfall over this part of the region.

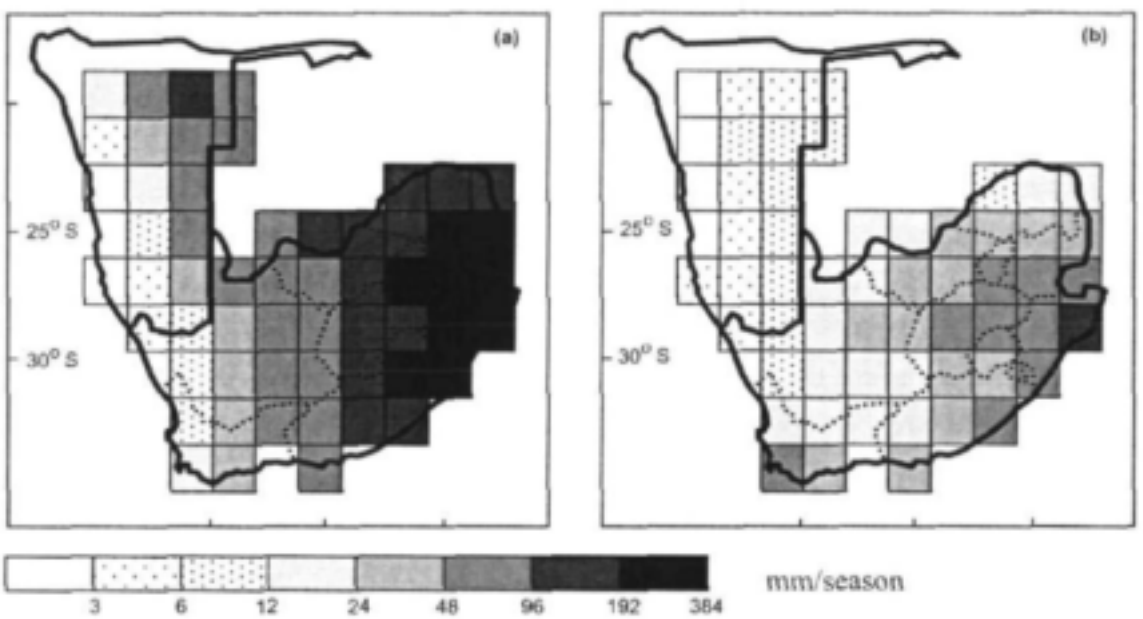

FIGURE 2.7 The AGCM simulated rainfall climate for the (a) austral *summer* season (October to March) and (b) austral *winter* season (May to August) in millimetres per day over southern Africa.

2.3.2.4 Statistical methods

Principal component (PC) analysis (Kachigan, 1991; Harrison, 1984), which represents unrotated eigenvectors of the covariance matrix, is applied to both the observed and AGCM simulated rainfall data on the spatial grid field depicted in figure 2.5. Detrended rainfall data for the summer season (October to March), mid-summer season (December and January) and winter season (May to August) for the 30-year period (1961 to 1990) are separately analysed. Detrending eliminates long-term changes in the rainfall and is essential when dealing with inter-seasonal rainfall fluctuations (Smith, 1994). The empirical orthogonal function (EOF) spatial patterns (also referred to as the PC patterns), with the associated amplitude time series, are calculated for each one of the three seasons. Due to the high percentage variance explained by the first observed rainfall PC and as a result of the complexity of SST-rainfall associations, we focus on the dominant rainfall (or PC1) patterns (figures 2.8 to 2.13).

In the search for SST-rainfall associations, correlation analyses are applied to compare rainfall PC1 patterns over southern Africa with the corresponding time series at each GISST grid point on the globe (figures 2.14 and 2.15). Standardised departures are used for comparisons, meaning that the anomaly for each data value in the rainfall PC and GISST time series is expressed in terms of

a fraction of the standard deviation. This allows for the correlation of data sets with diverse statistical features, and reduces the bias in data series with a high temporal variability. Correlation between the different seasonal rainfall PC1 patterns and the Niño4 SST anomalies are obtained by applying the same method.

The 1961-1990 summer and mid-summer rainfall PC1 time series have sample sizes of 29, while the 1961-1990 wintertime series has 30 values (figures 2.8 to 2.13). Significance levels for the different seasonal SST-rainfall comparisons (figures 2.14 and 2.15) are derived by a Monte Carlo approach, and levels greater than 95% are regarded as statistically significant.

2.3.2.5 Observed and model simulated rainfall (Summer season (October - March))

The observed summer rainfall PC1 pattern with the associated amplitude time series is illustrated in figure 2.8.

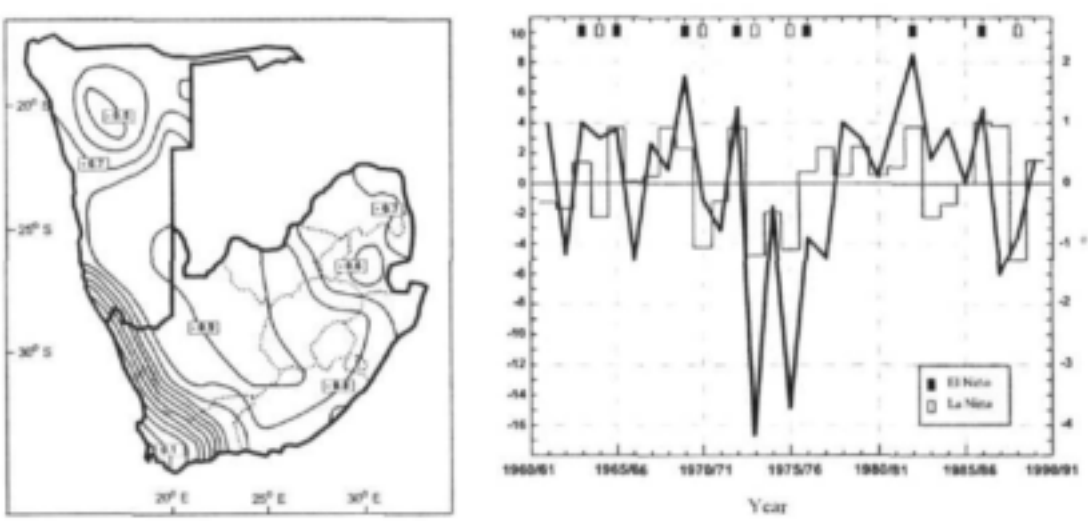

FIGURE 2.8 The first *observed* summer (October-March) rainfall principal component pattern (PC1) with the associated amplitude time series (1961-1990) for southern Africa. The pattern accounts for 54% of the total variance. The bar chart depicts the Niño4 Sea Surface Temperature (SST) variation in Kelvin. Because of negative spatial loadings the PC scores are inverted so that negative values indicate wet conditions.

This pattern accounts for 54% of the total variance, and corresponds well with the first January component revealed by Harrison (1984). The PC1 spatial pattern is characterised by a strong northwest to southeast trough located over the central continental part of southern Africa, with a steep gradient towards the southwest. Lindesay and Vogel (1990) and van Heerden *et al.* (1988) demonstrated that the area with the strongest spatial coherent correlation between the phase of the ENSO (in this case the Southern Oscillation Index or SOI) and observed summer rainfall also lies over the central continental part of southern Africa. The contours of these correlation patterns closely relate to those of the observed summer rainfall PC1 spatial pattern, indicating that the observed summer rainfall PC1 time series is strongly ENSO related. These results are confirmed by the strong relationship between the observed summer rainfall PC1 time series and SST anomalies over the central equatorial Pacific Ocean (Niño1.2, 3, 3.4 and 4 which are also regions

A, B, C and D respectively in figure 2.14). Linear correlation analyses (table 1) reveal significant coefficients (r = 0.48, 0.54, 0.56 and 0.57) between the observed summer rainfall PC1 time series and the Niño1.2, 3, 3.4 and 4 SST anomalies (r is significant at the 99% level if it exceeds 0.47). The strongest relation is with the Niño4 SST anomalies depicted by bars in figure 2.8. Figure 2.8 also indicates that six of the seven (86%) El Niño events coincided with below-normal summer rainfall, while above-normal summer rainfall has been experienced during four of the five (80%) La Niña events. The extremely wet summers during the 1973/74 and 1975/76 seasons, as well as the prevailing drier conditions during the early 1980s are well captured by the observed summer rainfall time series (figure 2.8).

TABLE 1

Correlation coefficients (r) between the observed rainfall first principal component (PC1) time series, CSIRO9(T63) AGCM rainfall PC1 time series of the ensemble mean and mean ensemble and the Niño1.2, 3, 3.4 and 4 SST anomalies (1961-1990) for the summer, mid-summer and winter seasons. The geographical location of the Niño1.2, 3, 3.4 and 4 SST regions are depicted as A, B, C and D in figure 10. The summer and mid-summer coefficients are all greater than the 99% significance level (r= 0.47), while low coefficients have been calculated for the winter.

1961 to 1990	SUMMER (October to March)	MID-SUMMER (December and January)	WINTER (May to August)
Niño12 *versus*			
Observed PC1	0.48	0.52	-0.16
Ensemble mean PC1	0.51	0.49	0.31
Mean ensemble PC1	0.47	0.47	0.27
Niño3 *versus*			
Observed PC1	0.54	0.61	-0.18
Ensemble mean PC1	0.64	0.52	0.20
Mean ensemble PC1	0.59	0.50	0.15
Niño 34 *versus*			
Observed PC1	0.56	0.65	-0.12
Ensemble mean PC1	0.72	0.55	0.21
Mean ensemble PC1	0.70	0.51	0.19
Niño 4 *versus*			
Observed PC1	0.57	0.68	0.01
Ensemble mean PC1	0.82	0.59	0.29
Mean ensemble PC1	0.79	0.55	0.26

Figure 2.9 illustrates the AGCM simulated summer rainfall PC1 pattern with its associated amplitude time series. The pattern accounts for 39% of the total variance and, as for the observed rainfall, the correlation of model simulated rainfall with the phase of the ENSO is strongest over the central continental parts of southern Africa.

Although less extreme than the observed rainfall, the wet conditions simulated during the 1973/74 and 1975/76 summer seasons are well captured by the PC1 amplitude time series (figure 2.9). Noticeable ENSO associations are also evident. Six of the seven (86%) El Niño events coincided with below-normal AGCM simulated summer rainfall while all (100%) the La Niña events were associated with above-normal AGCM simulated summer rainfall. Table 1 reveals that the AGCM simulated summer rainfall PC1 time series (constructed from the ensemble mean) was more strongly correlated than observed rainfall with the Niño1.2, 3, 3.4 and 4 SST anomalies (r = 0.5, 0.64, 0.72 and 0.82). The latter should be interpreted carefully since the ensemble mean has the

advantage over the observations of being less noisy. For this purpose mean ensemble correlations are additionally listed in table 1. These values are obviously slightly lower than the correlations for ensemble means, but still superior to correlations for observed rainfall. It is important to note that the PC1 time series of the model rainfall accounts for a smaller fraction of the total variance (54%) than the corresponding time series for observed rainfall (39%), implying that the higher correlations obtained from model results do not necessarily provide adequate information concerning model sensitivity as a result of SST forcing.

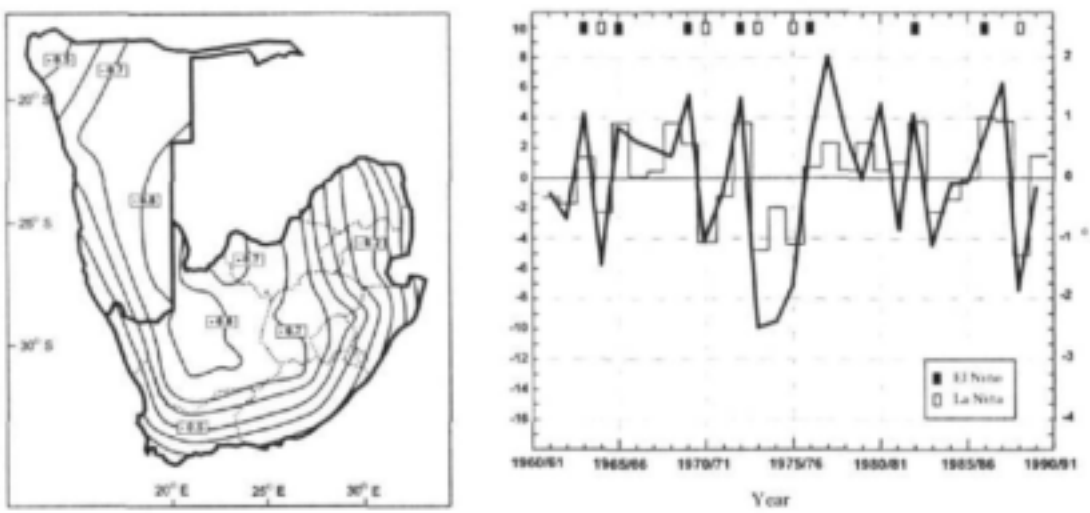

FIGURE 2.9 The first *AGCM simulated* summer (October-March) rainfall principal component pattern (PC1) with the associated amplitude time series (1961-1990) for southern Africa. The pattern accounts for 39% of the total variance. The bar chart depicts the Niño4 Sea Surface Temperature (SST) variation in Kelvin. Because of negative spatial loadings the PC scores are inverted so that negative values indicate wet conditions.

As a consequence of the lower percentage of variance, ENSO signals may also be present in other PCs of the model. It is, however, suggested that a large percentage of the model rainfall variability emanates from SST forcing over those global regions whose SSTs are observed to be associated with southern Africa's rainfall.

Note that the correlation coefficient (r = 0.49) between the observed and AGCM simulated summer rainfall PC1 amplitude time series is greater than the 99% significance level (table 2).

The second observed and AGCM simulated summer rainfall PC patterns, which respectively account for 9% and 16% of the total variance and are more obvious along the south and south-east coast line, correlates poorly (r = 0.22 in table 2). This is also applicable for the remaining higher PC patterns. It is, however, important to note that unless two PCs represent the same features of rainfall variability, and unless the percentage variance explained is sufficiently high, correlation analysis is not a definite way of identifying whether the AGCM captures the observed rainfall variability accurately.

TABLE 2

Correlation coefficients (r) between the CSIRO9(T63) AGCM and observed rainfall time series (1961 to 1990) for the first two principal components (PC1 and PC2). The coefficients are provided in terms of summer, mid-summer and winter seasons. The light and dark shaded cells denote significance greater than the 95% (r=0.37) and 99% (r=0.47) levels respectively.

1961 to 1990	SUMMER (October to March)	MID-SUMMER (December and January)	WINTER (May to August)
OBSERVED PC1 versus CSIRO-9 PC1 *(95% / 99%) significance level*	0.49 *(0.37 / 0.47)*	0.44 *(0.37 / 0.47)*	0.05 *(0.36 / 0.46)*
OBSERVED PC2 versus CSIRO-9 PC2 *(95% / 99%) significance level*	0.22 *(0.37 / 0.47)*	-0.06 *(0.37 / 0.47)*	0.12 *(0.36 / 0.46)*

2.3.2.6 Observed and model simulated rainfall (Mid-summer season (December and January))

Sufficient rainfall during the months December and January (mid-summer) is of vital importance for agricultural purposes in southern Africa, and therefore the rainfall frequency for these two months is investigated separately.

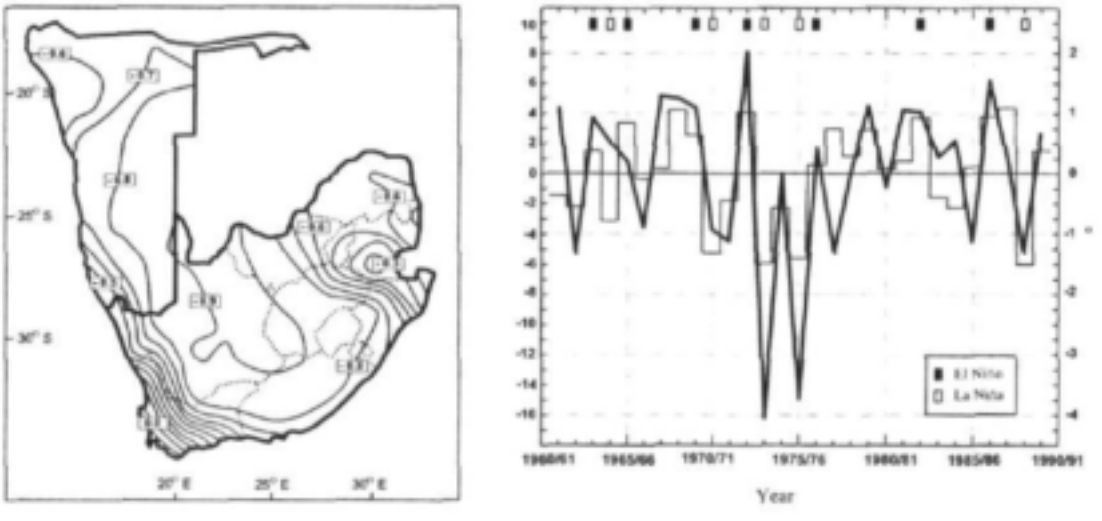

FIGURE 2.10 The first *observed* mid-summer (December, January) rainfall principal component pattern (PC1) with the associated amplitude time series (1961-1990) for southern Africa. The pattern accounts for 54 % of the total variance. The bar chart depicts the Niño4 Sea Surface Temperature (SST) variation in Kelvin. Because of negative spatial loadings the PC scores are inverted so that negative values indicate wet conditions.

The observed mid-summer rainfall PC1 pattern with the associated amplitude time series (figure 2.10) accounts for 54% of the total variance. Similar to the summer rainfall pattern, the spatial observed mid-summer rainfall PC1 pattern is characterized by a distinctive northwest to southeast ENSO related trough over the southern African interior.

Table 1 indicates significant correlation coefficients (r = 0.52, 0.61, 0.65 and 0.68) between the Niño1.2, 3, 3.4 and 4 SST anomalies and the observed mid-summer rainfall PC1 amplitude time series. These coefficients are stronger than calculated for the summer season. All the coefficients are equal or greater than the 99% significance level (r = 0.47). The Niño4 SST anomalies, which correlate the strongest, are expressed in terms of bar charts in figure 2.10. The strong ENSO associations are emphasized by the 100% (80%) of the El Niño/La Niña events that coincided with below-normal/above-normal rainfall (figure 2.10).

The spatial distribution and amplitude time series of the AGCM simulated mid-summer PC1 pattern is depicted in figure 2.11. A percentage of 29% of the total variance is explained by this pattern. This pattern is, in accordance with previous patterns, centred over the central continental part of southern Africa, but gradients towards the coast are noticeably stronger than found in the PC analysis of observed rainfall (figure 2.10).

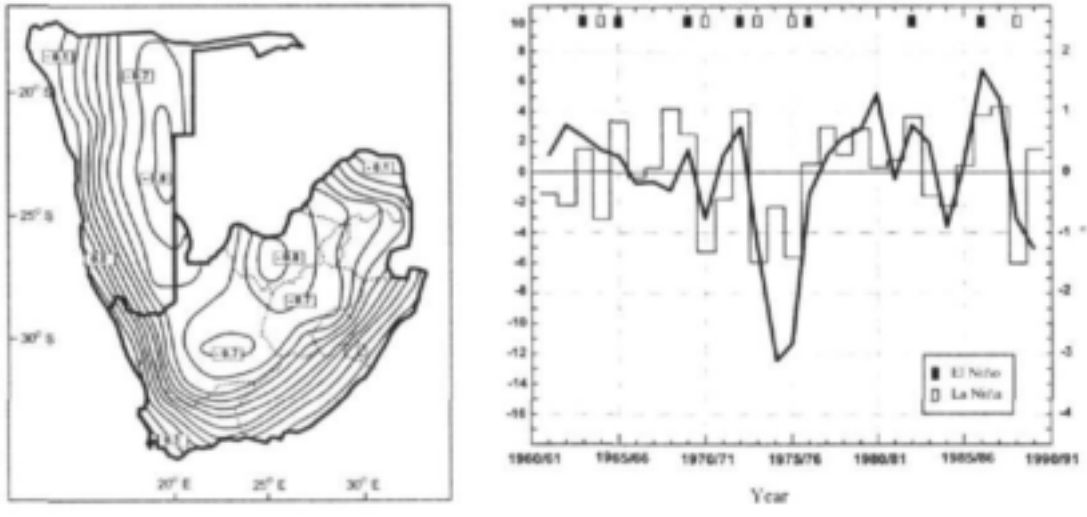

FIGURE 2.11 The first *AGCM simulated* mid-summer (December, January) rainfall principal component pattern (PC1) with the associated amplitude time series (1961-1990) for southern Africa. The pattern accounts for 29 % of the total variance. The bar chart depicts the Niño4 Sea Surface Temperature (SST) variation in Kelvin. Because of negative spatial loadings the PC scores are inverted so that negative values indicate wet conditions.

Unlike the summer pattern, equatorial Pacific Ocean SSTs relate less strongly to the AGCM simulated rainfall PC1 pattern than to the observed rainfall PC1 pattern (table 1). This could indicate that the AGCM simulations have a longer season of strong ENSO influence than the observations. Coefficients, however, are still in excess of the 99% significance level (r = 0.49, 0.52, 0.55 and 0.59 for the Niño1.2, 3, 3.4 and 4 regions respectively). The El Niño (La Niña)

events coinciding with below-normal (above-normal) rainfall are identical to those found in the observed mid-summer analysis.

The correlation (r = 0.44) between the observed and AGCM simulated mid-summer rainfall PC1 time series is slightly weaker than the corresponding summer correlation (Table 2), but still falls between the 95% and 99% significance level. The weaker correlation may be partly because of the fact that the two PC1 time series do not quite represent the same features of rainfall variability. It may also be possible that the ENSO signal is apparent in more than one rainfall PC in the model. Comparisons were found to be insignificant for the remaining higher mid-summer rainfall PC patterns.

2.3.2.7 Observed and model simulated rainfall (Winter season (May - August))

The observed and AGCM simulated winter rainfall PC1 patterns are illustrated in figures 2.12 and 2.13. The two patterns respectively account for 36% and 55% of the total rainfall variance and are both spatially most obvious over the central interior of southern Africa.

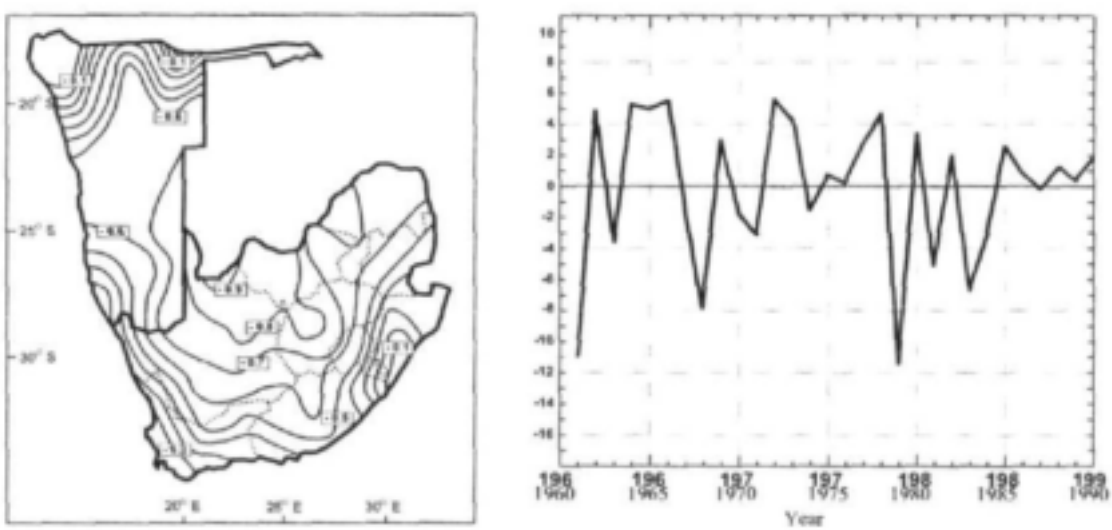

FIGURE 2.12. The first *observed* winter (May-August) rainfall principal component pattern (PC1) with the associated amplitude time series (1961-1990) for southern Africa. The pattern accounts for 36 % of the total variance. Because of negative spatial loadings the PC scores are inverted so that negative values indicate wet conditions.

Very little precipitation occurs over this region during winter months since the winter rainfall region is geographically located over the southwestern part of the analysis region. Relatively low correlation coefficients (r = 0.05 and 0.12) between the observed and AGCM winter rainfall PC1 and PC2 amplitude time series are shown in table 2. Table 1 confirms the well-known fact that the winter rainfall variability over southern Africa corresponds poorly with global SST perturbations in the equatorial Pacific Ocean. No further analyses in terms of seasonal forecasting will be done for winter rainfall, since the coarser resolution CSIRO9(R21) AGCM produces similarly poor model simulations.

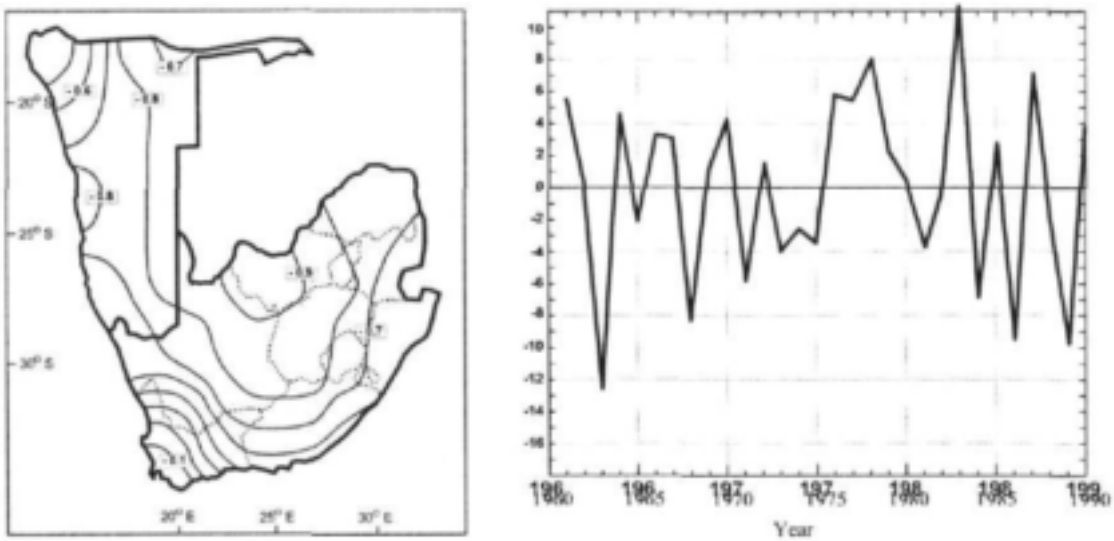

FIGURE 2.13 The first *AGCM simulated* winter (May-August) rainfall principal component pattern (PC1) with the associated amplitude time series (1961-1990) for southern Africa. The pattern accounts for 55 % of the total variance. Because of negative spatial loadings the PC scores are inverted so that negative values indicate wet conditions.

2.3.2.8 Global sea surface temperature correlation patterns

The dominant (PC1) summer season amplitude time series (1961 to 1990) for the observed and AGCM simulated rainfall patterns over southern Africa are compared with the temporal SST variability at each global GISST grid point (figures 2.14 and 2.15). The spatial correlation is significant at the 95% and 99% levels if the value of r exceeds 0.37 and 0.47 respectively.

Summer season (October - March)

Spatial correlation patterns between global GISST data and temporal PC1 summer rainfall variability (observed and AGCM simulated) are depicted by figures 2.14 and 2.15 respectively.

Shaded areas reflect the 99% significance level. Since ensemble averages are often used to produce standard model output in seasonal forecasting experiments, correlation patterns of the individual ensemble members have not been determined. The most significant positive spatial correlation patterns ($r > 0.6$ and 0.8 for the observed and AGCM simulated summer rainfall PC1 amplitude time series respectively) occur over the central equatorial Pacific Ocean. These values are considerably higher than the 99% significance level. The high correlation patterns derived from the AGCM simulated analysis ($r > 0.8$ in figure 2.15) indicate that the AGCM overemphasised the effect of ocean thermal fluxes from the Pacific Ocean on the leading summer rainfall pattern (PC1 pattern) over southern Africa. These results correspond well with the notably stronger SST-rainfall links earlier identified (table 1) between the CPC derived SST anomalies in the Niño1.2, 3, 3.4 and 4 regions and AGCM simulated summer rainfall PC1 amplitude time series over southern Africa.

No statistically significant links appear between the observed summer rainfall PC1 pattern and the SST variability over the southern Atlantic Ocean (figure 2.14). As for the Pacific Ocean analysis, AGCM simulated rainfall-SST links ($r < -0.4$ in the south and $r > 0.4$ in the north) are over emphasised in certain regions of the Atlantic Ocean (figure 2.15).

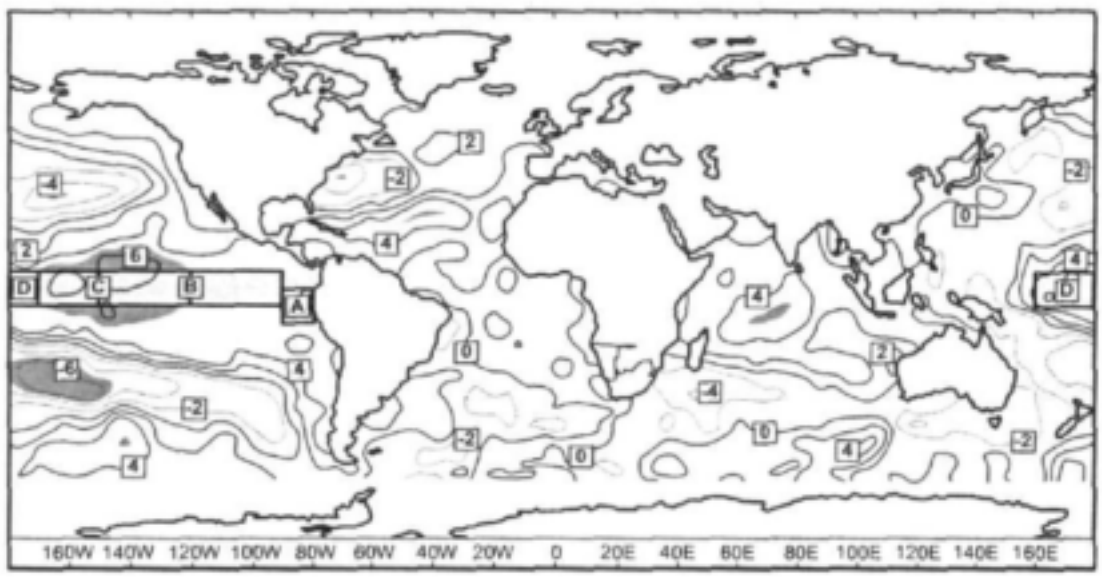

FIGURE 2.14. Correlation coefficients (r x 10) between the *observed* summer (October-March) rainfall PC1 time series (Figure 2.8) over southern Africa and global observed sea-surface temperatures (SSTs). Solid and dashed lines denote positive and negative values respectively. Spatially coherent correlations with values higher than the 99% significance level (0.47) are shaded. The symbols A, B, C and D denote the geographical location the Niño1.2 (0°-5°S)(90 °-80°W), Niño3 (5°N-5°S)(150°-90°W), Niño3.4 (5°N-5°S)(170°-120°W) and Niño4 (5°N-5°S)(160E °-150°W) regions respectively.

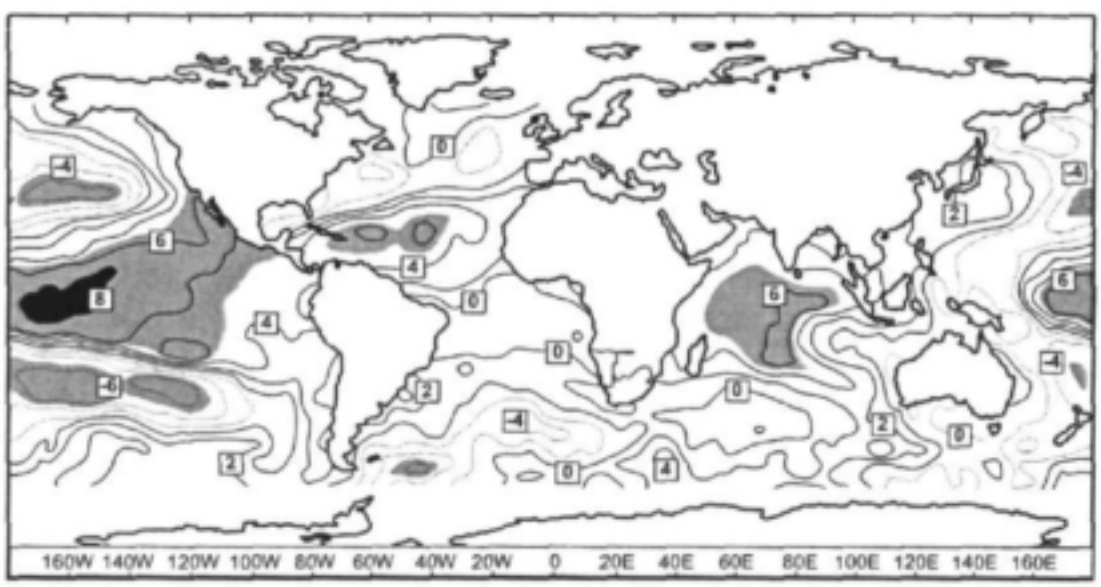

FIGURE 2.15 Correlation coefficients (r x 10) between the *AGCM simulated* summer (October-March) rainfall PC1 time series (Figure 2.9) over southern Africa and global observed sea-surface temperatures (SSTs). Solid and dashed lines denote positive and negative values respectively. Spatially coherent correlations with values higher than the 99% significance level (0.47) are shaded.

The observed difference in sign between SST correlation patterns in the south-western (Reason and Mulenga, 1999) and central equatorial parts (at approximately 10° south) of the Indian Ocean is well depicted in Figure 2.14 (Walker,1990; Jury and Pathack,1993). This involves statistically significant positive correlations ($r > 0.4$; greater than the 95% significance level) over the central equatorial Indian Ocean, and negative correlations ($r < -0.4$) over the ocean to the southeast of southern Africa. AGCM related patterns indicate that the core of positive and negative correlation fields are located eastwards in relation with observed patterns (figure 2.15). Here, the ocean region with stronger negative anomalies does not appear to the east of South Africa.

2.3.2.9 Discussion

The study focuses on the response of the atmosphere, and in particular rainfall over South Africa and Namibia (or southern Africa), to globally observed SST boundary forcing for the period 1961 to 1990.

Comparisons between global SST and observed rainfall variability are in accordance with associations obtained from previous studies. On the global scale, these comparisons indicate that above-normal/below-normal austral summer rainfall usually coincides with La Niña/El Niño events (Ropelewski and Halpert, 1987) as well as cold/warm SSTs over the tropical western Indian Ocean (Jury et al., 1996 and Tennant 1996). Landman and Mason (1999), however, demonstrated that the latter association was more profound prior to the late-1970s, and that warm (cold) events in the tropical western Indian Ocean are, at present, more frequently associated with above-normal (below-normal) rainfall conditions over southern Africa. Regional SST anomalies to the southeast of South Africa also appear to be related to South African rainfall fluctuations (Reason and Mulenga, 1999). Walker (1990), Jury and Pathack (1993) and Mason (1995) have also revealed other regional teleconnections.

The CSIRO-9 (Mark II) AGCM with a T63 spectral resolution (McGregor *et al.*, 1993) has been forced with global monthly-observed SST anomalies (1961 to 1990). The AGCM's rainfall response to this imposed SST forcing has been examined over southern Africa by means of PC analysis. Global ocean correlation patterns have subsequently been constructed for the dominant (PC1) AGCM simulated and observed rainfall variability.

Strong signals in the rainfall PC1 spatial patterns have been characterised by a distinctive northwest to southeast trough over the continental parts of the region under investigation. This applies to the observed as well as AGCM simulated summer, mid-summer and winter rainfall variability, and corresponds well with an area exhibiting the strongest spatial coherent correlations between the ENSO and summer (also mid-summer) rainfall over southern Africa (van Heerden *et al.* 1988; Lindesay and Vogel, 1990). Since the major winter rainfall region is located to the southwest of the area under investigation, little rain occurs over the region with stronger PC1 signals during winter months. Both the observed summer and mid-summer rainfall PC1 patterns account for 54% of the total variance, while only 39% and 29% of the total variance is accounted for in the corresponding AGCM patterns. These percentages (39% and 29% respectively) are not only smaller, but also more dispersed in the associated AGCM patterns. It is therefore likely that the observed and AGCM rainfall PC1 patterns do not represent the same features of summer rainfall variability.

As illustrated by the associated PC1 amplitude time series, some of the most extreme observed summer rainfall anomalies, such as the wet conditions that occurred during the 1973/74 and 1975/76 seasons, are to some extent captured in the AGCM simulations. Even though the PC1 patterns of observed and AGCM simulated summer rainfall might not necessarily represent the

same rainfall variability features, large correlations still exist between the two amplitude time series (table 2). Both these amplitude time series are also strongly ENSO related (table 1), as indicated by statistically significant and spatially coherent correlation patterns over the equatorial Pacific and Indian Oceans (figures 2.14 and 2.15). Here, correlation patterns of the AGCM amplitude time series are noticeably stronger than those calculated for the observed time series. With this in mind, and since the percentage of the total variance accounted for by the AGCM simulated summer rainfall PC1 pattern is noticeably lower than for the observed, it is possible that these ocean signals are also apparent in the remaining higher AGCM PCs. Unlike the summer patterns, winter rainfall variability corresponds poorly with global SST perturbations.

Despite differences in the percentage variability of the dominant (PC1) observed and AGCM simulated summer rainfall patterns, it is postulated the CSIRO9(T63) AGCM seems capable of capturing at least some of the important observed remote signals from the global equatorial oceans (ENSO and tropical Indian Ocean).

The model may therefore be regarded as suitable for future use in seasonal rainfall forecasting research, either in atmosphere-ocean coupled mode or with forecast SSTs imposed as boundary forcing. Probabilistic rainfall projections might be of significant value for hydrological planning and water resource management.

CHAPTER 3

CSIRO9(R21) AGCM RAINFALL PROJECTIONS FROM STATISTICAL SST FORECASTS

3.1 INTRODUCTION

In this chapter a two-phase forecasting procedure (figure 1.1) using the CSIRO9(R21) AGCM is employed in a first attempt to retrospectively forecast rainfall for a early-summer (OND 1998) and late-summer (JFM 1999) season. Tropical SST anomalies over the Indian, Atlantic and Pacific Oceans were firstly predicted using an empirical technique namely CCA (Landman and Mason, 2001), whereafter these anomalies were prescribed as ocean boundary forcing for the AGCM simulations (in CHAPTER 5 forecast SSTs produced by the COCA CGCM will be prescribed as boundary forcing).

To achieve this rainfall regions were defined according to model grid box resolution and observed station data were area averaged for the two seasons under consideration. Three separate twelve-month AGCM forecast simulations, each initiated from a different month (January, June and August 1998) were completed for the 1989/99 summer season. Based on a 12-year hindcast simulation forced with observed SSTs (1985 to 1996), rainfall probability distributions for the early-summer and late-summer seasons were constructed in order to establish categories of below-normal (BN), near-normal (NN) and above-normal (AN) rainfall. AGCM simulated forecasts were validated by comparisons with observed fields using a straightforward hit-score approach.

3.2 RAINFALL REGIONS

To begin with, seven regular model grid boxes that cover South Africa (G1 to G7 in figure 3.1(a)) were used as the basic rainfall regions for South Africa. Since it is recommended that area averages over more than one grid box are considered when analysing numerical forecasts, a composite of four model grid boxes was defined to form a central continental region (A1 in figure 3.1(b)), and a composite of the seven model grid boxes to form one region (SA) that covers most of South Africa (figure 3.1(c)).

Region A1 (a composite of grid boxes G2, G3, G4 and G5) represents the best fit of the area containing the leading (first) observed summer (October to March) rainfall PC pattern (figure 2.8). The relatively higher summer rainfall experienced over the northeastern interior is included in grid box G1. Rainfall patterns in regions G7 and G6 have diverse characteristics. Region or grid box G6 covers a semi-arid winter rainfall (May to August) region, while most parts of region or grid box G7 receive rain throughout most of the year.

One model grid box has a dimension of approximately 180 km x 317 km at latitude 30^{O} south (R21 spectral resolution of the CSIRO9 AGCM as discussed in SECTION 2.2.1).

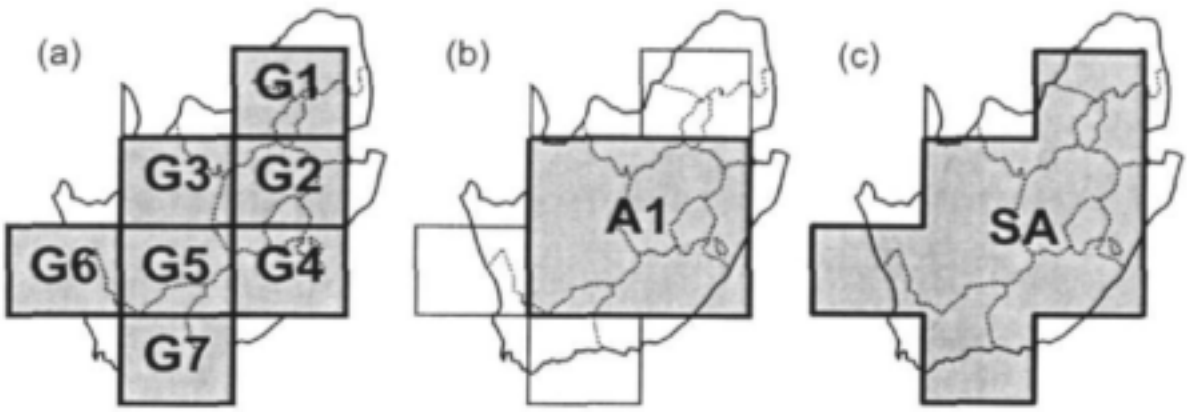

FIGURE 3.1 Spatial regions used in the forecast analyses namely (a) seven separate model grid boxes (G1 to G7), (b) a composite of four model grid boxes to form a central continental region (A1) and (c) a composite of seven model grid boxes to form one region (SA) that covers most parts of South Africa.

3.3 GRID AVERAGES OF RAINFALL

Model grid points are located at the centre of each grid box. Each observed grid point value represents the non-weighted spatial mean of the climatic variable considered in the appropriate grid box. Observed rainfall values for grid boxes in figure 3.1(a) were obtained by calculating area averages from observed continental rainfall stations alone. In model grid boxes where the ocean forms part of the grid box area (figure 3.2), it was assumed that the average rainfall over the land fraction represents the total grid average rainfall.

FIGURE 3.2 Area averages of observed rainfall calculated from land rainfall records alone (grey areas). In model grid boxes where the ocean forms part of the grid box area, it was assumed that the average rainfall over the land fraction represents the total grid average rainfall.

Observed monthly averaged rainfall has been obtained from the SAWS. The approximate number (missing data occurred in some of the most recent months) of rainfall stations (observed data points) used in each grid box area is listed in Table 3.

TABLE 3
Number of rainfall stations (observed data points) used per model grid box for boxes G1 to G7 in figure 3.1(a) for calculating area averages.

Region	G1	G2	G3	G4	G5	G6	G7
Number of rainfall stations	261	369	135	312	198	30	111

The climate of CSIRO9(R21) AGCM simulated rainfall for the OND and JFM seasons has been verified against observed fields in SECTION 2.3.1 (Maps in figures 2.1 to 2.4)

3.4 SEA SURFACE TEMPERATURE PROGNOSES

Three-month averaged CCA predicted SST anomalies, issued on a monthly basis by the Research Group for Statistical Studies (RGSCS) at the SAWS (Landman and Mason, 2001), were prescribed as model ocean boundary forcing for a period of nine months in advance.

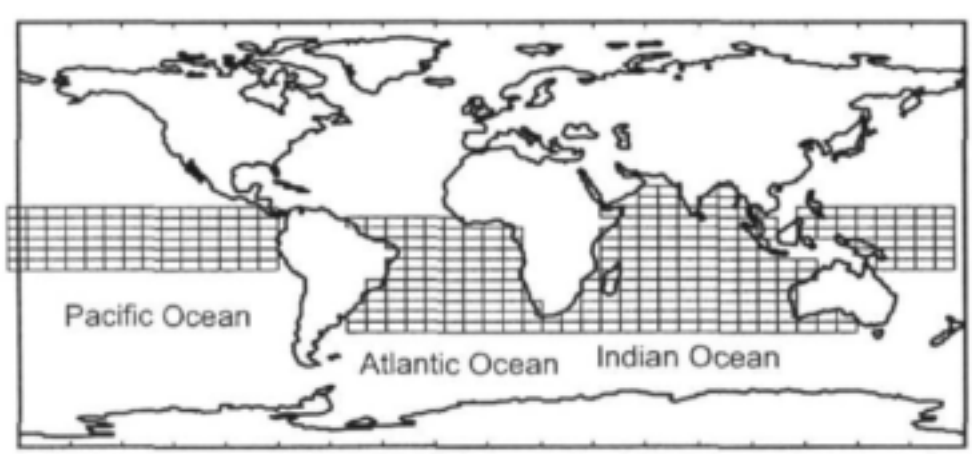

FIGURE 3.3 Spatial distribution of the SST anomaly grid used as AGCM boundary input during rainfall forecast simulations.

As indicated by figure 3.3, SST anomalies are generally forecast for lower (equatorial) latitudes covering the Pacific, Atlantic and Indian Oceans. A point of concern is that the CCA SST fields have a much coarser resolution (4° by 6° spatial resolution) than that of the CSIRO9(R21) AGCM meaning that relatively smoothed SST were forecast.

Examples of average CCA SST anomaly forecasts issued during May 1998 for July, August, September (JAS) 1998 and October, November, December (OND) 1998 are illustrated in figures 3.4 and 3.5. The CCA model indicated that the ENSO was entering a cold phase, which was in

agreement with observed trends during the 1998/1999 summer season. Note that the CCA forecast cold ENSO event was somewhat milder than observed. These SST anomaly forecasts (and updated fields) were used to produce the numerical rainfall projections discussed later in this chapter.

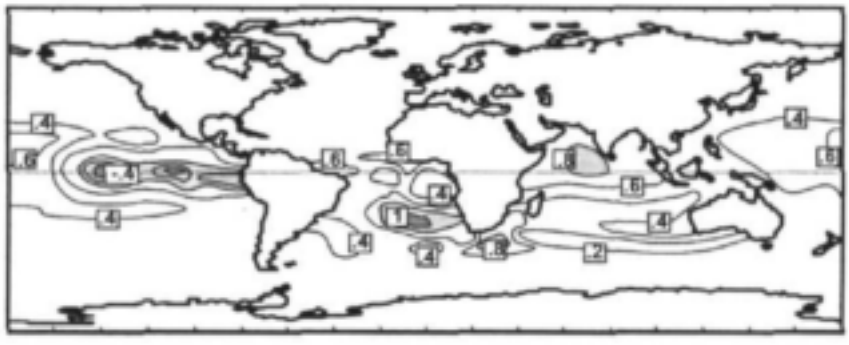

FIGURE 3.4 Canonical Correlation Analysis (CCA) Sea Surface Temperature (SST) anomaly forecast issued during May 1998 for the July, August, September (JAS) 1998 season

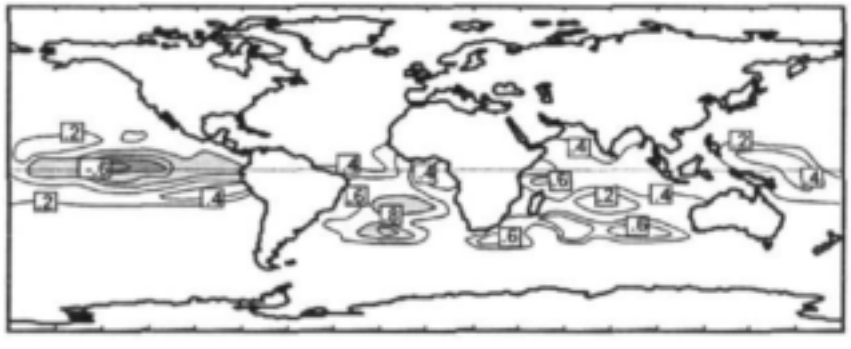

FIGURE 3.5 Canonical Correlation Analysis (CCA) Sea Surface Temperature (SST) anomaly forecast issued during May 1998 for the October, November, December (OND) 1998 season

3.5 RAINFALL FORECASTING PROCEDURE

Rainfall forecasts were prepared for regions G1, G6, G7, A1 and SA (figure 3.1). Three 12-month AGCM forecast simulations with prescribed SST anomalies (figure 3.6) were completed. The first simulation was initiated from January 1998 while the second and third started from April and July 1998, respectively. Rainfall forecasts from each simulation represent the average of five ensemble members. In the first simulation, globally observed SST anomalies (shaded boxes in figure 3.6) were imposed for the first three months (January, February and March) while three month averaged CCA predicted SST anomalies (white boxes in figure 3.6) were prescribed for the remaining nine months (April, May, June; July, August, September; October, November, December) over the region indicated in figure 3.3. A similar procedure was followed in the second and third AGCM simulations.

Results from three/two forecast runs are therefore available to calculate rainfall forecasts for the OND1998/JFM1999 seasons (figure 3.6). Weights, according to three-month average time lags, were allocated to the forecast rainfall totals before seasonal averages were calculated.

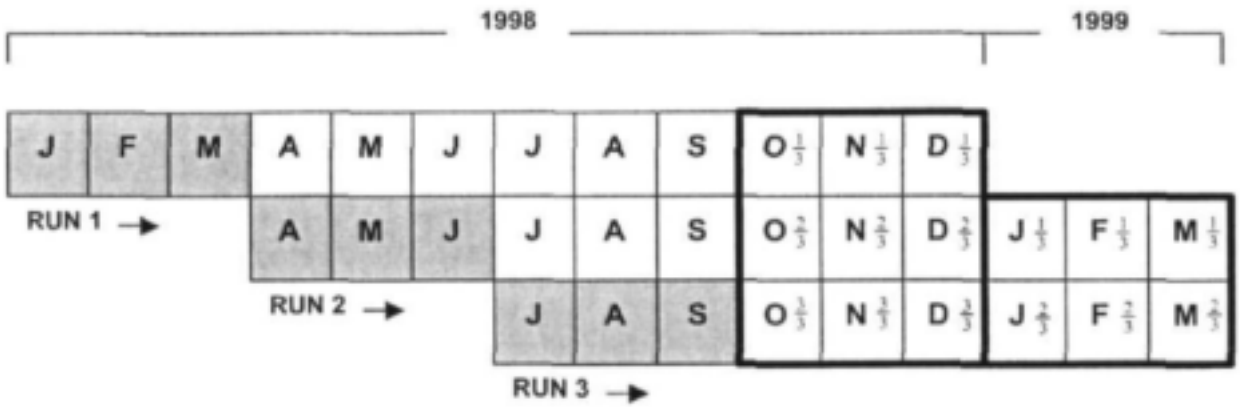

FIGURE 3.6 Three separate twelve-month AGCM rainfall forecast simulations, each initiated from a different month (namely January, April and June 1998), and each representing a five-member ensemble mean, have been compiled. Monthly Sea Surface Temperature (SST) anomalies were prescribed as ocean boundary forcing. Shaded/unshaded months denote observed/predicted SSTs. Forecasted SSTs were issued as three-month averages. Weights of 1/3, 2/3 and 3/3 were applied to rainfall forecasts with 3, 2 and 1 month lead times, respectively in the forecast seasons (October, November, December (OND) 1998 and January, February, March (JFM) 1999).

Apart from rainfall forecast simulations, five rainfall simulations (five ensemble members) were generated for evaluation against observed rainfall. During these simulations, observed SST anomalies from 1985 to 1996 (12-years) were imposed as ocean boundary forcing over grid areas G1, G6, G7, A1 (depicted in figure 3.1). Five-member ensemble means of model-simulated rainfall were calculated for the four AGCM rainfall regions over South Africa. In each one of the regions, monthly simulated rainfall was ranked to obtain tercile values. The ranked rainfall data series was classified into three categories namely rainfall smaller than *tercile 1* (BN), rainfall between *tercile 1* and *tercile 2* (NN) and rainfall greater than *tercile 2* (AN). The AGCM rainfall time series for each month comprises 12 values (1985 to 1996) implying that only four values were available per tercile category for rainfall verification.

Monthly area averaged observed rainfall (1985 to 1996) was also calculated for each one of the four rainfall regions (G1, G6, G7, A1), and similar to model simulations, categorized in terms of terciles. These results were used to determine the percentage probability for BN, NN or AN AGCM-simulated rainfall to appear over a given region.

3.6 HINDCAST SIMULATIONS AND MODEL SKILL

The AGCM's ability in reproducing monthly rainfall for each one of the rainfall regions (G1, G6, G7, A1 in figure 3.1), as well as for South Africa in total (region SA in figure 3.1(c)), is expressed in terms of the percentage of months in which model simulated rainfall (from the 12-year hindcast simulation) falls in the same category (AN, NN, BN) as the observed rainfall (figure 3.7). This is based on a simple hit rate score approach where the model scores one point when the observed and model-simulated rainfall falls in the same category, and zero points when rainfall categories differ. The number of points scored out of 12 (the total number of hindcasts) is expressed as a percentage that gives an indication of model performance (or skill) relative to what has been observed. A similar hit rate score will be used in the final CGCM forecasts discussed in CHAPTER 5. In figure 3.7, the points scored in the 12 months are expressed in terms of percentages. Scores lower than 33.3% may be attributed to chance (random forecasts), while hit

rate scores greater than 33.3% may indicate that a certain degree of skill exists in the ability of the AGCM to forecast rainfall.

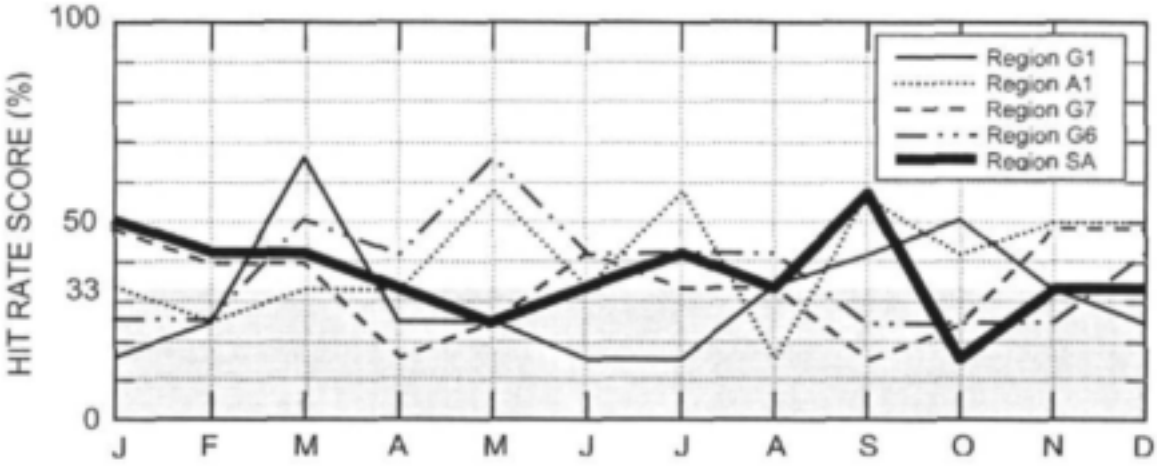

FIGURE 3.7 Percentage of months (from the 12-year hindcast) where the model simulated and observed rainfall fell in the same category (hits). Categories are in terms of terciles indicating above-normal (AN), near-normal (NN) and below-normal (BN) rainfall.

3.7 RAINFALL FORECASTS (1998/1999)

3.7.1 ACCUMULATED RAINFALL VERIFICATION

Figures 3.8(a), 3.8(b), 3.8(c), 3.8(d) and 3.8(e) depict time series of the accumulated numerical-forecast monthly rainfall compared with the corresponding observed series for the OND 1998 and JFM 1999 seasons over the four rainfall regions as defined in figure 3.1. Time series for regions G1, G6, G7 and A1as well as for South Africa in total (region SA) are provided. Thin lines in the figures also illustrate rainfall projections by the separate ensemble members. The range of the NN categories is shown by vertical thick black and shaded bars for the observed and AGCM simulated (forecast) rainfall, respectively.

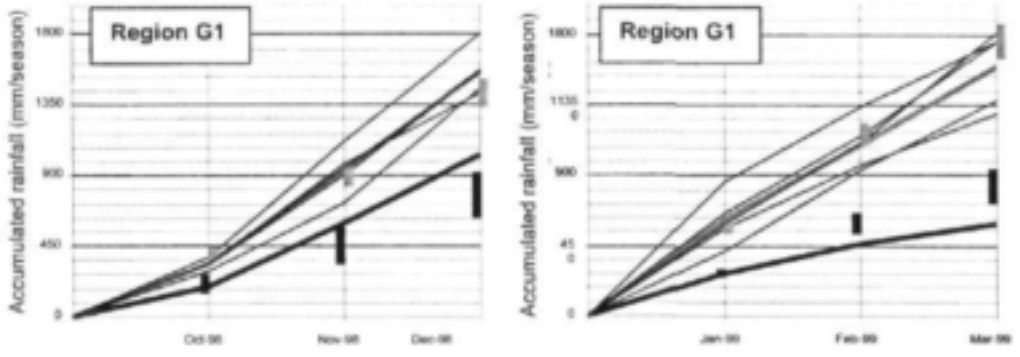

FIGURE 3. 8(a) Accumulated monthly observed rainfall (thick black line), forecast rainfall (shaded line) and the five ensemble members (thin black lines), measured in mm/season, for the OND 1998 and JFM 1999 seasons over region G1. Vertical thick black and shaded bars depict the near-normal (NN) category for the observed and AGCM simulated (forecast) rainfall respectively.

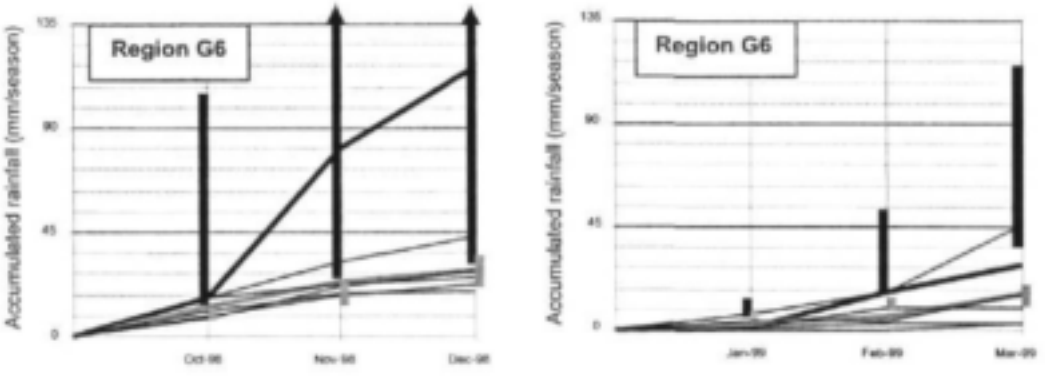

FIGURE 3. 8(b) As figure 3.8(a) but for region G6

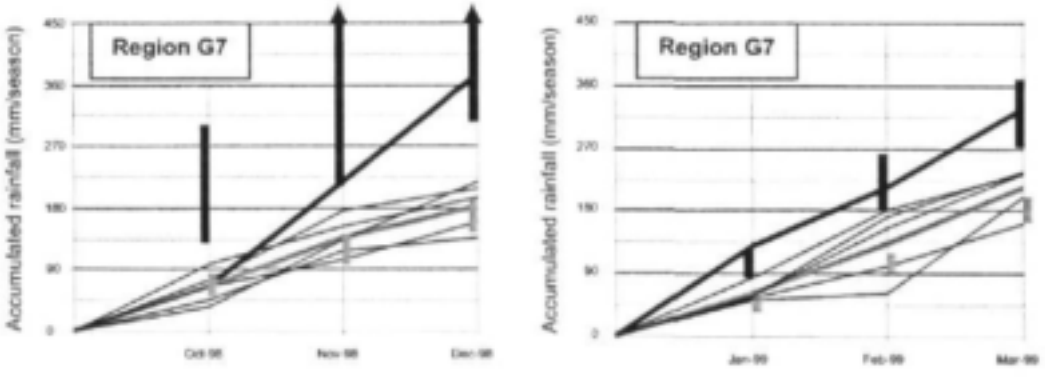

FIGURE 3. 8(c) As figure 3.8(a) but for region G7

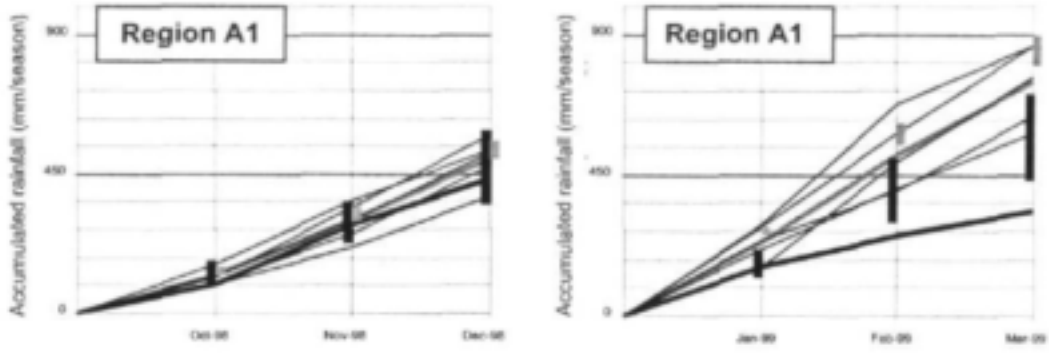

FIGURE 3. 8(d) As figure 3.8(a) but for region A1

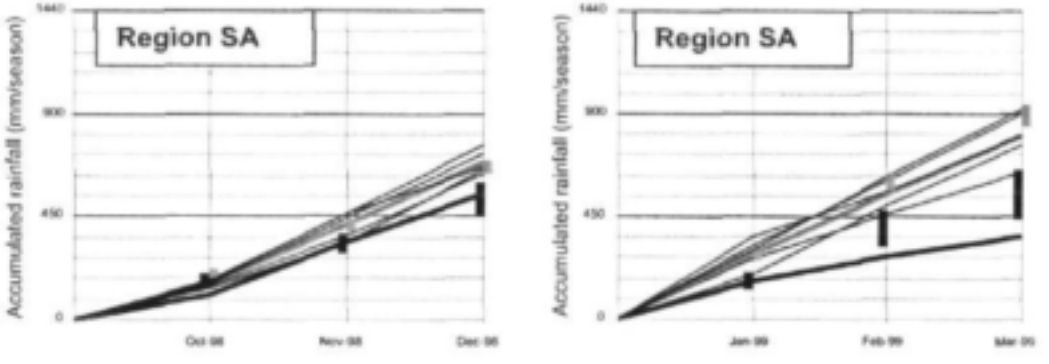

FIGURE 3. 8(e) As figure 3.8(a) but for region SA

3.7.2 SPATIAL RAINFALL VERIFICATION

Categorical probabilistic forecasts expressed in percentages of rain occurring in the AN, NN and BN categories, as well as the associated categories (AN, NN, BN) of observed rainfall for the OND 1998 and JFM 1999 seasons, are depicted in figures 3.9(a) and 3.9(b). These forecasts are for regions G1, G6, G7 and A1 (as defined in figure 3.1) and might differ from the almost deterministic categorical forecasts given in figures 3.8(a) to 3.8 (e).

If the model simulates rainfall in the AN category, it does not necessarily means that AN rainfall was actually observed – the percentage probabilities might show that NN or BN rainfall might have occurred historically.

The probabilistic forecasts in figures 3.9(a) and 3.9(b) depend upon the AGCM's skill (figure 3.7). It is strongly recommended that a measure of skill (based upon hindcast simulations) be allocated to any probabilistic numerical forecast. This measure of skill is embedded in the percentage probabilities indicated in figures 3.9(a) and 3.9(b).

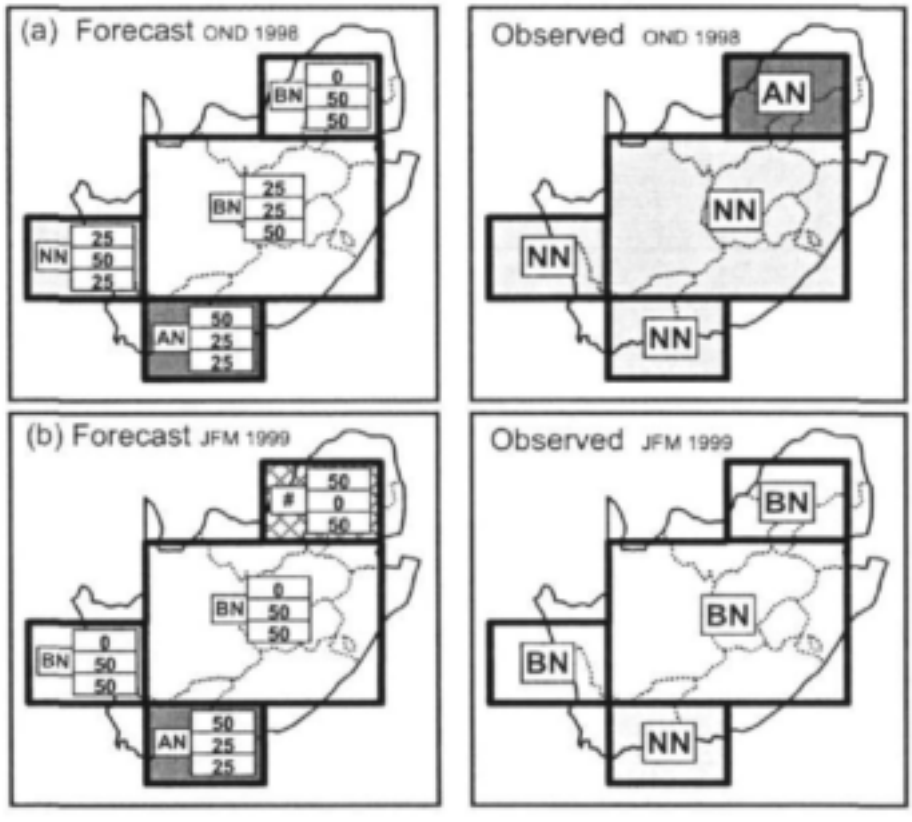

FIGURE 3.9 Categorical probabilistic rainfall forecasts (left) for the (a) OND 1998 and (b) JFM 1999 seasons over regions G1, G6, G7 and A1. Observed rainfall catogaries are shown on the right. Probabilities have been derived from a 12-year hindcast simulation. The interpertation of the forecast probabilities is depicted by figure 3.10.

An interpretation of the forecast probabilities displayed on the maps of figures 3.9(a) and 3.9(b) (left) is provided in figure 3.10.

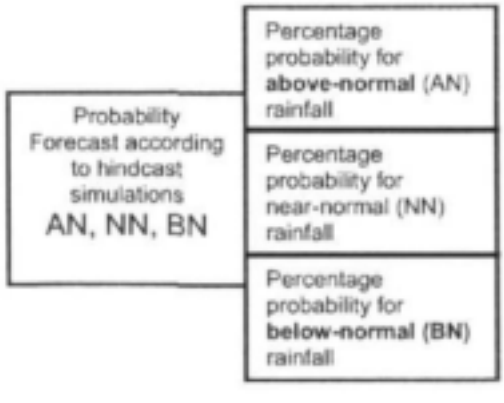

FIGURE 3.10 Interpretation of the diagram printed in the forecast regions (maps on the left in figure 3.9(a) and (b))

3.8 SUMMARY

Rainfall forecasts depicted in figure 3.8 are categorically correct for both the OND 1998 and JFM 1999 seasons in region G1, for the OND 1998 season in regions G6 and G7 and for the JFM 1999 season in region A1. This implies that 63% (5 from 8) of the forecasts fell in the same category as observed. The two rainfall forecasts issued for the SA region (figure 8(e)) are also categorically correct.

The percentage probabilistic rainfall forecasts (figure 3.9) are based upon the model's performance over a twelve-year hindcast run (1985 to 1996). As illustrated by figure 3.9(a), the model fails to forecast the good rain (NN to AN) which occurred over the summer rainfall region (regions G1 and A1) during the OND 1998 season. For this case, the forecast probabilities are overwhelming in favour of NN to BN rainfall. The AGCM, however, correctly forecast the OND 1998 rainfall over region G7. Percentage probabilistic rainfall forecasts improved in the JFM 1999 season, when the model succeeded in forecasting probabilities in favour of the drier conditions experienced over regions A1 and G6. The model forecast an equal probability for AN and BN rainfall in region G1, implying either a lack of skill or too narrow a NN range in the tercile category distribution (an issue that will be addressed in CHAPTER 5).

CHAPTER 4

A COUPLED ATMOSPHERE-OCEAN GENERAL CIRCULATION MODEL FOR SEASONAL FORECASTING

Contributions made to this chapter by ***Dr Steve Wilson*** *from the CSIRO Atmospheric Research in Australia are greatly acknowledged.*

4.1 INTRODUCTION

As indicated in this CHAPTER the configuration of the COCA CGCM (also known as the Coupled Oasis CAR-AGCM ACOM2 model) forms the basis of the research and is unique in the world. Examples from similar coupled model simulations have been examined, and with the various advantages and shortcomings in mind, a new coupling procedure has been constructed. It was therefore decided to include a detailed description of components of the CGCM configuration. The CGCM configuration and forecasting initialisation is summarised in a flow diagram at the end of the CHAPTER.

4.2 THE ATMOSPHERIC MODEL (AGCM)

The AGCM used is the T63 version of the CSIRO9 AGCM (McGregor *et al.*,1993) that has been used in a number of coupled model studies (see for example Hirst *et al.*,1996; Gordon and O'Farrel, 1997; Hirst,1999 and Hirst *et al.*, 2000). A description of the AGCM can be found in SECTION 2.2.2.

4.3 THE OCEAN MODEL (OGCM)

The OGCM used is the ACOM2 (Schiller *et al.*,1997) global domain configuration of the Geophysical Fluid Dynamics Laboratory (GFDL) Modular Ocean Model version 2.0 (MOM2) code (Pacanowski,1995).

The CSIRO Marine Research in Australia has developed the ACOM2 OGCM configuration. A detailed description of the configuration is given in Schiller *et al.* (1997). The model is global and has a tropically enhanced latitudinal resolution of 0.5° within 8° of the equator, increasing gradually to 5.9° at the poles. The longitudinal resolution is uniformly 2°. The zonal and meridional viscosity is latitude dependent to maintain numerical stability despite the strong change from high latitudinal resolution at the equator to coarse resolution at the poles. Meridional viscosity is in the order of 2.0×10^3 $m^2 s^{-1}$ from the equator to poles. Zonal viscosity is set to 2.0×10^4 $m^2 s^{-1}$ at the equator and increases to 3.1×10^5 $m^2 s^{-1}$ at the poles. Horizontal diffusivity is uniformly set to $4.0 \times 10^3 m^2 s^{-1}$.

The OGCM's vertical structure has 25 vertical levels with a maximum depth of 5000m. There are 8 x 15m uniform thickness levels in the upper 120m. Below 120m level, thickness expands gradually at first, so that there are 12 levels in upper 185m, and then expands more strongly to an almost 1000m depth thickness at 5000m. Bathymetry is a smoothed approximation to that of

Gates and Nelson (1975) and has been further modified in the Indonesian Through Flow region to allow transport of water through Lombok Strait and the Timor Sea. Surface heat flux is partitioned below the ocean surface by a solar penetration scheme that employs spatially varying extinction coefficients (Simonot and Le Treut 1988; Wilson 2000b). The model includes active salinity with surface forcing by relaxation to Levitus (1982) salinity on a time scale of 17 days. Vertical mixing is parameterised using a formulation of the Chen *et al.* (1994) vertical mixing scheme. To improve vertical mixing performance at low latitudes this scheme has been modified to use the IP mixing profile (Wilson, 2000a; 2000b; 2000c) that is based on the observations of Peters, Gregg and Toole (1988). Sea ice is constrained to a seasonal cycle defined by the GISST SST climatology.

4.4 COUPLING PROCEDURE

The AGCM and OGCM are synchronously coupled with a time step of 15 minutes. The misalignment of the ocean and atmosphere cells, particularly at the equator and in the modified Indonesian Through Flow region, has required use of the interpolation and filling procedures provided by the OASIS coupler (Terray *et al.*,1995) to exchange wind stresses (τ), heat fluxes (Q) and SSTs between the OGCM and AGCM. All of the additional coupling procedures that are described below have been done outside of the OASIS coupler. These procedures have all been done within the OGCM and on the OGCM's grid.

Anomaly coupling is used to correct the AGCM's wind stresses before using them to force the OGCM. The anomaly wind stress coupling is achieved by first using the AGCM wind stress (τ_m) to calculate an AGCM wind stress anomaly (τ'_m) relative to the AGCM wind stress climatology, so that $\tau'_m = \tau_m - \underline{\tau}_m$. The procedure for obtaining $\underline{\tau}_m$ will be described in detail in the next section. To obtain the wind stress that is used to force the OGCM, the AGCM wind stress anomaly is then superimposed onto an observed global wind stress climatology, $\underline{\tau}_o$, so that $\tau = \tau'_m - \underline{\tau}_o$. Both the model and observed climatologies are stored as monthly mean seasonal cycles and linear temporal interpolation between adjacent months is used to obtain values at the current model time. The observed wind stress climatology is the mean seasonal cycle of 1985-1990 Florida State University (FSU) (Goldberg and O'Brien, 1981; Legler *et al.*,1989 and Stricherz *et al.*,1992) wind stresses for both the Indian and Pacific Oceans, that are combined with a mean seasonal cycle of global Hellerman and Rosenstein (1983) (hereafter HR) wind stresses. The FSU stresses are obtained with a constant drag coefficient, $C_D = 1.5 \times 10^{-3}$, and as these stresses are available only within 30°N-30°S in the Indian and Pacific Oceans, they are embedded within the global HR stresses. To avoid discontinuities in the transition between the FSU and HR stresses, data are blended over three grid points.

SSTs are directly coupled (that is, without anomaly coupling) but, to stabilise the CGCM's climatology, the OGCM SSTs (SST_m) are gently nudged toward the observed global 1985 to 1990 Reynolds (1988) SST climatology ($\underline{SST}_o$). To do so, the heat flux (Q) that forces the OGCM is calculated by adding a weak stabilising heat flux relaxation term (Ji *et al.* 1998) to the AGCM's heat fluxes (Q_m).

$$Q = Q_m + \gamma_s(\underline{SST}_o - SST_m) \qquad (4.1)$$

where the stabilising relaxation coefficient (γ_s) varies latitudinally and is $\gamma_s = 5$ W m^{-2}K^{-1} from the equator to 5°N and 5°S, and then varies with a *cos* function from $\gamma_s = 5$ W m^{-2}K^{-1} at 5°N and 5°S to $\gamma_s = 15$ W m^{-2}K^{-1} at 15°N and 15°S, and then is maintained at $\gamma_s = 15$ W m^{-2}K^{-1} poleward of 15°N and 15°S.

4.5 USE OF A "HEAT FLUX-SST COUPLED SPIN-UP" TO OBTAIN AGCM WIND STRESS CLIMATOLOGY

It is well understood that OGCMs cannot reproduce the observed SST climatology without significant systematic errors. Errors occur even under quite strong relaxation toward the observed SST climatology, and are considerably worse in a CGCM (Mechoso *et al.*, 1995). The SST climatology that forces the atmosphere in a CGCM therefore differs significantly from the observed SST climatology. However, despite this difference, the normal procedure for an anomaly wind stress coupling is to use, as the AGCM's wind stress climatology, the climatology that the atmosphere produces when forced by the observed rather than coupled SST climatology. Thus, when the CGCM is run and the coupled SSTs systematically differ from the observed SST, the wind stress climatology actually produced by the atmosphere model will systematically differ from that used in the anomaly coupling. This has the potential to bias the wind stress anomalies produced by the anomaly coupling.

A coupled spin-up procedure has therefore been developed to avoid such a bias and to obtain an AGCM wind stress climatology ($\underline{\tau}_m$) that is compatible with the coupled OGCM's SST climatology. In this coupled spin-up procedure, the ocean model alone is spun up for 20 years by forcing it with the observed wind stress climatology ($\underline{\tau}_o$) and by relaxing toward the observed SST climatology, $\underline{SST}_o$, with a strong forcing relaxation coefficient, γ_f = 48 W $m^{-2}K^{-1}$. The resulting 20-year forced ocean-state is then saved. The CGCM is then started, using the 20–year OGCM's forced state as the OGCM initial condition[1], and the CGCM is run for a further 20 years. The coupling is as described in the section above, with the exception that the wind stress anomaly coupling is disabled by zeroing the AGCM's wind stress anomalies (τ'_m). The ocean is therefore forced only by the observed wind stress climatology, ($\underline{\tau}_o$). Consequently, during this "heat flux-SST coupled spin-up" the ocean is forced by the same wind stress climatology that it is forced by during full anomaly coupling, and inter-related coupled SST and heat flux climatologies evolve.

These coupled inter-relationships arise because during this spin-up, the AGCM is forced by the evolving coupled SST climatology. In response to these SSTs, the atmosphere produces a climatology of heat fluxes that, in turn, force the coupled SSTs. Thus SSTs feedback on heat fluxes and on SSTs, and so on, in a coupled inter-relationship. Meanwhile, in response to the coupled SSTs, the AGCM is also producing wind stresses. Because the anomaly wind stress coupling is disabled during this spin-up, these AGCM wind stresses are not communicated to the OGCM, but the data are saved for averaging into a climatology. A hovmoeller plot (not shown) reveals that SSTs settle into their new-coupled climatology after about two model years. Therefore, from the last 18 years of this 20-year coupled spin-up, the AGCM's wind stresses are averaged to form the AGCM's wind stress climatology ($\underline{\tau}_m$) for use in the anomaly wind stress coupling. SSTs are also averaged to form a corresponding coupled ocean model SST climatology ($\underline{SST}_m$) that is needed for initialising the model in ENSO forecast mode.
Thus the heat fluxes interact with the ocean model to produce the OGCM's coupled SST climatology, whilst the SST climatology interacts with the AGCM to produce the cliamtology of heat fluxes.

4.6 FORECASTING INITIALISATION

A coupled-nudging technique is used to generate the initial model condition for launching 12-month seasonal forecasts. This technique is similar that first used by Chen *et al.* (1995) to

[1] The atmosphere model's initial condition is not as important as that for the ocean because the atmosphere model "forgets" its initial condition after about a month and is then forced by the ocean condition.

initialise the Lamont model (Cane *et al.*,1986; Zebiak and Cane 1987). Here the CGCM assimilates data by nudging towards time varying monthly observations of surface anomalies, with the forecast initial condition obtained by nudging the CM for a period of some years up to the forecast starting time. The present CGCM has been nudged for 5 years prior to the starting time of the first hindcast experiments in 1985, and for a further 15 years prior to the starting time of current year 2000 forecast experiments.

In Chen *et al.* (1995) coupled-nudging with wind stress data alone was used to initialise the Lamont model. This technique achieved much better results than their previous technique for initialising the Lamont model in which the ocean model alone was forced by the same wind stress data and then coupled to the atmosphere model. Chen *et al.* (1995) believed that this good result arose because use of coupled-nudging avoided coupling shock and filtered noise out of the wind stress observations. In a later paper, Chen *et al.* (1997) also investigated two cases of coupled-nudging with SST data, but reported problems. In the first case they tried initialising the OGCM alone by forcing it with observed wind stress whilst nudging the OGCM's SST anomalies toward observations. In the second case they tried coupled-nudging in which both wind stress and SST anomalies were nudged toward observations. In both cases Chen *et al.* (1997) found that use of SST-nudging degraded their forecast initialisation. They speculated that the poor performance of their SST-nudging "…..could result from a poor choice of nudging parameters or systematic errors in model winds introduced by assimilating SST. The latter is known to be a potential problem, from the results of Zebiak (1986)." They also note that they had not attempted an SST-only coupled-nudging experiment because "of the serious errors in off-equatorial winds" produced by their simple atmosphere model (Zebiak, 1990).

Oberhuber *et al.* (1998) have conducted an SST-only coupled-nudging experiment in which they used only SST data to initialise their model. They reported success, where many other models had failed, in correctly predicting the onset of the 1997/1998 El Niño event and mid-1998 onset of the subsequent La Niña event. Although only used for a single experiment, these results suggest that SST-nudging can be successfully used for model initialisation.

A degradation in ENSO forecast skill of the Lamont model during the late 1990s has been attributed to its sole dependence upon wind stress data and equatorial upwelling dynamics for initialisation (Chen *et al.*, 1998). In particular, for the 1997/1998 El Niño, poor forecast skill has been attributed to easterly winds in the east Pacific that were too strong before onset in the FSU data (Chen *et al.*, 1999). In the present coupled nudging technique, both observed wind stress and SST data are used to generate the initial CGCM condition. SSTs such as the satellite-derived Reynolds (1988) data have higher temporal and spatial resolution than the surface FSU wind observations and so have the potential to provide additional information to the CGCM initialisation. There are also a number of reasons why we believe that coupled SST nudging will improve initialisation of the present model, rather than degrade it as in the Chen *et al.* (1997) model:

a) *There is the success of the Oberhuber et al. (1998) model.*

b) *SSTs are used not just to nudge the SSTs that force the AGCM, but an additional constraint is applied by also using the SSTs to nudge the heat flux fields that force the coupled ocean model - as explained below.*

c) *The present atmosphere GCM may not suffer the same serious errors in SST-forced winds as in Zebiak's simple atmosphere model.*

d) *Finally, the present model's "heat flux/SST coupled spin-up" (as described above) ensures that the wind stress climatology used in the anomaly wind stress coupling is compatible with the CGCM's SSTs. This eliminates one potential source of the systematic wind stress errors that occurred when Chen et al. (1997) assimilated SST.*

The present model's coupled-nudging technique is as follows:

At each time step, for wind stress (τ) and SST, a nudging anomaly (subscript n) is obtained by a linear- weighting of the anomaly generated by the CGCM (subscript m) with the observed anomaly (subscript o) using the following linear weighting

$$\tau'_n = \omega_\tau \tau'_o + (1 - \omega_\tau) \tau'_m \qquad (4.2)$$

$$SST'_n = \omega_{SST} SST'_o + (1 - \omega_{SST}) SST'_m \qquad (4.3)$$

where ω_τ and ω_{SST} are weighting coefficients for wind stress (τ) and SST respectively. As described in more detail below, both the observed and model anomalies are calculated by subtracting the appropriate climatology from the current value. Again, because these climatologies and the current observations are stored as monthly values, a linear temporal interpolation between adjacent months is used to obtain values at the current model time.

For wind stress, the weighting coefficient (ω_τ) is set to a spatially uniform value of 0.5. An observed wind stress anomaly (τ'_o) is obtained by subtracting the observed wind stress climatology ($\underline{\tau}_o$) from the time varying 1985 through to 1999 observations (τ_o). These observations contain FSU data in the tropical Pacific and Indian Oceans and have been blended with the global HR climatology in the same manner described above for the observed climatology. The model wind stress anomaly (τ'_m) is obtained by subtracting the model's wind stress climatology ($\underline{\tau}_m$) from the AGCM's wind stress (τ'_m). After applying a linear-weighting in accordance with equation (4.2), the resulting nudged wind stress anomaly (τ'_n) is used to nudge the coupled ocean model. To do so, the nudged wind stress anomaly (τ'_n) replaces the model wind stress anomaly (τ'_m) in the anomaly wind stress coupling, so that $\tau = \tau'_n + \underline{\tau}_o$.

For SSTs, the blending coefficient (ω_{SST}) varies linearly with latitude from 0.5 at 5°N and S to 0.75 at 15° N and S. The observed SST anomaly (SST_o'), is obtained by subtracting the observed SST climatology ($\underline{SST}_o$) from the time varying monthly global Reynolds SST observations from 1985 through to 1999 (SST_o). The model SST anomaly (SST'_m) is obtained by subtracting the model's SST climatology, ($\underline{SST}_m$), from the OGCM's SST (SST_m). Equation (4.3) is then used to calculate the nudged SST anomaly (SST'_n). As a consequence of the "heat flux-SST coupled spin-up" described above, the wind stress anomaly coupling is based on the CGCM's true SST climatology ($\underline{SST}_m$). Consequently, the nudged SST (SST_n), is calculated by superimposing the nudged anomaly, (SST'_n), onto the CGCM's SST climatology ($\underline{SST}_m$), rather than the conventional approach of superimposing these anomalies onto the observed SST climatology ($\underline{SST}o$). The nudged SST (SST_n) is then used to force the AGCM.

In using the model in nudged mode, it was found that the OGCM's SST anomalies at high-latitudes did not correspond well to observed SST anomalies. The upper ocean dynamical and thermal structures are largely determined by wind forcing (Chen et al.,1999b), so this lack of correspondence in SSTs is probably because the time varying FSU wind stress observations do not extend beyond latitudes 30°N and S. To correct the OGCM's SST anomalies at high latitudes,

an additional heat flux nudging term $\gamma_n(SST'_o - SST'_m)$ based on the difference between the observed SST anomaly (SST'_o) and the model's SST anomaly (SST'_m) is added to the atmosphere's heat fluxes, together with a modified form of the weak stabilising heat flux relaxation term described above. This term is modified to use the current SST observations (SST_o) rather than the observed SST climatology, ($\underline{SST}o$), so that equation (4.1) becomes

$$Q = Q_m + \gamma_s(SST_o - SST_m) + \gamma_n(SST'_o - SST'_m) \qquad (4.4)$$

Because the difference between the SST anomalies ($SST'_o - SST'_m$ is quite small) a strong nudging coefficient, $\gamma_n = 100\ Wm^{-2}K^{-1}$ is used. At the transition from coupled nudging to coupled prediction, the nudging scheme is wound-off over the last month of nudging by linearly reducing the coefficients ω_τ, ω_{SST} and γ_n from the values specified above at the beginning of the last month, to 0 at the end of the month. Additionally, a linear-weighting is used to make a transition of the weak stabilising relaxation (term γ_s) from using current SST observations in equation (4.4) back to using the observed SST climatology as in equation (4.1). This linear weighting is, $SST_o = \omega_Q SST_o + (1-\omega_Q)\ \underline{SST}_o$, where ω_Q is 1 during nudging and is linearly reduced to 0 during the last month.

FIGURE 4.1 DIAGRAM OF COCA CGCM COUPLING (CSIRO9(T63) AGCM AND ACOM2 OGCM)

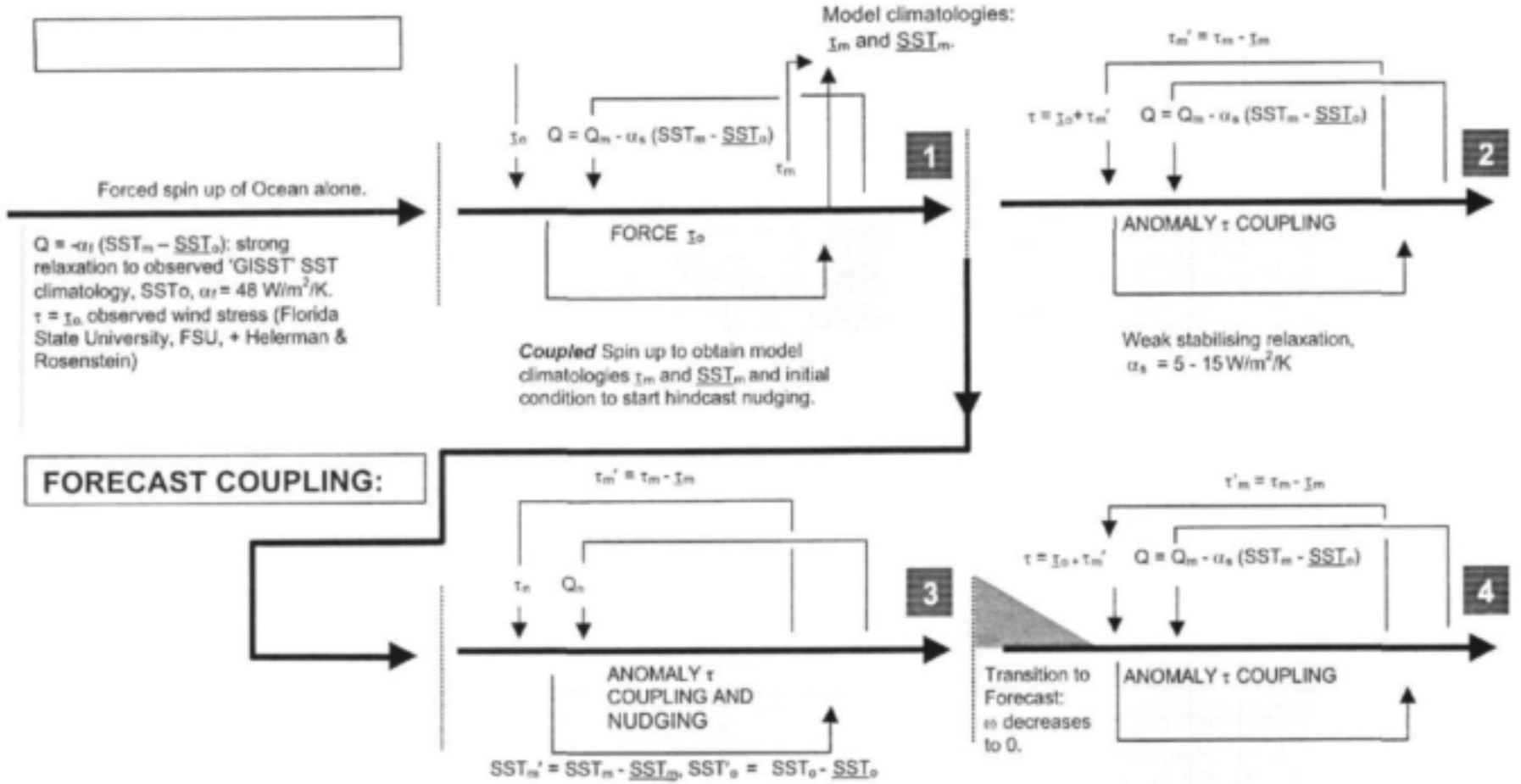

Coupled fields are '*nudged*' towards the observations with α_n = 100 W/m²/K strongly nudging SST anomalies towards the observed anomalies.

(a) $\tau_n' = \omega_\tau \tau_o' + (1-\omega_\tau)\tau_m$, $\therefore \tau_n = \underline{\tau}_o + \tau_n'$

(b) $SST_n' = \omega_{SST} SST_o' + (1-\omega_{SST}) SST_m'$ $\therefore SST_n = \underline{SST}_m + SST_o'$

(c) $Q_n = Q_m - \alpha_s (SST_m - SST_o) - \alpha_n (SST_m' - SST_o')$

Four stage Coupling for initialising the ENSO Prediction System:

1. Spinning up Coupled Climatologies
2. Free ENSO Mode
3. Coupled-nudged initialisation with observed SST_o and wind stress, τ_o
4. ENSO Prediction mode (as for 2 but after nudged initialisation)

CHAPTER 5

CSIRO9(R21) AGCM RAINFALL PROJECTIONS FROM CGCM SST FORECASTS

Contributions made to this chapter by ***Mr Richard Sewell*** *from the South African Weather Service and* ***Dr Ian Smith*** *from the CSIRO Atmospheric Research are greatly acknowledged*

5.1 INTRODUCTION

The ultimate objective of the CLIPWATER project is to produce seasonal rainfall forecasts modulated by forecast SST boundary forcing from the COCA CGCM discussed in CHAPTER 4. As mentioned earlier, rainfall forecasts were simulated by the CSIRO9(R21) AGCM on a local super computer. This introductory section gives a brief overview of the content of CHAPTER 5 where the achievements during the final phase of the research project are outlined.

Before introducing any forecasting procedure, an assessment of the ability of the COCA CGCM to produce the boundary SST forecast fields (measure of skill) is required. Persistence and blended statistical SST forecasts are employed as a baseline against which these CGCM results are compared. It is indicated that the CGCM's SST forecasts outscore forecasts from both these methods when the relationship between forecast and observed SST fields are statistically significant. This gives a good motivation why SST forecasts from the CGCM are superior and more appropriate to use. The verification analysis was based upon 13 (1987 to 1999) hindcast simulations, and is only valid for the NINO34 region in the eastern equatorial Pacific Ocean.

Four ensembles of an 18 year (1982 to 1999) hindcast simulation were completed on a local super computer using the CSIRO9 (R21) AGCM, forced with observed SSTs, to generate an ensemble averaged model simulated monthly rainfall database for model skill assessment and category classification. Observed monthly rainfall fields for the same period have been calculated for the seven model grid boxes that cover South Africa (G1 to G7 in figure 3.3). Three different category classifications of AN, NN and BN in the model simulated and observed rainfall distribution are considered and compared in the skill score analyses. The conventional tercile distribution employed in CHAPTER 3 has been employed.

Seasonal rainfall forecast simulations produced by the CSIRO9(R21) AGCM, with SST boundary forcing input from the CGCM, have been completed for the OND 2001 and JFM 2002 seasons, and categorical probabilistic forecasts for these seasons are issued for the seven grid boxes (G1 to G7) and areas (A1 and SA) as defined in figure 3.3.

5.2 CGCM SST FORECAST VERIFICATION

In order to determine the skill or verify the performance of the COCA CGCM, multiple hindcast simulations have been generated for a historical period of 13 years (1987 to 1999). Different epochs from this period have been considered in the verification process where SSTs from the

CGCM was compared to those of other models used in South Africa. The CGCM, which employs a "nudging" initialisation technique to incorporate observations, has been released at the beginning of the months January, April, July and October to generate monthly SST projections for a period of 12 months in advance. These predicted SST fields were time averaged over three-months to obtain forecasts for the JFM, AMJ, JAS and OND seasons.

Model performance in 48 hindcast simulations (see figure 5.1), with differed time lags (months), is first measured against persistence (SECTION 5.2.1) in the NINO34 region (5° North to 5° South and 170° West to120° West; figure 2.14 in CHAPTER 2). Here, persistence will serve as a baseline against which the CGCM SST forecasting performance is measured. In addition to persistence seasonal (3 month average) CGCM SST hindcasts for the NINO34 region will also be compared with results from a blended statistical forecasting model (CCA SST forecasts blended with Principal Oscillation Patterns (POPs) SST forecasts or CCA/POPs forecasts) developed by Sewell (2001; *personal communication*) at the SAWS (SECTION 5.2.2). Similar to persistence, the CCA/POPs model's performance will serve as a second baseline against which the CGCM SST forecasting performance is measured.

Apart from the NINO34 analyses, global spatial anomaly correlation patterns between 48 6-month lead-time forecasts and the associated observed fields are also illustrated and discussed in SECTION 5.2.3.

5.2.1 CGCM SST FORECASTS AGAINST PERSISTENCE

To begin with, CGCM simulated SST hindcasts are compared with the most basic form of forecasting (also refered to as "poor" man's forecasting), namely persistence. Persistence implies that one assumes that observed SSTs measured during a specific month persist in the following (forecast) months.

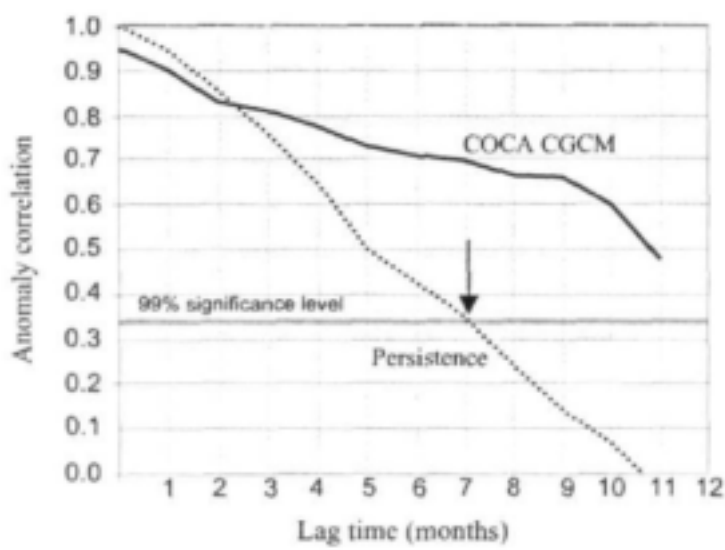

FIGURE 5.1 Anomaly correlations between CGCM forecast SSTs and persistence over the NINO34 region. The correlations have been calculated from 48 hindcast simulations where the model was initialised at the beginning of January, February, March (1987 to 1999 = 13 years) and October (1990 to 1998 = 9 years). The 99% significance level is 0.33.

In figure 5.1 anomaly correlations between the monthly observed and persisted (forecast) SSTs are calculated for different lead times in the NINO34 region. These correlations represent comparisons between observed and 48 forecast SST fields initialised from January, April, July (1987 to 1999 = 13 years) and October (1990 to 1998 = 9 years).

Figure 5.1 indicates that the CGCM outscores persistence in forecasts with a time lag of three months and longer. The correlation between persistence and observations at the point of release will obviously be perfect, while CGCM comparisons shows a correlation of approximately 0.95. This may be attributed to the fact that although model simulated SSTs are nudged towards observations, they are still not equal to observed fields. CGCM forecast SSTs retain a relatively high correlation (above the 99% significance level), even over a period of 11 months in advance (correlation = 0.49). The 95% and 99% significance levels are 0.29 and 0.33, respectively.

5.2.2 CGCM AND CCA/POPs SST FORECAST COMPARISONS

In SECTION 5.2.1 it has been indicated that the CGCM forecasts outscores persistence in the NINO34 region with forecasts with a time lag of 3 months and longer. In this section seasonal (3 month average) CGCM SST forecasts (JFM, AMJ, JAS, OND) for the NINO34 region are compared with results from the CCA/POPs model (Sewell, 2001; *personal communication*). In addition to persistence, the CCA/POPs model's performance will also serve as a baseline against which the CGCM SST forecast performance is measured.

The aim of this verification experiment is to compare the output of the CGCM with that of the CCA/POPs model over a period of 13 years (1987 - 1999). For each year, four seasons are predicted namely JFM, AMJ, JAS, OND which will be denoted S_n, S_{n+1}, S_{n+2}, S_{n+3}, respectively. This is done using each season S_n, (n=1,4) as predictor, so that if (n+r) > 4 for (r=1,3) S_{n+r} falls in the following year. There is one difference in the method employed to produce seasonal forecasts between the CGCM and CCA/POPs model. The CGCM uses the first month of the first season, S_n, as the initialised state and then predicts the individual months up to 12 months ahead as predictands. These are then averaged to obtained seasons. The rationale behind this is that in the case of the statistical model the data is already in the form of seasons and because of the nature of the model S_{n-1} is used to predict S_{n+r}, (r=0.3, n=1,4). Note that in the case of n=1, JFM, S_{n-1}, falls in the previous year.

The treatment of the data in the preparatory phase is the same in both the statistical models (CCA and the POPs model). The data for the predictor and the predictand is averaged over a 3-month period, centred and standardised. This is done for each of the 13 years under consideration, giving a time series for each grid point in the domain of the model. In order to reduce the amount of data and thus to scale down the problem from a computational aspect and to eliminate noise the data is transformed into mode space using EOF analysis. Only the first 10 modes are retained using a refinement of the 'scree' (Jackson, 1991) method as arbiter. The refinement involves determining the cut-off point, namely the point where the difference in the eigenvalues is less than the difference in the differences.

In both the CCA and the POPs methods the prediction equations can be expressed in the form:

$$\mathbf{Y} = \underline{\mathbf{M}}\,\mathbf{X}$$

where **Y** is the predicted anomaly vector and **X** is the value of the predictor anomaly vector. $\underline{\mathbf{M}}$ is the transformation matrix as derived by either CCA (Glahn 1968) or the POPs technique (von Storch *et al.*, 1988; Penland, 1989).

The CCA/POPs model used reconstructed historical SSTs from 1987 to 1995 (Smith *et al*.,1996), together with the latest optimal interpolation data from 1996-1999 (Reynolds and Smith, 1994) to compile a 13-year (1987 - 1999) record length. Prior to the use of satellite retrievals in the early 1980s, SST data analysis depended largely on 'in situ' data which was adequate to describe SST patterns between 30°S and 60°N except the eastern tropical and South Pacific (Reynolds, 1988). The data is supplied on a 1° by 1° grid. To make the problem more tractable this is interpolated to a 4° by 6° grid (1°E to 397°E and 45°S to 45°N). This spatial grid configuration has previously been illustrated in figure 3.3.

The initialisation method employed to produce CGCM SST forecasts has been discussed in detail in CHAPTER 4. The SST output from the CGCM is supplied on a global 192 by 96 grid which is the grid resolution of the CSIRO9(T63) AGCM. For direct comparison with the output of the CCA/POPs model, this is linearly interpolated to the same 4° by 6° spatial resolution as introduced to the statistical models (figure 3.3).

SST forecasts in the NINO34 region, as generated by both the CGCM and CCA/POPs models, have been compared with observations for the four seasons (OND, JFM, AMJ, JAS) with different three-month time lags. In an effort to compare the performance of the two models, anomaly correlations between model and observed SSTs have been calculated. Results are displayed in figures 5.2 (a), (b), (c) and (d) as well as in table 4.

OND SST forecasts (figure 5.2(a)) from the CGCM (solid black line) are superior to those produced by the CCA/POPs model (dotted black line) in the interval where the anomaly correlations are above the 95% significance level. This applies for forecasts of 3 months in advance. Forecasts in the interval where the CCA/POPs model performs better that the CGCM are not regarded as statistically significant. The same conclusion can be made for the JFM SST forecasts (figure 5.2(b)). The CCA/POPs model performs better with JFM forecasts of six, nine and twelve moths in advance, but it is again important to note that these forecasts are not statistically significant. In relation to the CCA/POPs model, the CGCM performs exceptionally well (an anomaly correlation coefficient difference of approximately 0.2) with AMJ SST forecasts (figure 5.2(c)) in the interval above the 95% significance level. The CAC/POPs model, however, performs better with twelve-month time lag forecasts where relative small anomaly correlation coefficients have been calculated. The JAS forecasts of the CGCM outscore the CCA/POPs forecasts with the three, nine and twelve month forecasts (figure 5.2(d)). To conclude, the CGCM performs better than the CCA/POPs model in the interval above the 95% significant level for all seasons (OND, JFM, AMJ and JAS).

In table 4 the magnitude of the anomaly correlation values for the CGCM and CCA/POPs models (graphically displayed in figures 5.2 (a), (b), (c) and (d)) are listed. Cases where one of the two anomaly correlations is above the 95% significance level are in bold. In all these cases anomaly correlation coefficients calculated for the CGCM are larger than those of the associated CCA/POPs coefficients.

Model performance during 48 hindcast simulations, with differed time lags (months), was measured against persistence (SECTION 5.2.1) in the NINO34 region as well as against CCA/POPs SST forecasts. Persistence and CCA/POPs SST forecasts served as a baseline against which the CGCM SST forecasting performance was measured. In both comparisons the CGCM generally performed better than the other models, which justifies the prescription of CGCM SST forecasts as surface boundary forcing in the final CSIRO9(R21) rainfall forecast analyses.

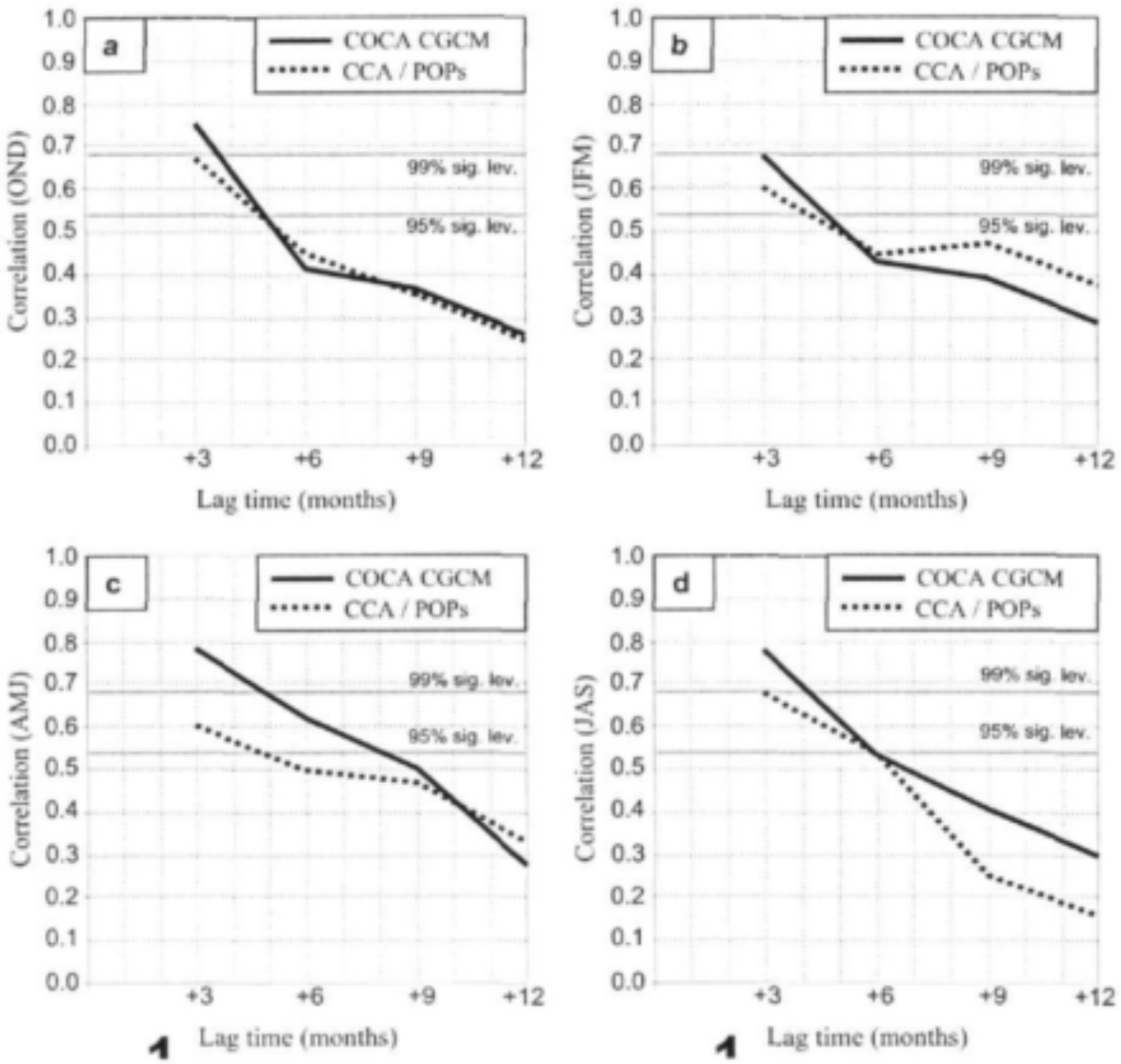

FIGURE 5.2 Anomaly correlations between COCA CGCM SST forecasts (solid black lines) and observations, and CCA/POPs (dotted black lines) SST forecasts and observations in the NINO34 region over a 13-year period (1987 to 1999) for different month lag times (+3, +6, +9, +12). Correlations are for the seasons (a) OND, (b) JFM, (c) AMJ and (d) JAS. The 95% and 99% significance levels are 0.54 and 0.69 respectively.

Up to this point the verification analyses focused on forecasting performance in the NINO34 region alone. It is, however, a well-known fact that remote and regional responses from other ocean regions might also have a significant influence on rainfall variability over Southern Africa. The following section will give some insight concerning the SST forecasting performance of the CGCM over the global oceans as well as in regional oceans in the vicinity of South Africa.

TABLE 4
Anomaly correlation coefficients between COCA CGCM SST forecasts and observations, and CCA/POPs SST forecasts and observations in the NINO34 region over a 13-year period (1987 to 1999) for different month lag times and seasons. The 95% and 99% significance levels are 0.54 and 0.69 respectively. Coefficients greater than the 95% significance level are in bold.

Lag times	OND correlation CCA/POPs - CGCM	JFM correlation CCA/POPs - CGCM	AMJ correlation CCA/POPs - CGCM	JAS correlation CCA/POPs - CGCM
+3 months	**.68 - .74**	**.60 - .68**	**.60 - .78**	**.68 - .78**
+6 months	.45 - .41	.44 - .43	.50 - **.61**	.54 - .54
+9 months	.36 - .37	.48 - .40	.48 - .51	.25 - .41
+12 months	.24 - .25	.39 - .29	.33 - .29	.17 - .30

5.2.3 SPATIAL SST CORRELATION PATTERNS

The same hindcast results obtained from the 48 forecast simulations discussed in section 5.2.1 have been used to calculate global spatial correlation between CGCM forecast and observed SST patterns. Composite correlations have been calculated from all the seasonal forecasts that have been initiated from January, April, July and August. Forecast SST fields with a 6-month time lag have been compared with observations. These correlations fields are depicted in figure 5.3. The CGCM exhibits most skill in the Pacific Ocean, especially over the eastern equatorial Pacific Ocean where correlations in access of 0.8 occur. In contrast, the CGCM has very little or no skill to predict SST patterns 6 months in advance over the Atlantic and Indian Oceans. As far as regional correlations in the vicinity of South Africa are concerned, the model shows slightly improved skill (0.3 and higher: > 95% significance level) in the northern Mozambique Channel, along the western coastline of South Africa and over extensive areas to the southeast of the African continent (shaded in figure 5.3).

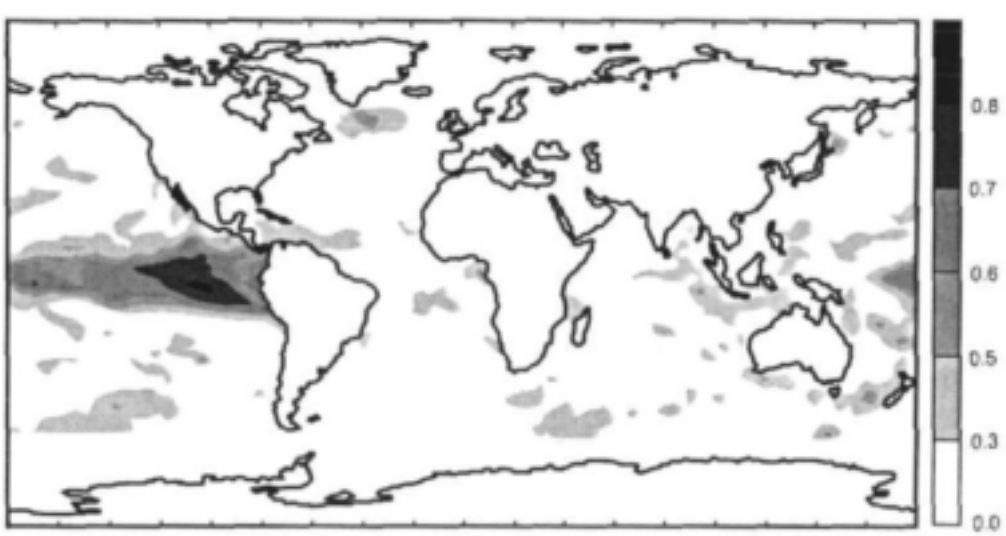

FIGURE 5.3 Global spatial anomaly correlations between CGCM forecast SSTs with a time lag of 6 months and observations. The correlations have been calculated from 48 hindcast simulations where the model was initialised at the beginning of January, April, July (1987 to 1999 = 13 years) and October (1990 to 1998 = 9 years). The 95% and 99% significance levels are 0.29 and 0.33 respectively.

If selected periods from the 48 hindcasts are chosen, anomaly correlation patterns in the South African region improve noticeably. Note that figure 5.3 gives the composite average anomaly correlation patterns between forecasts with a time lag of 6 months and observations derived from all (48) the hindcast simulations initiated from the beginning of four different months (January, April, July and October). In contrast, figure 5.4 (a) and (b) give the associated anomaly correlations calculated from the hindcast simulations initiated from the individual months June and January alone, to forecast for January and June (6 months in advance). Figure 5.4(a) and (b) illustrate anomaly correlations calculated from 13 hindcast simulations, implying that the 95% and 99% significance levels are 0.54 and 0.69, respectively.

Encouraging are the higher anomaly correlation patterns to the south of the continent, and especially over the Mozambique Channel (figures 5.4(b) and 5.4(b)) depicted by shaded areas (> 95% significance level). The January forecast shows significant skill over an area to the northeast of Madagascar in the Indian Ocean and the south western Indian Ocean (figure 4.5(a)). The July forecasts show improved skill in the Mozambique Channel. These local ocean regions might influence rainfall patterns over South Africa (Reason and Mulenga; 1999) implying that the forecasting of regional SST patterns is important.

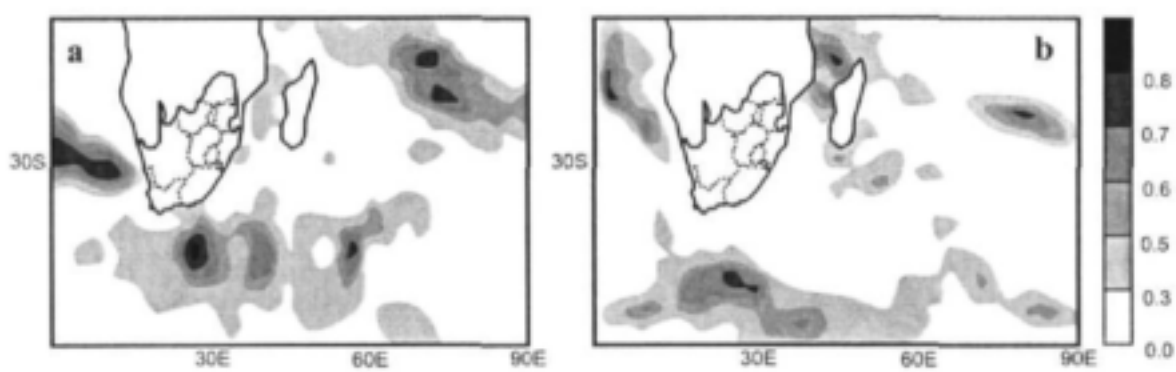

FIGURE 5.4 Regional spatial anomaly correlations between CGCM forecast SSTs with a time lag of 6 months and observations. The correlations have been calculated from 13 hindcast simulations (1987 to 1999 = 13 years) where the model was initiated at the beginning of (a) July to forecast for January and (b) January to forecast for July. The 95% and 99% significance levels are 0.54 and 0.69 respectively.

5.3 *CSIRO9 (R21) AGCM RAINFALL VERIFICATION*

Seasonal rainfall projections are generated by using CSIRO9(R21) AGCM (the same AGCM that has been used for rainfall forecasts in CHAPTER 3). The COCA CGCM provides the monthly SST forecasts (predictor), which will then be prescribed as thermal boundary forcing for the CSIRO9(R21) AGCM to simulate the rainfall (predictand) response. A two-tiered forecasting procedure is therefore applied (illustrated in figure 1.1). In SECTION 1.2.2 it was emphasised that the problem of numerical seasonal forecasting is inherently probabilistic by nature. A requirement is therefore to issue rainfall forecasts in terms of percentage probabilities in the BN, NN or AN categories. These percentage probabilities are calculated by comparing historically observed rainfall records to model simulated rainfall results emanating from hindcast AGCM simulations forced by perfectly observed SST patterns.

5.3.1 HINDCAST SIMULATIONS

Four ensembles of an 18 year (1982 to 1999) hindcast simulation were completed on a local super computer using the CSIRO9 (R21) AGCM, forced with observed SSTs (Smith *et al.* (1996) and Reynolds and Smith (1994)), to generate an ensemble averaged model simulated monthly rainfall database for model skill assessment and category classification. Observed monthly rainfall fields for the same period have been calculated for the seven model grid boxes that cover South Africa (G1 to G7 in figure 3.3). Three different category classifications of AN, NN and BN in the model simulated and observed rainfall distribution are considered and compared in the skill score analyses. The conventional tercile distribution employed in CHAPTER 3 has been employed.

5.3.2 RAINFALL CATEGORY CLASSIFICATION

The CSIRO9(R21) AGCM's ability to reproduce monthly rainfall episodes for each rainfall region (G1 to G7 and A1 in figure 3.1 (a) and (b)), as well as for South Africa in total (region SA in figure 3.1(c)), is expressed in terms of the percentage of events where model simulated rainfall (from the 18-year hindcast simulation) falls in the same category (AN, NN and BN) as the associated observed rainfall. In this chapter AN, NN and BN categories are obtained from a data series that consists of 18 rainfall values.

The most commonly used category classification is the tercile classification. However, if the AN and BN category percentages are both significantly larger than the NN category percentage in a rainfall forecast distribution, a noticeable fraction of the NN variability might still be captured in the AN and BN distribution. In this study, it was found that this often happened in the tercile category distribution, which could result in poor forecasts of the more extreme wet and dry rainfall events. The tercile category classification of the 18 rainfall values (6:6:6 classification or classification A in table 5) therefore often appears not to be the best choice. An alternative approach would be to create a category distribution where the AN and BN rainfall events are defined in such a way that they are, to a great extent, excluded from the normal variability in a rainfall distribution. To avoid noise from the normal distribution affecting the AN and BN categories, it is recommended that a wider range in the rainfall distribution be allocated to the NN category. This may be achieved by introducing an 5:8:5 and 4:10:4 category classifications, or classifications B and C in table 5.

TABLE 5

The three category classifications (A,B,C) of the rainfall distribution from 18 values considered in the skill score analysis of this chapter. Category classification A represents the usual tercile classification, while classifications B and C allow for a wider range in the near-normal (NN) category.

	Classification A	Classification B	Classification C
ABOVE-NORMAL (AB)	**6** (33%)	**5** (28%)	**4** (22%)
NEAR-NORMAL (NN)	**6** (33%)	**8** (44%)	**10** (56%)
BELOW-NORMAL (BN)	**6** (33%)	**5** (28%)	**4** (22%)
TOTAL YEARS 1882-1990	**18**	**18**	**18**

Consider a time series that consists of 18 rainfall values and is ranked from the smallest to largest value, namely w_i, i=1, 18.

The median of such a time series (denoted in figures 2.3 and 2.4 for the rainfall used in this study) would be

$$\frac{w_9 + w_{10}}{2}$$

More precise formulations of classifications A, B and C (table 5) are:

a) *Classification A (6:6:6 or tercile classification)*

Below Normal (BN)	Near Normal (NN)	Above Normal (AN)
$w_i \leq \frac{w_6 + w_7}{2}$	$\frac{w_6 + w_7}{2} < w_i < \frac{w_{12} + w_{13}}{2}$	$w_i \geq \frac{w_{12} + w_{13}}{2}$

b) *Classification B (5:8:5 classification)*

Below Normal (BN)	Near Normal (NN)	Above Normal (AN)
$w_i \leq \frac{w_5 + w_6}{2}$	$\frac{w_5 + w_6}{2} < w_i < \frac{w_{13} + w_{14}}{2}$	$w_i \geq \frac{w_{13} + w_{14}}{2}$

c) *Classification C (4:10:4 classification)*

Below Normal (BN)	Near Normal (NN)	Above Normal (AN)
$w_i \leq \frac{w_4 + w_5}{2}$	$\frac{w_4 + w_5}{2} < w_i < \frac{w_{14} + w_{15}}{2}$	$w_i \geq \frac{w_{14} + w_{15}}{2}$

A well-known disadvantage in the verification of current AGCM ensemble hindcast simulations is the relatively short time series that are available for category classification (Goddard *et.al.*, 2001). This will certainly have a negative influence on skill-score estimations, and that is also why rainfall in this study is verified in terms of an elementary hit rate score. Had a longer record been available, more advanced evaluation scores such as Linear Error in Probability Space (LEPS) scores could have been be calculated.

In this chapter a relatively short time series of 18 years is examined. The worst case would be that probabilistic forecast percentages in the AN and BN categories (classification C in Table 5) are confined to a factor of 25% (100/4) since only 4 rainfall values occur in these categories. Despite these constraints, category classifications A, B and C are all examined in the skill score analysis.

5.3.3 MODEL SKILL

The AGCM's ability to reproduce rainfall events for each rainfall region (G1, G6, G7, A1 in figure 3.1), as well as for South Africa in total (region SA in figure 3.1(c)), is expressed in terms of the percentage of events where model-simulated rainfall (from the 18-year hindcast simulation) falls in the same category (AN, NN, BN) as the observed rainfall. Similar to the procedure followed in CHAPTER 3 (SECTION 3.6), model verification is based on a hit-rate score approach. In this chapter, however, hit-rate scores (expressed as percentages) are calculated for

all the regions and for each one of the three category classifications in table 5. Model performance in terms of individual months as well as three-month average seasons is analysed.

5.3.3.1 Percentages of hit rate scores for monthly simulations

TABLE 6(a)
Percentages of monthly hit rate scores for the AN, NN and BN categories in regions G1 to G7, A1 and SA. Hit rate scores are calculated for three category classifications (6:6:6, 5:8:5 and 4:10:4) as defined in table 5. Periods with scores bigger than 33% are shaded.

	Jan	*Feb*	*Mar*	*Apr*	*May*	*Jun*	*Jul*	*Aug*	*Sep*	*Oct*	*Nov*	*Des*
Region G1												
6:6:6	28	38	22	28	28	39	28	50	44	28	22	39
5:8:5	39	43	19	39	34	37	26	37	50	22	34	26
4:10:4	53	37	28	42	33	48	37	40	33	25	25	33
Region G2												
6:6:6	33	22	50	56	50	28	28	39	44	27	39	44
5:8:5	41	33	39	50	43	48	33	33	33	22	37	61
4:10:4	40	33	30	42	57	45	45	33	42	22	40	68
Region G3												
6:6:6	33	44	33	22	22	50	33	28	22	28	44	33
5:8:5	28	41	37	19	19	58	39	26	26	26	30	35
4:10:4	22	40	37	25	22	63	45	25	25	22	28	42
Region G4												
6:6:6	17	39	50	33	33	44	39	33	28	28	39	61
5:8:5	26	37	57	37	37	65	48	33	23	39	33	54
4:10:4	40	37	53	36	40	65	45	48	25	33	33	53
Region G5												
6:6:6	39	28	22	17	39	39	33	33	11	22	17	33
5:8:5	33	30	26	13	48	48	43	15	23	30	23	33
4:10:4	37	43	37	13	45	40	57	22	28	37	35	37
Region G6												
6:6:6	33	44	33	22	28	22	28	44	44	22	39	28
5:8:5	30	54	41	19	43	26	28	39	41	23	41	37
4:10:4	25	37	37	28	53	22	45	33	28	32	32	40
Region G7												
6:6:6	39	33	50	28	17	22	39	28	28	28	44	39
5:8:5	58	48	43	26	19	23	33	30	41	19	43	41
4:10:4	60	60	45	22	25	25	48	28	40	22	37	40
Region A1												
6:6:6	33	39	28	39	28	28	39	50	44	33	39	28
5:8:5	37	24	26	26	37	33	33	43	50	41	39	26
4:10:4	25	18	25	33	37	37	33	57	45	37	33	25
Region SA												
6:6:6	33	28	33	22	39	22	50	33	33	50	39	44
5:8:5	26	22	43	28	33	18	54	28	19	43	37	54
4:10:4	13	22	45	42	37	18	53	30	28	45	48	68

The higher percentages in hit rate scores in classification B (5:8:5) and C (4:10:4) (table 6(a)) might be attributed to biases as a result of the wider range in the rainfall distribution allocated to the NN category. This means that more hits might occur in the NN category of these distributions than in the NN category of classification A (6:6:6). To estimate to what extent extreme rainfall (AN and BN categories) is captured by the AGCM, selected hit rate scores for the more extreme AN and BN rainfall categories are calculated in table 6(b).

TABLE 6(b)

Percentages of monthly hit rate scores for the more extreme AN and BN categories in regions G1 to G7, A1 and SA. Hit rate scores are calculated for three category classifications (6:6:6, 5:8:5 and 4:10:4) as defined in table 5. Periods with scores bigger than 33% are shaded.

	Jan	*Feb*	*Mar*	*Apr*	*May*	*Jun*	*Jul*	*Aug*	*Sep*	*Oct*	*Nov*	*Des*
Region G1												
6:6:6	34	42	25	33	17	33	34	50	42	33	17	34
5:8:5	40	40	10	40	20	30	20	30	50	20	20	20
4:10:4	50	25	13	38	25	38	25	25	25	13	13	25
Region G2												
6:6:6	25	25	50	59	50	33	25	33	42	34	33	50
5:8:5	30	30	40	50	40	40	30	30	30	20	30	60
4:10:4	25	25	25	38	50	38	38	25	38	13	25	63
Region G3												
6:6:6	34	42	33	25	17	50	42	33	17	25	33	42
5:8:5	30	30	30	10	10	50	40	20	20	20	20	40
4:10:4	13	25	25	13	13	50	38	13	13	13	13	38
Region G4												
6:6:6	17	33	59	33	33	50	33	42	25	42	42	59
5:8:5	20	30	60	30	30	60	40	30	10	40	30	50
4:10:4	25	25	50	25	25	63	38	38	13	25	25	50
Region G5												
6:6:6	42	25	59	9	33	34	42	34	9	25	9	33
5:8:5	30	20	20	0	40	40	40	10	10	20	10	30
4:10:4	25	25	25	0	38	25	50	13	13	25	13	25
Region G6												
6:6:6	33	42	33	17	33	25	33	50	42	17	33	25
5:8:5	20	50	30	10	40	20	30	40	30	10	30	30
4:10:4	13	25	25	13	50	13	38	25	13	13	13	25
Region G7												
6:6:6	42	34	50	25	9	17	42	25	25	25	50	33
5:8:5	50	40	40	20	10	10	30	20	30	10	40	30
4:10:4	50	7	50	38	13	13	13	38	13	25	13	25
Region A1												
6:6:6	33	50	25	42	25	34	42	50	50	33	50	25
5:8:5	30	30	20	20	30	30	30	40	50	30	40	20
4:10:4	13	13	13	25	25	25	25	50	38	25	25	13
Region SA												
6:6:6	34	33	42	25	42	33	50	33	25	50	34	50
5:8:5	20	20	40	30	30	20	50	30	10	40	30	50
4:10:4	0	13	38	38	25	13	50	25	13	38	38	63

5.3.3.2 Percentages of hit rate scores for three-month average (seasonal) simulations

TABLE 7(a)

Percentages of three-month averaged (seasonal) hit rate scores for the AN, NN and BN categories in regions G1 to G7, A1 and SA. Hit rate scores are calculated for three category classifications (6:6:6, 5:8:5 and 4:10:4) as defined in table 5. Periods with scores bigger than 33% are shaded.

	JFM	*FMA*	*MAM*	*AMJ*	*MJJ*	*JJA*	*JAS*	*ASO*	*SON*	*OND*	*NDJ*	*DJF*
Region G1												
6:6:6	28	33	33	22	17	27	33	39	50	39	33	39
5:8:5	28	22	28	28	22	26	41	22	26	43	37	39
4:10:4	22	10	30	45	30	33	37	13	25	33	45	33
Region G2												
6:6:6	22	50	50	44	44	44	22	22	44	39	33	44
5:8:5	33	54	50	68	43	37	33	23	37	54	50	39
4:10:4	37	48	57	65	60	40	33	28	40	45	57	45
Region G3												
6:6:6	22	28	50	44	56	33	22	28	17	28	39	33
5:8:5	15	30	39	28	54	33	22	23	11	26	37	15
4:10:4	25	20	22	22	45	22	25	28	22	22	37	25
Region G4												
6:6:6	17	39	50	44	39	39	22	17	17	33	50	33
5:8:5	23	58	50	28	39	39	34	30	11	11	39	37
4:10:4	28	68	45	30	30	42	37	37	22	13	33	25
Region G5												
6:6:6	28	17	44	33	39	50	39	39	11	28	28	17
5:8:5	30	30	43	33	33	50	34	34	17	37	26	37
4:10:4	28	28	33	45	45	57	35	28	20	37	37	37
Region G6												
6:6:6	28	39	50	22	39	22	33	11	29	44	28	17
5:8:5	33	37	48	34	48	28	30	23	23	33	30	22
4:10:4	25	40	33	28	37	22	43	32	28	33	20	33
Region G7												
6:6:6	33	28	17	22	22	33	39	22	33	39	28	50
5:8:5	52	33	19	17	13	33	48	26	37	35	26	41
4:10:4	48	33	13	20	16	45	36	28	42	30	33	37
Region A1												
6:6:6	28	28	44	39	28	39	28	44	33	28	17	28
5:8:5	26	28	43	43	48	43	33	28	28	26	22	22
4:10:4	22	30	45	48	60	57	45	22	22	25	13	22
Region SA												
6:6:6	22	39	39	44	33	39	39	44	33	50	33	56
5:8:5	26	37	33	46	33	39	37	41	41	43	43	50
4:10:4	25	40	22	30	45	57	37	37	37	57	33	45

Similar to the monthly verification, higher percentages in hit rate scores in classification B (5:8:5) and C (4:10:4) (table 7(a)) might be attributed to biases as a result of the wider range in the rainfall distribution allocated to the NN category. This means that more hits might occur in the

NN category of these distributions than in the NN category of classification A (6:6:6). To estimate to what extend extreme rainfall (AN and BN categories) is captured by the AGCM, selected hit rate scores for the more extreme AN and BN rainfall categories are calculated in table 7(b).

TABLE 7(b)

Percentages of three-month average (seasonal) hit rate scores for the more extreme AN and BN categories in regions G1 to G7, A1 and SA. Hit rate scores are calculated for three category classifications (6:6:6, 5:8:5 and 4:10:4) as defined in table 5. Periods with scores bigger than 33% are shaded.

	JFM	*FMA*	*MAM*	*AMJ*	*MJJ*	*JJA*	*JAS*	*ASO*	*SON*	*OND*	*NDJ*	*DJF*
Region G1												
6:6:6	42	42	42	42	33	17	25	25	42	50	42	33
5:8:5	40	30	20	30	30	20	20	30	20	20	40	30
4:10:4	25	13	0	25	38	25	25	25	0	13	25	38
Region G2												
6:6:6	50	34	50	58	58	42	42	25	17	42	42	42
5:8:5	40	30	50	50	70	40	30	30	10	30	50	50
4:10:4	38	25	38	50	63	50	25	25	13	25	38	50
Region G3												
6:6:6	33	17	17	50	50	59	42	25	25	17	33	42
5:8:5	10	10	20	40	30	50	30	20	10	10	20	30
4:10:4	13	13	0	13	13	38	13	13	13	13	13	25
Region G4												
6:6:6	33	17	42	59	50	50	50	17	17	17	42	50
5:8:5	30	10	50	50	30	40	40	20	20	10	10	40
4:10:4	13	13	63	38	25	25	38	25	25	13	0	25
Region G5												
6:6:6	25	25	17	50	33	42	50	33	25	0	33	33
5:8:5	30	20	20	40	30	30	50	20	20	0	30	20
4:10:4	25	13	13	25	38	38	50	13	13	0	25	25
Region G6												
6:6:6	25	33	33	50	17	34	25	25	9	17	42	25
5:8:5	20	30	30	40	20	40	30	20	10	10	30	20
4:10:4	25	13	25	25	13	25	13	25	13	13	25	0
Region G7												
6:6:6	42	33	25	17	17	17	42	42	25	34	50	33
5:8:5	30	40	30	10	0	0	30	40	20	30	40	20
4:10:4	25	38	25	0	0	0	38	25	13	38	25	25
Region A1												
6:6:6	25	25	33	42	42	33	42	34	50	34	33	25
5:8:5	20	20	30	40	40	40	40	30	30	30	20	20
4:10:4	13	13	25	38	38	50	50	38	13	13	13	0
Region SA												
6:6:6	59	25	34	42	50	42	50	33	33	34	50	42
5:8:5	50	20	30	30	50	30	40	30	30	30	40	40
4:10:4	38	13	25	13	25	38	50	25	25	25	50	25

A number of conclusions can be made when Tables 6(a), 6(b), 7(a) and 7(b) are examined. Most obviously are:

(a) Tables 6(a) and 7(a) indicate that in most regions percentage hit rate scores for the AN, NN and BN categories improve from classification A (6:6:6) towards classifications B (5:8:5) and C (4:10:4). This improvement might be attributed to biases as a result of the wider range in the rainfall distribution allocated to the NN category, meaning that more hits might occur in the NN category of classifications B (5:8:5) and C (4:10:4) than in the NN category of classification A (6:6:6).

To a certain extent the latter is confirmed in tables 6(b) and 7(b). These tables might be of value when one has to decide which category classification (classification A, B or C defined in table 5) is the most appropriate to use. The category classification with the highest hit rate score in these tables indicate that AN or BN (AN and BN) rainfall is well captured in AGCM simulations. The following will help with the interpretation of tables 6(a), 6(b), 7(a) and 7(b):

Hit rate score for AN, NN, BN (tables 6(a) and 7(a))	**Hit rate score for AN, BN (tables 6(b) and 7(b))**	**Implication**
High	Low	NN distribution too wide
Low	High	NN distribution too narrow
High	High	High general skill
Low	Low	Low general skill

Higher percentage probabilities of rainfall towards category classification C (4:10:4) of AN **or** BN (NOT AN **and** BN) could be of great value for seasonal forecasts because such probabilities will indicate that the AGCM captures the variability of more extreme rainfall events.

(b) Percentage hit rate scores do not improve significantly from monthly to three-month averaged rainfall analyses in individual grid boxes (regions G1 to G7 and even A1 in figures 6(a) and 6(b)).

(c) Percentage hit rate scores do improve noticeably when area averages are considered with time-averaged rainfall analyses (region SA in figures 6(a) and 6(b)).

5.4 CGCM SST FORECASTS FOR THE 2001/2002 SUMMER SEASON

The CGCM was employed to generate global SST forecasts for the 2001/2002 summer season. These simulations were performed at the CSIRO Atmospheric Research in Australia. Surface temperatures fields from the atmospheric component of the CGCM with a T63 horizontal resolution, which are equivalent to SST fields over the oceans, were used. In order to obtain a final ENSO outlook for 2001/2002, a number of SST forecasts were analysed. Four SST forecast simulations with the CGCM that were initiated from the beginning of July and August 2001 tend to indicate neutral ENSO conditions for the 2001/2002 summer season (figure 5.5 (a)). The two predictions initialised from August 1 (dotted lines in figure 5.5 (a)) indicate slightly positive anomalies in the NINO34 region for a few months, eventually decaying by early 2002. These forecasts give no strong indication of the development of persistent neutral ENSO conditions.

In addition to the NINO34 SST forecasts where the CGCM has significant skill, global SST forecasts were also issued. One of these forecasts, namely OND/JFM SST anomalies of globally forecast SSTs initiated from the beginning of August 2001, served as boundary forcing for the

CSIRO9 (R21) AGCM. Anomalies of global SST forecasts for December 2001, initiated from the beginning of August 2001, are displayed in figure 5.5(b).

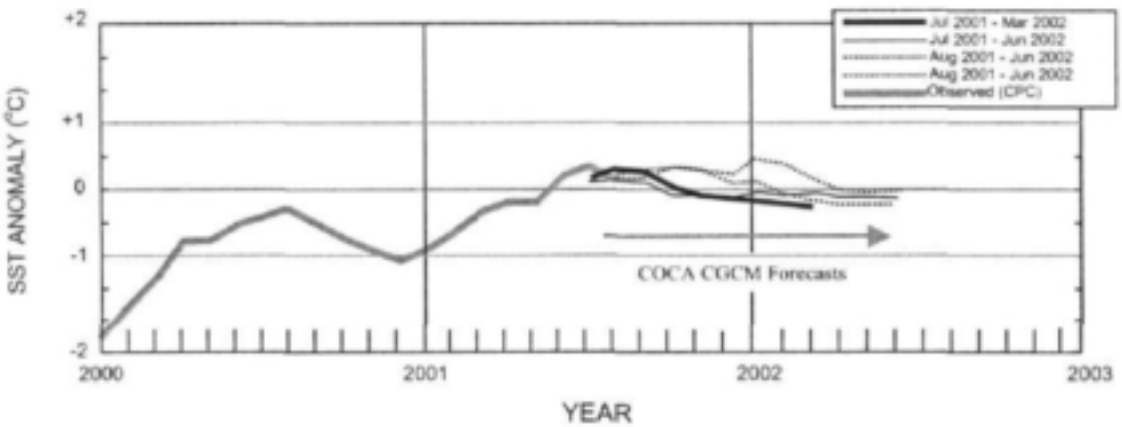

FIGURE 5.5(a) NINO34 SST forecast simulations by the COCA CGCM for the 2001/2002 summer season. Neutral ENSO conditions are expected.

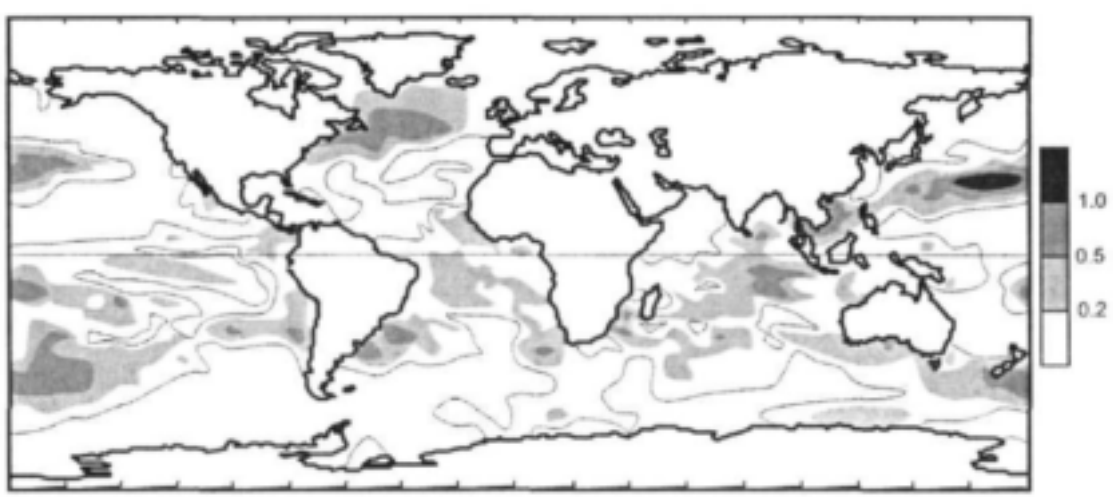

FIGURE 5.5(b) CGCM forecast Sea Surface Temperature (SST) anomalies for December 2001 measured in °C. The forecast simulation has been initialised from the beginning of August 2001. The dotted line represent the zero isotherm and the shaded areas has temperatures of 0.2 degrees and higher.

A matter of interest is that global and ENSO related SST forecasts being produced by the COCA CGCM are now issued on a routine basis by the CSIRO Atmospheric Research[1].

[1] http://www.dar.csiro.au/res/cm/coca.htm

5.5 PROBABILISTIC RAINFALL FORECASTS FOR 2001/2002

Seasonal cycle model simulations with the CSIRO9(R21) AGCM were performed with global COCA CGCM forecast SSTs prescribed as boundary forcing. SST fields from the CGCM simulations initiated from the beginning of August 2001, were prescribed. A spin-up simulation, where observed SSTs were prescribed for April, May, June and July 2001, preceded the AGCM rainfall forecast simulations. Four-member ensemble averages were calculated from CSIRO9(R21) AGCM rainfall simulations to yield monthly rainfall fields for the grid boxes that cover South Africa. Each ensemble run was initialised with slightly different initial conditions. Monthly model simulated rainfall fields were time averaged to produce rainfall forecasts for the OND 2001 and JFM 2002 seasons.

Category classifications A, B and C have been used to prepare categorical probabilistic rainfall forecasts for each one of the South African grid boxes (G1 to G7) and regions (A1 and SA). AGCM simulated rainfall forecast totals for the OND 2001 and JFM 2002 seasons have been compared to values of AN, NN and BN rainfall categories obtained from the 18-year hindcast simulation to determine the forecast category. From here, percentage probabilistic forecasts, depicted in figures 5.6 (a), (b), (c), figures 5.7 (a), (b), (c) and figures 5.8 (a), (b), and (c), have been prepared.

5.6 DISCUSSION

Percentage probabilistic rainfall forecasts for the early-summer period (OND 2001) over regions G1 to G7 in figures 5.6(a), 5.7(a) and 5.8(a) favoured AN rainfall over the eastern parts of the country. AN conditions were consistently forecast for grid G2 (Free State Province and Lesotho) in all three the category classifications. The associated forecasts for the late-summer season (JFM 2002) indicated that drier conditions in the NN category might follow. Category classification C (4:10:4) indicates that BN conditions were most likely to occur over grid box G7 (eastern parts of the Western Cape and western parts of the Eastern Cape) during the JFM 2002 season. There is also an indication that NN to AN conditions might have occured over the West Coast region for the rest of the summer season. There is no consistent signal for rainfall over the central parts of the country, although NN conditions becoming somewhat drier in the late-summer season might have been expected to occur for region A1.

Figures 5.6(b), 5.7(b) and 5.8(b) exhibited no forecasting skill for region A1 in category classification A (6:6:6), while BN and NN rainfall were forecast in classifications B (5:8:5) and C (4:10:4), respectively. This applies for both the OND 2001 and JFM 2002 seasons. The percentage probabilistic rainfall forecasts indicated that the expected rainfall in region A1 should be similar for both seasons.

In general the forecasting patterns pointed towards a wetter early-summer (OND 2001) and drier late-summer (JFM 2002) season (region SA in figures 5.6(c), 5.7(c) and 5.8(c)). This is particularly significant in figure 5.8(c) where the model forecast a 50% chance for AN conditions to occur during OND 2001 in the 4:10:4 classification, followed by drier conditions during JFM 2002.

If observed rainfall is considered, the OND 2001 season was indeed wetter than the JFM 2002 season – an indication that the seasonal forecasting method discussed in this chapter exhibits significant skill and could therefore produce rainfall forecasts for the two seasons under consideration.

5.5.1 *Rainfall forecasts with category classification A (6:6:6)*

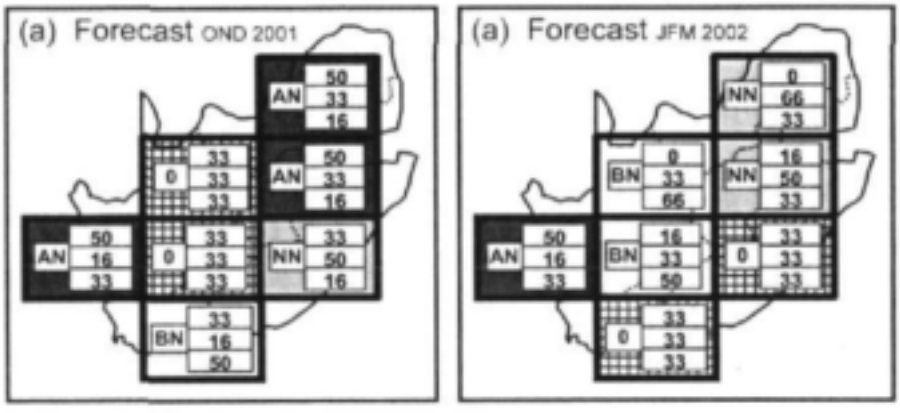

FIGURE 5.6(a) Categorical probabilistic rainfall forecasts for the (a) OND 2001 and (b) JFM 2002 seasons over regions G1 to G7 as calculated for category classification A (6:6:6). Probabilities have been derived from a 18-year hindcast simulation. The interpretation of the forecast probabilities is depicted by figure 3.10.

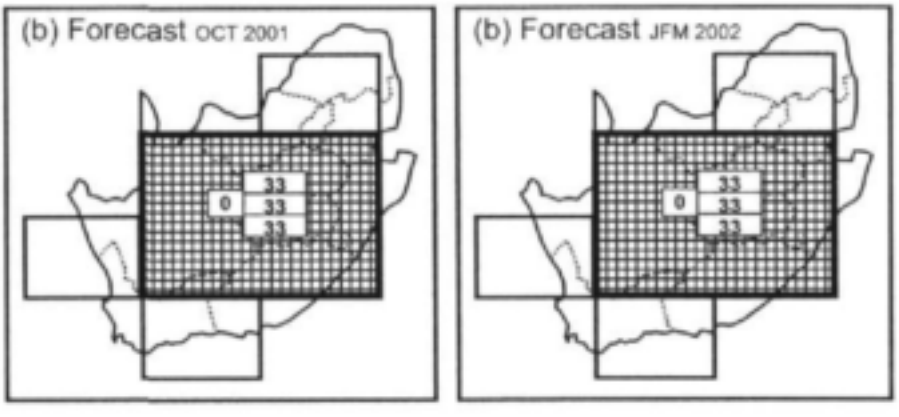

FIGURE 5.6(b) As figure 5.6(a) but for region A1.

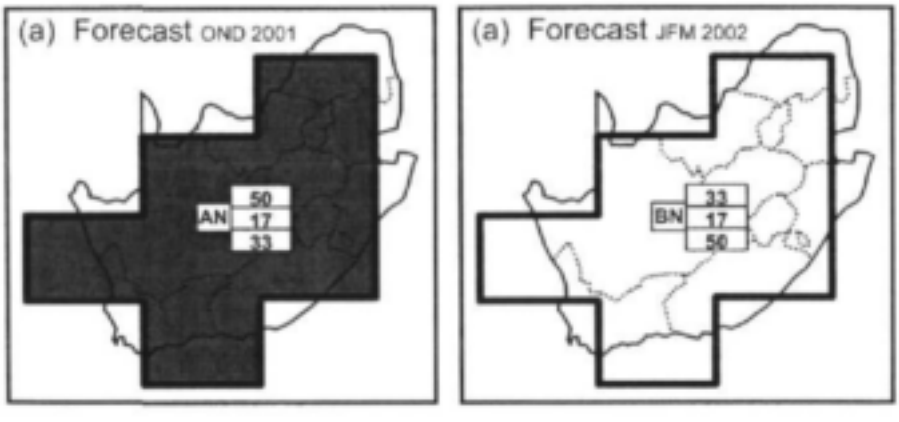

FIGURE 5.6(c) As figure 5.6(a) but for region SA.

5.5.2 *Rainfall forecasts with category classification B (5:8:5)*

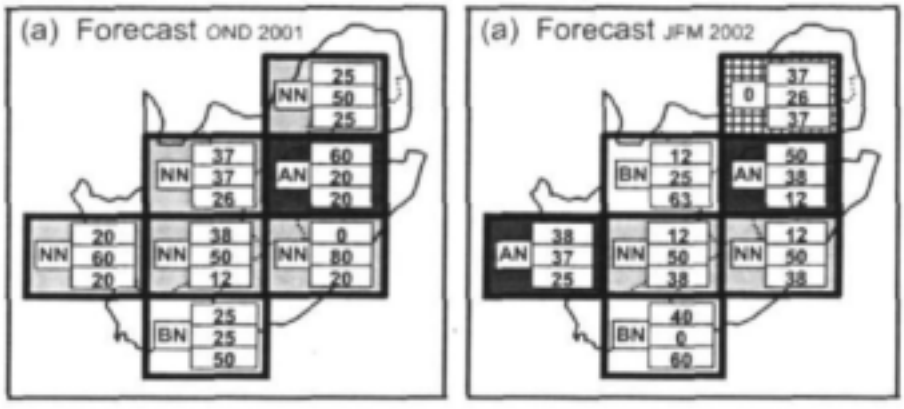

FIGURE 5.7(a) Categorical probabilistic rainfall forecasts for the (a) OND 2001 and (b) JFM 2002 seasons over regions G1 to G7 as calculated for category classification. B (5:8:5) Probabilities have been derived from a 18-year hindcast simulation. The interpretation of the forecast probabilities is depicted by figure 3.10.

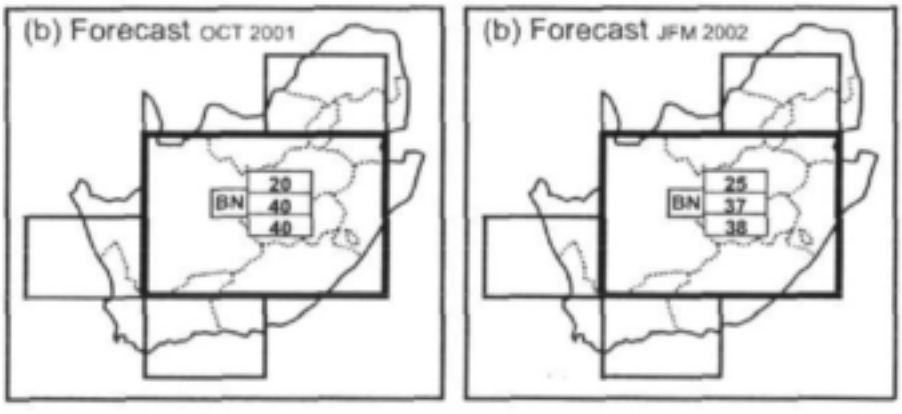

FIGURE 5.7(b) As figure 5.7(a) but for region A1.

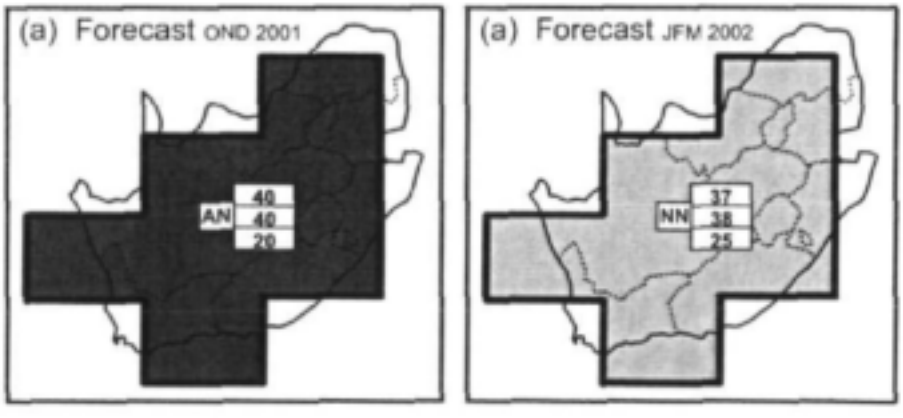

FIGURE 5.7(c) As figure 5.7(a) but for region SA.

5.5.3 *Rainfall forecasts with category classification C (4:10:4)*

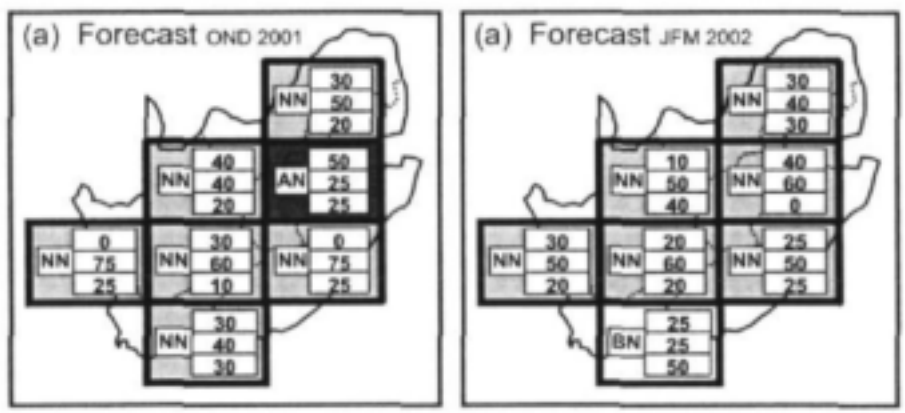

FIGURE 5.8(a) Categorical probabilistic rainfall forecasts for the (a) OND 2001 and (b) JFM 2002 seasons over regions G1 to G7 as calculated for category classification C (4:10:4). Probabilities have been derived from a 18-year hindcast simulation. The interpretation of the forecast probabilities is depicted by figure 3.10.

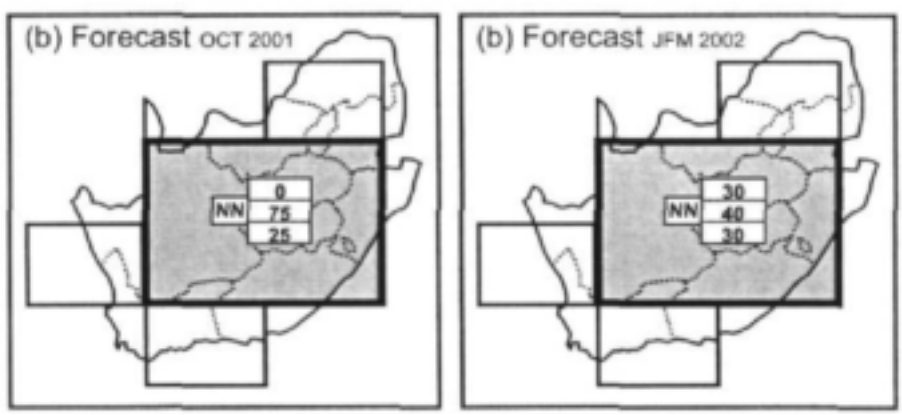

FIGURE 5.8(b) As figure 5.8(a) but for region A1.

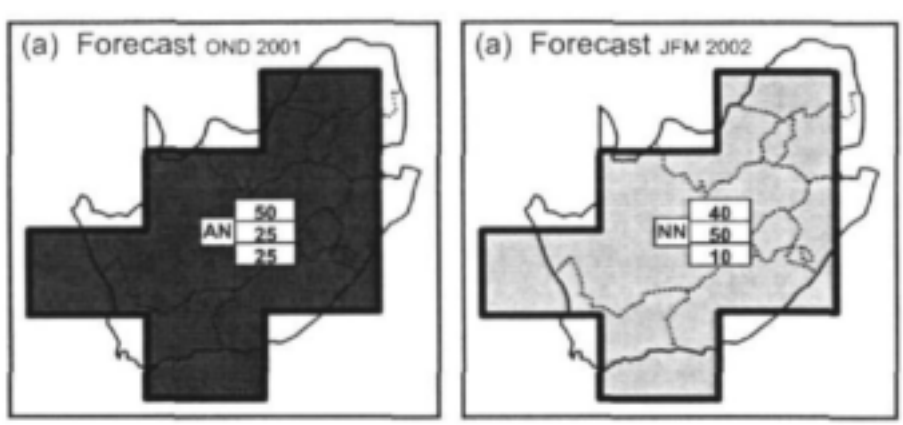

FIGURE 5.8(c) As figure 5.8(a) but for region SA.

CHAPTER 6

CONCLUSION

6.1 SUMMARY OF RESEARCH

In this study observed rainfall over South Africa was analysed from spatial and temporal perspectives and was compared with the associated AGCM simulated rainfall, where rainfall climatologies were derived in accordance with the CSIRO9(R21) and T(63) spectral resolutions. These climatologies formed the basis from which deviations in forecast rainfall were assessed.

A first numerical rainfall forecast was obtained by using the CSIRO9(R21) AGCM for the 1998/1999 summer season and verified against observations. Instead of CGCM SST forecasts, statistical Canonical Correlation Analysis (CCA) SST forecasts were employed as surface boundary forcing in this first experiment.

The research team collaborated closely with Australian scientists during the development phase of the COCA CGCM. Aspects of anomaly coupling, nudging and the initialisation procedure for forecast simulations were addressed and complex processes involved in ocean-atmosphere coupling as well as forecasting procedures were considered. In this project the COCA CGCM was primarily used for global SST forecasts.

Finally, COCA CGCM SST forecasts were evaluated against persisted SST forecasts and compared with forecasts generated by a statistical model. The CGCM forecasts outscored persistence and statistical forecasts, which motivated why CGCM SST forecasts were used. Spatial anomaly correlation patterns between observations and CGCM SST forecasts were illustrated and ocean regions with significant skill were highlighted.

The CSIRO9(R21) AGCM was forced with CGCM SST forecast fields to in an effort to generate probabilistic seasonal forecasts for the 2001/2002 summer season. An 18-year hindcast simulation was used to determine the skill of the AGCM, and different rainfall categories were defined. Hit rate scores were calculated. CGCM SST forecasts for the October, November, December (OND) 2001 and January, February, March (JFM) 2002 seasons were prescribed as boundary forcing for the AGCM and rainfall simulations were performed. Probabilistic forecasts were prepared for the three rainfall categories.

The OND 2001 (early-summer) and JFM 2002 (late-summer) forecasts favoured wetter conditions during the early-summer season followed by somewhat drier conditions during the late-summer season. ***These forecasts agreed with observations during the 2001/2002 summer season.***

6.2 OUTLOOK FOR THE FUTURE

The CLIPWATER project established a firm basis for further research in the field of numerical-based rainfall forecasting. During the CLIPWATER project Ms Anna Bartman completed and submitted an MSc dissertation, which addresses the field of downscaling, and in particular focuses on recalibration techniques (Bartman, 2002). A most challenging prospect is to produce improved seasonal forecasts on the regional scale. The CLIPWATER research team will continue

with their efforts to investigate means of improving seasonal forecasts, and will most probably focus on the development of regional scale rainfall forecasting.

REFERENCES

1. Allan, R., Lindesay, J. and Parker, D. (1996) *El Niño Southern Oscillation & Climatic Variability*. CSIRO Publishing, 150 Oxford Street, Collingwood, VIC, Australia. ISBN 0-643-05803-6, 405 pp.

2. Bartman, A.G. (2002) *Pattern analysis and recalibration of a perfectly forced atmospheric general circulation model*. Unpublished MSc dissertation, University of Pretoria, Pretoria, 0002, South Africa, 75 pp.

3. Botha, L. (1997) *Rainfall as indicator of the agroclimate of Namibia*. Unpublished M.Dip. dissertation, Pretoria Technicon, Pretoria, South Africa, 131 pp.

4. Brundrit, G.B. and Shannon, L.V. (1989) Cape storms and the Aghulhas Current: a glimpse of the future? *South African J. Science*, **85**, 619-620.

5. Cane, M.A., S.C. Dolan, and S.E. Zebiak, (1986) Experimental forecasts of the 1982/83 El Nino. *Nature* (London), **321**, 827-832.

6. Chen, D., L.M. Rothstein, and A.Busalacchi, (1994) A Hybrid Vertical Mixing Scheme and Its Application to Tropical Ocean Models. *J. Phys. Oceanogr.*, **24**, 2156-2179.

7. Chen, D., S.E. Zebiak, A.J. Busalacchi, and M.A. Cane, (1995) An improved procedure for El Nino forecasting. *Science*, **269**, 1699-1702.

8. Chen, D., S.E. Zebiak, M.A. Cane, and A.J. Busalacchi, (1997) Initialization and Predictability of a Coupled ENSO Forecast Model. *Mon. Wea. Rev.*, **125**, 773-788.

9. Chen, D., M.A. Cane, S.E. Zebiak, and A.Kaplan, (1998) The impact of sea level data assimilation on the Lamont model prediction of the 1997/98 El Nino. *Geophys. Res. Lett.*, **25**, 2837-2840.

10. Chen, D., M.A. Cane, and S.E.Zebiak, (1999a) The impact of NSCAT winds on predicting the 1997/1998 El Nino: A case study with the Lamont-Doherty Earth Observatory model. *J. Geophys. Res. (Oc)*, **104**, 11,321-11,327.

11. Chen, D., W.T. Liu, S.E. Zebiak, Y.Kushnir, and D.Witter, (1999) Sensitivity of the tropical Pacific Ocean simulation to the temporal and spatial resolution of wind forcing. *J. Geophys. Res. (Oc.)*, 104, 11,261-11,271.

12. Crimp, S.J., Lutjeharms, J.R.E. and Mason, S.J. (1998) Sensitivity of tropical-temperate trough to sea-surface temperature anomalies in the Agulhas retroflection region. *Water SA*, **24** (2), 93-100.

13. Dix, M.R. and Hunt, B.G. (1995) Chatoc influences and the problem of deterministic seasonal predictions. *Int. J. Climatol.*, **15**, 729-752.

14. Folland, C.K. and Rowell, D.P (1995) *Workshop on simulations of the Climate of the Twentieth Century using GISST, 28-30 November 1994, Hadley Centre, Bracknell, UK.*

Climate Research Technical Note **56**, Hadley Centre, Meteorological Office, London Road, Bracknell, Berkshire RG12 2SY, UK.

15. Gates, W.L., and A.B. Nelson, (1975) *A new (revised) tabulation of the Scripps topography on a 1° global grid. Part 1: Terrain heights.* Technical Report R-1276-1-ARPA, The RAND Corporation.

16. Goddard, L., Mason, S.J., Zebiak, S.E., Ropelewski, C.F., Basher, R., Cane, M.A. (2001) Current Approaches to Seasonal to Interannual Climate Prediction. *Int.J.Climatol.* **21(9)**, 1111-1152.

17. Goldberg, S.B., and J.J. O'Brien, (1981) Time and space variability of tropical Pacific wind stress. *Mon. Wea. Rev.*, **109**, 1190-1207.

18. Gordon, H.B. (1981) A flux formulation of the spectral atmospheric equations suitable for use in long-term climate modeling. *Mon.Wea.Rev.*, **109**, 56-64.

19. Gordon, H.B., and S.P. O'Farrell, (1997) Transient climate change in the CSIRO coupled model with dynamic sea ice. *Mon. Wea. Rev.*, **125**, 875-907.

20. Harrison M.S.J. (1984) A general classification of South African summer rain-bearing synoptic system. *J. Climatol.*, **4**, 547-560.

21. Hattle, J.B. (1968) Polar fronts of the Southern Hemisphere. *Notos: South African Weather Bureau*, **17**, 15-22.

22. Hellerman, S., and M.Rosenstein, (1983) Normal monthly wind stress over the world ocean with error estimates. *J. Phys. Oceanogr.*, **13**, 1093-1104.

23. Hirst, A., H.Gordon, and S.O Farrell, (1996) Global warming in a coupled climate model including oceanic eddy-induced advection. *Geophys. Res. Lett*, **23**, 3361-3364.

24. Hirst, A., S.O Farrell, and H.Gordon, (2000) Comparison of a Coupled Ocean Atmosphere Model with and without Oceanic Eddy-Induced Advection. Part I: Ocean Spinup and Control Integrations. *J. Climate*, **13**, 139 -163.

25. Hirst, A.C., (1999) The Southern Ocean response to global warming in the CSIRO coupled ocaen-atmosphere model. *Environmental Modelling and Software*, **14**, 227-241.

26. Hunt B.G., Zebiak, S.E. and Cane, M.A. (1994) Experimental predictions of climatic variability for lead-times of twelve months. *Int.J.Climatol.*, **14**, 507-526.

27. Hunt B.G. (1997) Prospects and problems for multi-seasonal predictions: some issues arising from a study of 1992. *Int.J.Climatol.*, **17**, 137-154.

28. Jackson, J. E., (1991) *A user's guide to principal components*, Wiley, New York

29. Ji, M., D.W. Behringer, and A.Leetma, (1998) An Improved Coupled Model for ENSO Prediction and Implications for Ocean Initialization. Part II: The Coupled Model. *Mon. Wea. Rev.*, **126**, 1022-1034.

30. Joubert A.M. (1997) Simulations by the atmospheric model intercomparison project of atmospheric circulation over southern Africa. *Int. J. Climatol.*, **17**, 1129-1154.

31. Jury, M.R. and Pathack, B.M.R. (1993) Composite climatic patterns associated with extreme modes of summer rainfall over southern Africa: 1975-1984. *Theor. Appl. Climatol.*, **47**, 137-145.

32. Jury, M.R., Pathack, B., Rautenbach C.J.deW. and van Heerden, J. (1996) Drought over South Africa and Indian Ocean SST: Statistical and GCM results. *The Global Atmosphere and Ocean System*, **4**, 47-63.

33. Jury, M.R., (1996) Regional teleconnection patters associated with summer rainfall over South Africa, Namibia and Zimbabwe. *Int. J. Climatol.*, **16**, 135-153.

34. Kachigan, S.K. (1991) *Multivariate statistical analysis: A conceptual introduction.* Radius Press, P.O.Box 1271, FDR Station, New York, NY 10150, ISBN 0-942154-91-6.

35. Kumar, A., Hoerling, M., Ji, M., Leetmaa, A. and Sardeshmukh, P. (1996) Assesing a GCM's Suitability for Making Seasonal Predictions. *J. Clim.*, **9**, 115-129.

36. Landman, WA (1995) A canonical correlation analysis model to predict South African summer rainfall. *Experimental Longlead Forecast Bulletin,* **4** (4), 23-24.

37. Landman, W.A. (1997) *A study of rainfall variability of South Africa as revealed by multivariate analyses.* Unpublished MSc dissertation, University of Pretoria, Pretoria, 0002, South Africa, 134 pp.

38. Landman, W.A. (1999) Near-global forecasts of sea-surface temperatures using canonical correlation analysis. *NOAA Experimental Long-Lead Forecast Bulletin*, **8**, No 4, 26-27.

39. Landman, W.A. and Mason, S.J. (1999) Change in the association between Indian Ocean sea-surface temperatures and summer rainfall over South Africa and Namibia. *Int. J. Climatol.*, **19**, 1477-1492.

40. Landman, W.A. and Mason, S.J. (2001) Forecasts of near-global sea surface temperatures using cononical correlation analysis. *J.Clim.*, **14**(18), 3819-3833.

41. Lau, N.-C. and Nath, M.J. (1994) A Modelling Study of the Relative Roles of Tropical and Extratropical SST Anomalies in the Variability of the Global Atmosphere-Ocean System. *J. Clim.*, **7**, 1184-1207.

42. Legler, D., I.Navon, and J.O'Brien, (1989) Objective Analysis of pseudostress over the Indian Ocean using a direct-minimization approach. *Mon. Wea. Rev.*, **117**, 709-720.

43. Levitus, S., (1982) *Climatological Atlas of the World Ocean.* NOAA Professional Paper 13, National Oceanic and Atmospheric Administration, Rockville, Maryland.

44. Lindesay, J.A. (1988) *The Southern Oscillation and atmospheric circulation changes over southern Africa.* PhD Tesis, Univ Witwatersrand, Johannesburg, South Africa. 284pp.

45. Lindesay, J.A. and Vogel, C.H. (1990) Historical evidence for southern oscilation-southern African rainfall relationships, *Int. J. Climatol.*, **10**, 679-689.

46. Lorenz, E. M. N. (1964) The problem of deducing the climate from the governing equations. *Tellus*, **16**, 1-11.

47. Lutjeharms, J.R.E. and De Ruijter, W.M.P. (1996) The influence of the Agulhas Current on the adjacent coastal ocean: possible impacts of climate change. *J. Marine Sys.*, **7**, 321-336.

48. Majodina, M. and Jury, M.R. (1996) Composite winter cyclones south of Africa: Evolution during eastward transit over the Agulhas warm pool. *S.Afr.J.mar.Sci.*, **17**, 241-252.

49. Mason, S.J., Lindesay, J.A. and Tyson, P.D. (1994) Simulating drought in southern Africa using sea surface temperature variations. *Water SA*, **20**, No 1, 15-21.

50. Mason, S.J. (1995) Sea-surface temperature - South African rainfall associations, 1910-1989. *Int.J.Climatol.*,**15**, 119-135.

51. Mason, S.J., Joubert, A.M., Cosijn, C. and Crimp, S.J. (1996) Review of seasonal forecasting techniques and their applicability to Southern Africa. *Water SA*, **22**, No 3, 203-209.

52. Mechoso, C.R., A.W. Robertson, N.Barth, M.K. Davey, P.Delecluse, P.R. Gent, S.Ineson, B.Kirtman, M.Latif, H.L. Treut, T.Nagai, J.D. Neelin, S.G.H. Philander, J.Polcher, P.S. Schopf, T.Stockdale, M.J. Suarez, L.Terray, O.Thual, and J.J. Tribbia, (1995) The Seasonal Cycle over the Tropical Pacific in Coupled Ocean-Atmosphere General Circulation Models. *Mon. Wea. Rev.*, **123**, 2825-2838.

53. McGregor, J.L., Gordon, H.B., Watterson, I.G., Dix, M.R. and Rotstayn, L.D. (1993) *The CSIRO 9-level Atmospheric General Circulation Model.* CSIRO Division of Atmospheric Research Technical Paper No. **26**, Aspendale, VIC, Australia. 89 pp.

54. Oberhuber, J.M., E.Roeckner, M.Christoph, M.Esch, and M.Latif, (1998) Predicting the '97 El Nino event with a global climate model. *Geophys. Res. Lett.*, **25**, 2273-2276.

55. Pacanowski, R.C., (1995) *MOM2 Documentation User's Guide and Reference Manual.* Technical Report 3, GFDL.

56. Parker, D.E., Jackson, M. and Horton, E.B. (1995) *The GISST2.2 sea-surface temperature and sea-ice climatology.* Climate Research Technical Note **63**, Hadley Centre, Meteorological Office, London Road, Bracknell, Berkshire RG12 2SY, UK. 16 pp.

57. Palmer, T.N. and Anderson, L.T. (1994) The prospects for seasonal forecasting. *Q.J.Royal Meteorol. Soc.*, **120**, 755-793.

58. Penland, C. (1989) 'Random Forcing and Forecasting Using Principal Oscillation Pattern Analysis', *MWR*, **10**, 2165-2185

59. Peters, H., M.C. Gregg, and J.M. Toole, (1988) On the Parameterization of Equatorial Turbulence. *J. Geophys. Res. (Oc.)*, **93**, 1199-1218.

60. Phillips, N.A. (1957) A coordinate system having some special advantages for numerical forecasting. *J.Meteor.*, **14**, 184-185.

61. Preston-Whyte, R.A. and Tyson, P.D. (1993) *The atmosphere and weather of southern Africa*. Oxford University Press, ISBN 0-19-570496-7, 374 pp.

62. Rautenbach, C.J.deW. (1999) *Introduction of a hybrid vertical co-ordinate to an Atmospheric General Circulation Model.* Unpublished PhD thesis, University of Pretoria, Pretoria, 0002, South Africa, 149 pp.

63. Reason, C.J.C. (1998) Warm and Cold Events in the Southeast Atlantic / Southwest Indian Ocean Region and Potential Impacts on Circulation and Rainfall over Southern Africa. *Meteorol. Atmos. Phys.* **69**, 49-65.

64. Reason, C.J.C and Mulenga, H. (1999) Relationships between South African rainfall and SST anomalies in the southwest Indian Ocean. *Int.J.Climatol.*,**19**, 1651-1673.

65. Reynolds, R.W. (1988) 'A real-time global sea surface temperature analysis', *J. Climate*, **1**, 75-86

66. Reynolds, R.W. and Smith, T.M. (1994) 'Improved global sea sea-surface temperature analyses using optimum interpolation', *J. Climate*, **7**, 929-948.

67. Reynolds, R., (1999) A real-time global sea surface temperature analysis. *J. Climate*, **1**, 75-86.

68. Ropelewski, C.F. and Halpert, M.S. (1987). Global and regional scale precipitation patterns associated with the El Niño/Southern Oscillation, *Mon. Wea. Rev.*, **115**, 1606-1626.

69. Rotstayn, L.D. (1996) Inclusion of cloud microphysics in the CSIRO GCM: sensitivity of the parameterized processes to the time step. *Bureau of Meteorology Research Centre, BMRC Research Report*, **54**, 163-168.

70. Rotstayn, L.D. (1997) A physically based scheme for the treatment of stratiform clouds and precipitation in large scale models. Part I: Description and evaluation of the microphysical processes. *Q. J. R. Meteorol. Soc.*, **123** (541), 1227-1282.

71. Rowel, P.D. (1998) Assesing Potential Seasonal Predictability with an Ensemble of Multidecadal GCM Simulations. *J. Clim.* **11**, 109-120.

72. Schiller, A., J.S. Godfrey, P.M. McIntosh, and G.Meyers, (1997) *A Global Ocean General Circulation Model for Climate Variability Studies.* CSIRO Marine Laboratories Report 227, CSIRO Marine Research.

73. Schulze, B.R. (1980) *Climate of South Africa, Part 8, General Survey (WB 28).* South African Weather Bureau, 330 pp.

74. Simonot, J.Y., and H.L. Treut, (1986) A Climatological Field of Mean Optical Properties of the World Ocean. *J. Geophys. Res. (Oc.),* 91, 6642-6646.

75. Smith, I.N. (1994) Indian Ocean Sea-surface temperature patterns and Australian winter rainfall. *Int.J.Climatol.,* **14**, 287-305.

76. Smith, I.N., Budd, W.F. and P. Reid (1998) The sensitivity of Antarctic accumulation rates to temperature changes. *Annals of Glaciology*, **27**, 246-250.

77. Smith, I.N. (1999) Estimating mass balance components of the Greenland ice sheet from a long-term GCM simulation. *Global and Planetary Change*, **20**,19-32.

78. Stricherz, J.N., J.J. O'Brien, and D.M. Legler, (1992) *Atlas of Florida State University tropical Pacific winds for TOGA 1966-1985.* Technical report, Florida State University.

79. Tennant,W.J. (1996) Influence of Indian Ocean sea-surface temperature anomalies on the general circulation of southern Africa. *South African J. Science*, **92**, 289-295.

80. Terray, L., E.Sevault, E.Guilyardi, and O.Thual, (1995*) Ocean Atmosphere Sea Ice Soil. User's Guide and Reference Manual*, CERFACS.

81. Tyson, P.D. (1986) *Climatic change and variability over southern Africa.* Cape Town: Oxford University Press, ISBN 0-19-570430-4, 220 pp.

82. Van Heerden, J. Terblanche, D.E. and Schulze, G.C. (1988) The southern oscillation and South Africa summer rainfall. *J. Cilmatol.*, **8**, 577-597.

83. Von Storch, H., T. Bruns, I. Fischer-Bruns and K. Hasselman, (1988) Principal Oscillation Pattern Analysis of the 30-60 day oscillation in a GCM equatorial troposphere, *J. Geophys. Res.* **93**, 11020-11036.

84. Walker, N.D. (1990) Links between South African rainfall and temperature variability of the Agulhas and Benguela current systems. *J. Geophys. Res.*, **95**, **C3**, 3297-3319.

85. Webster, PJ (1981) Mechanisms determining the atmospheric response to sea surface temperature anomalies. *J. Atmos. Sci.* **38** 554-571.

86. Wilson, S.G., (2000a): An intercomparison of Richardson Number-based Vertical Mixing Schemes in a tropical Pacific Ocean GCM that avoids Accumulation of Warm Surface Water. *Submitted to Mon. Wea. Rev.*

87. Wilson S.G., (2000b): An Ocean GCM and Vertical Mixing Scheme which maintain a "Sharp" Equatorial Thermocline. *Submitted to J. Phys. Oceanogr.*

88. Wilson, S.G., (2000c): How ocean Vertical Mixing and Accumulation of Warm Surface Water influence the "Sharpness" of the Equatorial Thermocline. *J. Climate (in press).*

89. Yang, X.-Q., Anderson, J.L. and Stern, W.F. (1998) Reproducible forced modes in AGCM ensemble integrations and potential predictability of atmospheric seasonal variations in the extratropics. *J. Clim.*, **11**, 2942-2959.

90. Zebiak, S.E. and Cane, M.A. (1987) A model El Niño – Southern Oscillation. *Mon. Weather Rev.*, **115**, 2262-2278.

91. Zebiak, S.E., (1986) Atmospheric convergence feedback in a simple model for El Nino. *Mon. Wea. Rev.*, **114**, 1263-1271.

92. Zebiak, S.E., and M.A.Cane, (1987) A model El Nino-Southern Oscillation. *Mon. Wea. Rev.*, **115**, 2262-2278.

93. Zebiak, S.E., (1990) Diagnostic studies of Pacific surface winds. J. Climate, 3, 1016-1031.

94. Zhang, Y., Wallace, J.M. and Battisti, D.S. (1997) ENSO-like interdecadal variability: 1900-93. , *J. Cilmatol.*, **10**, 1004-1020.

Other related WRC reports available:

Development of statistical forecast models of summer climate and hydrological resources over Southern Africa

Mark R Jury

This research project seeks to develop prediction models for water, climate and related resources from the following realisations: - the climate of Southern Africa often exhibits large departures from average; - these unexpected events impact water resources and economic activity; - climate fluctuations are related to nearby tropical ocean – monsoon conditions; - the fluctuations can be replicated using various climate and oceanic indices; and – regression equations can be formulated at useful lead-times to predict the climate.

In summary, this WRC project has successfully studied, formulated and implemented models to predict the variability of Southern African climate and water resources, 3-6 months in advance. The project has built on past efforts and drawn ideas from graduate students and collaborating scientists, to provide Southern African water and resource managers with optimum statistical forecasts via the internet website: <http://www.1stweather.com/forecasts/cip seasonal outlook.shtml>

Report Number: 903/1/02 **ISBN: 1 86845 936 5**

TO ORDER: Contact **Rina** or **Judas** - Telephone No: 012 330 0340
Fax Number: 012 331 2565
E-mail: publications@wrc.org.za

Water Research Commission
Private Bag X03, Gezina, 0031, South Africa
Tel: +27 12 330 0340, Fax: +27 12 331 2565
Web: http://www.wrc.org.za